BIOACTIVE AGENT LOADED HYDROGEL SYSTEMS FOR DENTAL
TISSUE ENGINEERING APPLICATIONS

A THESIS SUBMITTED TO
THE GRADUATE SCHOOL OF NATURAL AND APPLIED SCIENCES
OF
MIDDLE EAST TECHNICAL UNIVERSITY

BY

DENİZ HAZAL ATİLA

IN PARTIAL FULFILLMENT OF THE REQUIREMENTS
FOR
THE DEGREE OF DOCTOR OF PHILOSOPHY
IN
ENGINEERING SCIENCES

SEPTEMBER 2021

Approval of the thesis:

BIOACTIVE AGENT LOADED HYDROGEL SYSTEMS FOR DENTAL TISSUE ENGINEERING APPLICATIONS

submitted by **DENİZ HAZAL ATİLA** in partial fulfillment of the requirements for the degree of **Doctor of Philosophy** in **Engineering Sciences, Middle East Technical University** by,

Prof. Dr. Halil Kalıpçılar
Dean, Graduate School of **Natural and Applied Sciences**   _____

Prof. Dr. Murat Dicleli
Head of the Department, **Engineering Sciences**   _____

Prof. Dr. Ayşen Tezcaner
Supervisor, **Engineering Sciences, METU**   _____

Prof. Dr. Vasıf Hasırcı
Co-Supervisor, **Medical Engineering, Acıbadem Mehmet Ali Aydınlar University**   _____

Examining Committee Members:

Prof. Dr. Dilek Keskin
Engineering Sciences, METU   _____

Prof. Dr. Ayşen Tezcaner
Engineering Sciences, METU   _____

Assoc. Prof. Dr. Eda Ayşe Aksoy
Basic Pharmaceutical Sciences, Hacettepe Uni.   _____

Prof. Dr. Halime Kenar
Medical Engineering, Acıbadem Mehmet Ali Aydınlar Uni.   _____

Assoc. Prof. Dr. Can Özen
Biotechnology, METU   _____

Date: 07.09.2021

I hereby declare that all information in this document has been obtained and presented in accordance with academic rules and ethical conduct. I also declare that, as required by these rules and conduct, I have fully cited and referenced all material and results that are not original to this work.

Name, Last Name: Deniz Hazal, Atila

Signature:

ABSTRACT

BIOACTIVE AGENT LOADED HYDROGEL SYSTEMS FOR DENTAL TISSUE ENGINEERING APPLICATIONS

Atila, Deniz Hazal
Doctor of Philosophy, Engineering Sciences
Supervisor: Prof. Dr. Ayşen Tezcaner
Co-Supervisor: Prof. Dr. Vasıf Hasırcı

September 2021, 176 pages

Use of tissue engineered oral restoration products is currently a popular approach for treating dental defects that adversely affect oral health in ageing populations. Among scaffolds composed of long-lasting porous ceramics and biodegradable natural or synthetic polymers with varying service lives, injectable hydrogels attract attention to regenerate dental pulp due to the capability of filling non-uniform voids such as pulp cavity. In this study, two types of injectable hydrogels were formulized by designing distinct morphologies with the utilization of different biomaterials. Firstly, Tideglusib (Td)-loaded hyaluronic acid hydrogels (HAH) incorporated with Rg1-loaded chitosan microspheres (CSM) were developed for vital pulp regeneration, providing controlled release of Td drug and a ginsenoside Rg1 for matching two basic requirements of pulp; (i) odontoblastic differentiation of human dental pulp stem cells (DPSC) and (ii) vascularization of pulp. Secondly, gelatin methacrylate (GelMA)/thiolated pectin (PecTH) hydrogels (GelMA/PecTH) incorporated with the electrospun core/shell fibers, i.e. melatonin (Mel)-loaded polymethylmethacrylate (PMMA)/Td-loaded silk fibroin (SF) as the core and the shell components respectively, were designed as an alternative injectable hydrogel for vital pulp

regeneration, providing controlled release of Td and Mel for inducing proliferation and odontoblastic differentiation of DPSC for a prolonged period. For the first formulation, the expression of the specific genes (COL1A1, ALP, OCN, Axin-2, DSPP, and DMP1) confirmed odontogenic differentiation of DPSC which were incubated with Td-loaded HAH hydrogels incorporated with Rg1-loaded CSM microspheres. Angiogenic potential of the Rg1-containing hydrogel systems among all the other groups were shown on Matrigels *in vitro* with HUVEC. For the second formulation, cell viability assay showed that DPSC proliferated more in the groups of GelMA/PecTH hydrogels incorporated with PMMA/SF with a Mel/Td ratio of 1/3. ALP activity tests demonstrated that DPSC had the highest odontogenic differentiation level in the hydrogels groups containing PMMA/SF with a Mel/Td ratio of 3/1. Therefore, these novel injectable hydrogels have a potential as candidate biomaterials for vital pulp regeneration.

Keywords: Tideglusib, Hydrogel, Electrospun Fibers, Microspheres, Dental Tissue Engineering

ÖZ

DİŞ DOKU MÜHENDİSLİĞİ UYGULAMALARINA YÖNELİK BİYOAKTİF AJAN YÜKLÜ HİDROJEL SİSTEMLERİ

Atila, Deniz Hazal
Doktora, Mühendislik Bilimleri
Tez Yöneticisi: Prof. Dr. Ayşen Tezcaner
Ortak Tez Yöneticisi: Prof. Dr. Vasıf Hasırcı

Eylül 2021, 176 sayfa

Yaşlanan popülasyonlarda ağız sağlığını olumsuz etkileyen diş kusurlarını tedavi etmek için doku mühendisliği ile geliştirilmiş ağız restorasyon ürünlerinin kullanımı günümüzde popüler bir yaklaşımdır. Uzun ömürlü gözenekli seramikler ve değişen hizmet ömrüne sahip biyobozunur doğal veya sentetik polimerlerden oluşan yapı iskeleleri arasında, enjekte edilebilir hidrojeller, pulpa boşluğu gibi düzdün olmayan boşlukları doldurma kabiliyeti ile diş pulpası yenilenmesi için idealdir. Bu çalışmada, farklı biyomalzemelerle farklı morfolojiler tasarlanarak iki tip enjekte edilebilir hidrojel formüle edilmiştir. İlk olarak, Td ilacının ve bir ginsenosid olan Rg1'in kontrollü salınımını sağlayan, Rg1 yüklü kitosan mikroküreleri (CSM) ile birleştirilmiş Tideglusib (Td) yüklü hyaluronik asit hidrojeller (HAH) vital pulpa rejenerasyonun iki temel gereksinimini; (i) insan dental pulpa kök hücrelerinin (DPSC) odontoblastik farklılaşması ve (ii) pulpanın vaskülarizasyonu karşılamak için geliştirildi. İkinci olarak, elektro-eğirilmiş çekirdek/kabuk fiberli yapıları (melatonin (Mel) yüklü polimetilmetakrilat (PMMA)/Td yüklü ipek fibroin (SF):çekirdek/kabuk) ile birleştirilmiş jelatin metakrilat (GelMA)/tiyollenmiş pektin (PecTH) hidrojelleri (GelMA/PecTH), DPSC'nin proliferasyonunu ve odontoblastik farklılaşmasını indüklemek için Td ve Mel'in kontrollü salınımını uzun bir süre

boyunca sağlayan, alternatif enjekte edilebilir hidrojeller vital pulpa rejenerasyonunu sağlamak amaçlı tasarlanmıştır. İlk formülasyon için, spesifik genlerin (COL1A1, ALP, OCN, Axin-2, DSPP ve DMP1) ifadesi, Rg1 yüklü CSM mikroküreleri ile birleştirilmiş Td yüklü HAH hidrojelleri ile inkübe edilen DPSC'nin odontojenik farklılaştığını doğrulamıştır. Rg1 içeren hidrojel sistemlerinin anjiyojenik potansiyeli HUVEC ile Matrijeller üzerinde *in vitro* gösterilmiştir. İkinci formülasyon için yapılan hücre canlılığı analizi, 1/3 Mel/Td oranıyla PMMA/SF ile birleştirilen GelMA/PecTH hidrojel gruplarında DPSC'lerin daha fazla çoğaldığını göstermiştir. ALP aktivite testleri, Mel/Td oranı 3/1 olan PMMA/SF içeren hidrojel gruplarında DPSC'nin en yüksek odontojenik farklılaşma seviyesine sahip olduğunu göstermiştir. Bu nedenle, bu yeni enjekte edilebilir hidrojeller, pulpa rejenerasyonunu sağlama potasiyeline sahip biyomateryallerdir.

Anahtar Kelimeler: Tideglusib, Hidrojel, Elektroeğirilmiş Fiberler, Microküreler, Diş Doku Mühendisliği (En fazla 5 anahtar kelime)

To my family,

ACKNOWLEDGMENTS

TABLE OF CONTENTS

xiii

CHAPTER 3

CHAPTER 4

APPENDICES

LIST OF TABLES

TABLES

LIST OF FIGURES

FIGURES

LIST OF ABBREVIATIONS

ALP	Alkaline Phosphatase
ANOVA	Analysis of Variance
ATR	Attenuated Total Reflectance
Axin-2	Axin-2 Protein
BCA	Bicinchoninic Acid
BDDE	1,4-butanediol diglycidyl ether
BSA	Bovine Serum Albumin
COL1A1	Collagen Type I
CSM	Chitosan Microspheres
DMEM	Dulbecco's Modified Eagle Medium
DMP1	Dentin Matrix Protein 1
DMSO	Dimethyl Sulfoxide
DPSC	Human Dental Pulp Stem Cells
DSPP	Dentin Sialophosphoprotein
EDX	Energy-dispersive X-ray spectroscopy
eNOS	Endothelial Nitric Oxide Synthase
FBS	Fetal Bovine Serum
FITC	Fluorescein Isothiocyanate
FTIR	Fourier Transform Infrared

GAPDH   Housekeeping Gene

Gel   Gelatin

GelMA   Methacrylated Gelatin

HA   Hyaluronic Acid

HAH   Hyaluronic Acid Hydrogels

HUVEC   Human Umbilical Vein Endothelial Cells

Mel   Melatonin

OCN   Osteocalcine

PBS   Phosphate Buffered Saline

Pec   Pectin

PecTH   Thiolated Pectin

PI   Propidium Iodide

PMMA   Poly(methyl methacrylate)

pNPP   p-Nitrophenyl Phosphate

Saos-2   Human Osteogenic Sarcoma Cell Line

SEM   Scanning Electron Microscopy

SF   Silk Fibroin

TCPS   Cells seeded on polystyrene tissue culture wells

Td   Tideglusib

TGA   Thermo-Gravimetric Analyses

UV   Ultra Violet

VEGFA   Vascular Endothelial Growth Factor-A

VEGFR2   Vascular Endothelial Growth Factor Receptor-2

XPS   X-Ray Photoelectron Spectroscopy

CHAPTER 1

INTRODUCTION

1.1   Dental Tissue

Teeth, 20% surface area holders of mouth, are considered as significant constituents of human body in terms of functioning such as mastication, speech, and facial expressions as well as other focuses such as defense purposes among animals and esthetic concerns in modern times (Yen & Sharpe, 2008). They serve endurance under attritional forces lifelong owing to unique structural design of soft and hard tissues (Galler & D'Souza, 2011). From outer to inner layers; enamel, dentin, dental pulp, cementum, periodontal ligament, lamina dura, and alveolar bone are the sequential tooth parts (Figure 1.1).
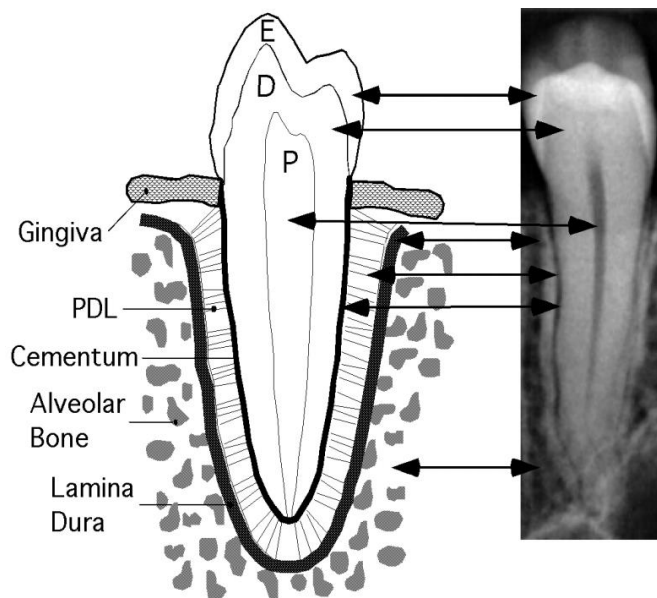
Figure 1.1 Sketch-radiograph of a tooth (Galler & D'Souza, 2011; Snead, 2008). Enamel (E): the visible tooth layer; Dentin (D): the bulk structural layer; Dental pulp

(P): the soft core of the tooth; Cementum: the coverage layer of root surface; Periodontal ligament (PDL): the connective tissue between cementum and alveolar bone; Alveolar bone: the attachment cavity of tooth in jaw; Lamina dura: the denser bone region between alveolar bone and PDL; Gingiva: the mucosal epidermal layer surrounding the tooth.

Crown surface acts in mastication process while root acts in attachment of the tooth to the alveolar bone (Nanci, 2007). Enamel deposited by ameloblasts (i.e., specialized dental epithelial cells), is the hardest tissue among mammalians with its inorganic hydroxyapatite content more than 90% in composition and is placed at the outermost layer of the tooth covering its entire visible surface in oral cavity (Galler & D'Souza, 2011). Dentin produced by odontoblasts (i.e., highly specialized mesenchymal cells), underlies below the enamel, and acquires a tubular bonelike architecture with an elastic feature possessing nearly 50% mineral content (Zaslansky, Friesem, & Weiner, 2006). Dental pulp composes the core of a tooth within which involves a living connective tissue; fibroblasts, odontoblasts, cementoblasts, nerve bundles, blood vessels, and lymph ducts (Yen & Sharpe, 2008). Odontoblasts align peripheral region of the dental pulp and form pre-dentin matrix which is a collagenous network, followed by mineralization of that matrix (Galler & D'Souza, 2011). Once the pre-dentin converts into dentin, each odontoblast has been protruded into a single dentinal tubule which is a connection channel between dental pulp and the outermost regions providing fluid flow from the pulp (Pashley, Livingston, & Greenhill, 1978). Dentin is an avascular but sensitive and regenerative layer since it can be restored by cytoplasmic extensions of odontoblasts or pulp cells through the tubules and can trigger self-deposition in the case of need (Nanci, 2007).

1.1.1   Dental Pulp

Pulp is in charge of two remarkable tasks for sustaining tooth viability which are (i) to supply nutrition by vascular network and (ii) to detect pathogen colonization for prevention of dental caries occurring due to bacterial invasion (W. Zhang & Yelick,

2

2010). In the case of pulp contamination, preservation of remaining viable pulp tissue is as important as elimination of microorganisms; since a tooth lacking pulp would be quite defenseless against further damage, eventually this leads to total tooth loss (Veerayutthwilai, Byers, Pham, Darveau, & Dale, 2007). Infected pulp often cannot be completely healed due to its physical location and tissue-specific properties (Farges et al., 2015).

1.2   Treatments for Diseased Dental Pulp

1.2.1   Endodontic Therapy

Endodontic therapy, i.e. root canal treatment, is one of the most commonly used methods in dentistry which is a procedure for the removal of contaminated or injured dental tissue, refilling, and sealing off the newly formed void with synthetic material to prevent potential future contamination (W. Zhang & Yelick, 2010). With advancements in antibiotic therapies, dental materials, and endodontic technology, the success rate of endodontic therapy has increased dramatically over the past decade (Prada et al., 2019). However, uncertain outcomes such as secondary root canal treatment may be needed (Hannahan & Eleazer, 2008) since current endodontic techniques replace the vital pulp with synthetic materials, rather than living tissue. Extruded endodontic materials can cause a foreign body reaction (Nair, 2006). Moreover, pulpless teeth lose their ability to sense environmental changes, making the progression of caries unnoticeable by patients (W. Zhang & Yelick, 2010).

1.2.2   Dental Pulp Regeneration

In order to avoid destroying the entire pulp by root canal treatments or tooth extractions, current strategies listed for treating diseased dental pulp include vital pulp therapy and dental pulp regeneration (Duarte Campos et al., 2020; Morotomi, Washio, & Kitamura, 2019). Vital pulp therapy consists of indirect and direct pulp

capping including pulpotomy, which all aim to protect the viability of remaining odontoblasts and provide a barrier against exogenous pathogens (Fuks, 2008). On the other hand, dental pulp regeneration strategies involve utilization of biomaterials, bioactive agents, cells, or various combinations of them to restore pulp tissue (Morotomi et al., 2019).

For functional pulp regeneration, two issues must be considered: (i) to induce odontogenic differentiation of stem cells for proper functioning and (ii) to ensure revascularization crucial for averting pulp necrosis and thus facilitating pulp regeneration (Gaihre, Uswatta, & Jayasuriya, 2017). The presence of differentiated odontoblasts lining the inner wall of the pulp chamber and root canal can facilitate repair of the functional dentin-pulp complex. However, when odontoblast differentiation occurs throughout the regenerated pulp, pulp stone formation may occur, which can block the blood supply, also prevent the transport of supplies which comes only from the narrow apical end of the tooth, and cause pulp necrosis (Berès et al., 2016). Therefore, differentiation rate of DPSC should be well-tuned.

1.2.3   Preformed Scaffolds

Fibrous meshes or moldable sponges have been utilized in tissue engineering of pulp tissue (F. Li, Zhao, & Song, 2010). In the literature, poly(ε-caprolactone) (PCL)/gelatin(Gel) scaffolds were electrospun with or without the addition of nano-hydroxyapatite (nHA) and behavior of human dental pulp stem cells (DPSC) seeded on these scaffolds were tested *in vitro* and *in vivo*. The subcutaneous pockets were created at the back of nude mice and scaffolds folded twice into a 4-layer were implanted. It was observed that electrospun composite scaffolds made of PCL/Gel/nHA and PCL/Gel, supported the proliferation and odontogenic differentiation of DPSC (X. Yang et al., 2010). Moreover, hard tissue formation was observed in the cell/scaffold composite groups *in vivo*. In another study, porous poly (L-lactic acid) (PLLA) scaffolds; (i) PLLA with solid-walled (SW) surface and (ii) PLLA nano-fibrous (NF) surface were produced by phase separation technique. Both

4

were tested *in vitro* using DPSC and *in vivo* by transplanting DPSC seeded scaffolds into two subcutaneous pockets after midsagittal incision on the dorsa of nude mice to observe the effect of fibrous or non-fibrous surfaces on dentin regeneration. Results showed that the NF-PLLA scaffolds enhanced the odontogenic differentiation of DPSC and mineralization of scaffolds was observed both *in vitro* and *in vivo* (J. Wang et al., 2011). In a different study, 3D cellulose acetate/oxidized pullulan/gelatin scaffolds with a tubular morphology were prepared by thermally induced phase separation and porogen leaching methods (Rad et al., 2019). The scaffolds were incorporated with boron (B) modified bioactive glass nanoparticles (BG-NPs), which stimulated the odontogenic differentiation of DPSC at most in the groups containing higher percents of B and BG-NPs *in vitro*.

1.2.4 Injectable Scaffolds

During determination of material type for successful pulp regeneration, several features of pulp tissue should be taken into account. For instance, fragility of pulp (soft tissue), irregular shape of pulp cavity, and small volume (~20 μm) of root canals all pose difficulties for pre-formed scaffolds with predetermined-shape during design and implantation into the defect site without causing harm (Fehrenbach & Popowics, 2015). Therefore, injectable scaffolds are preferred for dental pulp treatments owing to their superior characteristics such as (i) minimal invasiveness and maximal sterility, (ii) capability of filling non-uniform defects, and (iii) homogeneous delivery of bioactive molecules or cells by simply blending solutions prior to injection (Chang, Ahuja, Ma, & Liu, 2017; Gaihre et al., 2017).

Among all injectable scaffolds, hydrogels exhibit viscoelastic properties similar to soft connective tissue including dental pulp; thus enabling them to mimic native soft tissue extracellular matrix (ECM) by means of nutrient/waste transfer and cell encapsulation (Inuyama et al., 2010; L. A. Sharma & Love, 2019). Table 1.1 includes recently formulated injectable systems for dental tissue engineering, mainly for

dental pulp regeneration. To prepare injectable hydrogels, different polymers and crosslinking mechanisms were utilized as listed below.

Table 1.1 Injectable systems for dental tissue engineering.

Material	*Method*	*Aim*	*Findings*	*Reference*
HA hydrogels reinforced with cellulose nanocrystals and enriched with platelet lysate	Hydrazone cross-linking between hydrazide/amine and aldehyde groups of aldehyde and hydrazide derivatives of HA	To test the ability of the hydrogels to promote cells recruitment and proangiogenic activity *in vitro*.	Stimulation of chemotactic and pro-angiogenic activity by promoting DPSC recruitment and cell sprouting in DPSC/HUVEC co-cultures *in vitro* and in an *ex vivo* model by chick chorioallantoic membrane (CAM) assay.	(Silva et al., 2018)
Chlorhexidine (CHX)-loaded halloysite aluminosilicate nanotube-modified GelMA hydrogel	Photo-crosslinking	To examine the hydrogels *in vitro* and *in vivo* for sustained intracanal drug delivery applications in endodontics.	Minimum localized inflammatory responses and inhibition of bacterial growth due to successful drug delivery with minimal cell toxicity on human stem cells from exfoliated deciduous teeth.	(Ribeiro et al., 2020)

VEGF-encapsulated heparin-conjugated gelatin nanospheres immobilized in the nanofibers of an injectable PLLA microspheres	A combination of the water-in-oil-in-oil (W/O/O) double emulsion process, chemical crosslinking, and thermally induced phase separation	To regenerate living pulp tissues in a full-length root canal by mimicking clinical operation using freshly extracted human teeth.	Regeneration of pulp-like tissues that fulfilled the entire apical and middle thirds and reached the coronal third of the full-length root canal and regeneration of number of blood vessels throughout the canal *in vivo*.	(X. Li, Ma, Xie, Sun, & Liu, 2016)
DPSC and HUVEC-encapsulated peptide hydrogel PuraMatrix™	Gelation by gently running culture media down the side of the well on top of the hydrogel	To investigate the role of DPSC in triggering angiogenesis and the potential for regenerating vascularized pulp *in vivo*.	Formation of vascularized pulp-like tissue with patches of osteodentin after transplantation in mice in both the monoculture of DPSC and coculture groups of DPSC and HUVEC.	(Dissanayaka, Hargreaves, Jin, Samaranayake, & Zhang, 2015)

Commercially Available HA Hydrogel (Restylane)	Chemically crosslinked with BDDE	To examine survival, mineralization, and odontoblastic differentiation capacity of stem cells from apical papilla for pulp regeneration.	Promotion of survival, mineralization, and differentiation into an odontoblastic phenotype of stem cells from apical papilla by upregulation of DSPP, DMP1, and matrix extracellular phosphoglycoprotein (MEPE).	(Chrepa, Austah, & Diogenes, 2017)
Commercially available HyStem-C™ composed of polyethylene glycol diacrylate (PEGDA), HA, and gelatin components	Thiol-reactive gelatin and thiol-reactive HA solutions were mixed with disulfide bond added PEGDA (crosslinker).	To test the hypothesis that a PEGDA-HA based hydrogel combined with gelatin and fibronectin can support DPSC viability and spreading using an *in vitro* injectable 3D cell delivery strategy.	Enhancement of cell viability with the increasing ratios of HA to gelatin for 14 days. Enhancement of cell proliferation with added fibronectin (1.0-10.0 μg/mL) over time. Determination of fibronectin concentration (0.1 μg/mL) to induce cell spreading.	(Jones, Kefi, Sun, Cho, & Alapati, 2016)

Two types of PLLA microspheres with nanofibrous or smooth surface forming bioactive aggregates containing DPSC	Pouring the solution into liquid nitrogen & solvent exchange and traditional solvent evaporation	To examine the ability of the injectable systems to promote pulp regeneration in the root canal *in vivo.*	Confirmation of biocompatibility, biosafety and odontogenic potential of fibrous and smooth bioactive injectable microspheres. Promotion of dentin regeneration by the microspheres and DPSC *in vitro* and *in vivo*.	(Garzon et al., 2018)
Self-adhering phosphopullulan-functionalized calcium-silicate cement	Addition of phosphopullulan powder into calcium-silicate cement solution and shaking.	To evaluate the pulpal inflammatory reaction and reparative dentin-formation capacity by *ex vivo* human tooth-culture model and *in vivo* minipig animal study.	Stimulated of the formation of fibrous tissue and mineralized foci *ex vivo*. Promotion of early inflammatory reaction and regeneration of the pulp-tissue interface by phosphopullulan-functionalized cement and control after 7 and 70 days, respectively.	(Pedano et al., 2020)

Low-stiffness (235 Pa) and high-stiffness (800 Pa) oligomeric collagen matrices encapsulating DPSC	Self-assembly of type I oligomeric collagen derived from the dermis of market-weight pigs	To evaluate long-term cell survival, as well as endothelial and odontogenic differentiation following *in vitro* studies.	Upragulated expression of endothelial markers in the 235 Pa-matrices after 28 days, and the enhanced effect upon VEGF incorporation. Promotion of ALP activity in the 800 Pa-matrices. Enhancement of mineralization in BMP$_2$-modified matrices.	(Pankajakshan, Voytik-Harbin, Nör, & Bottino, 2020)
Hybrid RGD-alginate/laponite (RGD-Alg/Lap) hydrogel microspheres co-encapsulating DPSC and VEGF	Electrostatic microdroplet method	To support differentiation of DPSC *in vitro* and neotissue regeneration *in vivo* by using immunodeficient nude mice.	Stimulation of DPSC differentiation *in vitro* and pulp-like tissue regeneration *in vivo* after subcutaneous implantation with tooth slices in a nude mouse model for 1 month by the incorporation of laponite and the sustained release of VEGF.	(R. Zhang et al., 2020)

Glycol-chitosan (GC)-based single/dual-network hydrogels	Double network gelation under physiological environmental conditions through Schiff reaction and electrostatic interaction	To investigate the effect of hydrogel scaffolds on biological behavior of encapsulated DPSC.	Upregulation of DSPP, DMP1 and ALP expression significantly after 14 days in the dual-network hydrogels. Formation of more mineralization deposition and mass-shaped mineralized nodules in the dual-network hydrogels compared to single-network hydrogels.	(Cao, Yang, Qu, Han, & Wang, 2020)
Crosslinked HA gel containing tooth bud-derived dental mesenchymal cells and transforming growth factor-β1 (TGF-β1)	Crosslinking with BDDE and mixing with cells and TGF-β1	*In vivo* analyses by injection subcutaneously into nude mice as well as in empty tooth slices and the pulp chambers of mini pigs.	Formation of dentin–pulp-like tissue with a typical well-organized dentinal tubular structure and columnar odontoblast-like cells. High expression of the genes DSPP, DMP-1, MEPE and BSP. Neoformation of destroyed dentin.	(L. Tan et al., 2015)

Star-shaped block copolymer-poly(l-lactic acid)-block-poly(l-lysine) that self-assembles into unique nanofibrous spongy microspheres	Ring opening polymerization	To deliver hypoxia-primed DPSC and regenerate dental pulp with a rich vasculature and a complex histologic structure similar to that of the native dental pulp.	Enhancement of angiogenesis inside the pulp chamber and promotion of the formation of odontoblast-like cells lining along the dentin–pulp interface in the hypoxia group significantly compared to control after 4 weeks.	(Kuang et al., 2016)
Keratin hydrogels made by keratins extracted from sheep wool	10-12 h of incubation at 37°C	*In vivo* analyses of hydrogels implanted into rat upper molar teeth following partial pulpotomy.	Confirmation the biocompatibility of the hydrogels following 4 weeks after implantation in rat dental pulp. Organization of normal radicular pulp tissue with no adverse reactions. Observation of pulp healing to occur by a reparative response, with widespread DMP1 expression.	(Ajay Sharma et al., 2017)

Fibrin gels loaded with extracellular vesicles isolated from DPSC	Mixing the fibrinogen stock solution containing vesicles with the cell-loaded polymerization solution containing thrombin and CaCl$_2$	To test angiogenesis capacity as well as collagen deposition by using co-cultured endothelial cells and DPSC in the gels.	Facilitation of vascular-like structure formation in less than 7 days by increasing the release of VEGF. Promotion of the deposition of collagen I, III, and IV, and readily induced apoptosis during the initial stage of angiogenesis.	(S. Zhang et al., 2020)
Cellularized fibrin hydrogel supplemented with chitosan	Self-assembling	To support dental pulp tissue neoformation while confering antibacterial property.	Observation of a potent antibacterial effect of the chitosan in the fibrin network, and similar dental pulp-mesenchymal stem/stromal cell viability, fibroblast-like morphology, proliferation rate and type I/III collagen production capacity.	(Ducret et al., 2019)
Chitosan hydrogel	Pregel involving β-glycerophosphate	*In vitro* analyses using stem cells from the apical	Promotion of viability, proliferation, and migration of stem cells from the	(M. S. Moreira et al., 2021)

	disodium salt hydrate (crosslinker) becomes hydrogel at 37°C.	papilla and *in vivo* analyses using a rodent orthotopic dental pulp regeneration model under the influence of photobiomodulation therapy.	apical papilla *in vitro* when photobiomodulation therapy was applied especially with the energy density of 5 J/cm^2. Formation of pulp-like tissue inside the root canal *in vivo*.	
Silver-doped bioactive glass/chitosan hydrogel (Ag-BG/CS)	Pregel involving sodium β-glycerophosphate (crosslinker) and Ag-BG becomes hydrogel at 37°C.	To explore the molecular mechanisms of Ag-BG/CS in regards to its bioactive and anti-inflammatory properties.	Stimulation of dentin formation and preservation of vital pulp tissue. Enhancement of pulpal repair through the mitogen-activated protein kinase (MAPK) pathway by phosphorylation of p38 and ERK$_1$/2(p42/44).	(Zhu et al., 2019)

1.2.4.1   Hyaluronic Acid

Hyaluronan or hyaluronic acid (HA) holds great potential to be utilized as a raw material to prepare hydrogels for pulp tissue engineering since pulp ECM contains glycosaminoglycans like HA (Goldberg & Hirata, 2017) which contributes to the initial development of dental pulp (Inuyama et al., 2010) and induces odontoblastic differentiation of DPSC via CD44 (Ahmadian et al., 2019), suggesting that HA which can be formulated as an injectable hydrogel allowing cell infiltration and growth is ideal biomaterial for pulp repair and regeneration. Indeed, HA, a naturally occurring non-sulphated anionic polysaccharide, is composed of alternating units of a repeating disaccharide (β-1,4-D-glucuronic acid and β-1,3-N-acetyl-D–glucosamine), whose functional groups enable formation of new covalent bonds with surrounding tissue by continuously transforming it into necessary HA derivatives in the presence of biological molecules and signals (Ahmadian et al., 2019; G. Huang & Huang, 2018). These dynamic interactions and HA turnover are extremely important in physiological processes that are directly associated with rapidity of regeneration and wound repair (Fraser, Laurent, & Laurent, 1997).

In a previous study, injectable HA hydrogels reinforced with cellulose nanocrystals (CNCs) and enriched with platelet lysate (PL) were tested for endodontic tissue regeneration (Silva et al., 2018). The results demonstrated that the release of the chemotactic and pro-angiogenic growth factors (PDGF and VEGF) from the PL-laden hydrogels promoted (i) cell recruitment by chemotactic stimuli and (ii) cell sprouting by angiogenic stimuli in DPSC/HUVEC co-cultures *in vitro*. Moreover, the encapsulated DPSC was supported by the PL-laden hydrogels better when compared to the groups without PL *in vitro*. Furthermore, the hydrogels were capable of recruiting dental pulp-origin cells and enhancing new vessel-like structures sprouting in an *ex vivo* model (chick chorioallantoic membrane-CAM assay). In another study, HA hydrogels containing tooth bud-derived dental mesenchymal cells and transforming growth factor-β1 (TGF-β1) were prepared and injected

16

subcutaneously into nude mice as well as in empty tooth slices and the pulp chambers of mini pigs (L. Tan et al., 2015). In the nude mice model, a new tissue formation similar to dentin–pulp tissue with a typical well-organized dentinal tubular structure and columnar odontoblast-like cells were detected 7 weeks after injection. The following studies conducted by using empty tooth slices and the pulp chambers of mini pigs after the removal of total pulp and partial dentin confirmed the repairment of the dentin-pulp tissue.

1.2.4.2   Gelatin

Gelatin (Gel) is inexpensive, denatured collagen that can be derived from a variety of sources, while retaining natural cell binding motifs, such as RGD, as well as MMP-sensitive degradation sites (Galis & Khatri, 2002). In the literature, Gel was combined with alginate and bioplotted layer by layer to form 3D scaffolds, followed by post-crosslinking with glutaraldehyde (Pan, Song, Cao, & Wang, 2016) which were tested for dental pulp regeneration in a following study (Yu et al., 2019). Gel/alginate (20/4 wt%) scaffolds promoted biomineralization of DPSC *in vitro*. Moreover, the biomineralization-related genes (ALP, OCN, and DSPP) exhibited an upregulation in their expressions.

Gel derivatives have been utilized to bring out new properties of Gel-based biomaterials. For instance, addition of methacrylate groups to the amine-containing side groups of Gel are fuctional to make it photopolymerizable that can be converted into a hydrogel comprising stablility at 37 °C (Nichol et al., 2010), which is called photocrosslinkable gelatin methacryloyl or gelatin methacrylate (GelMA). Since GelMA consisted of modified natural ECM components (Van Den Bulcke et al., 2000), it is considered as a potentially attractive material for tissue engineering applications owing to its capability of cell/tissue adherence and biodegradability in the presence of matrix metalloproteinases (Ribeiro et al., 2020). In the literature, it was repoted that DPSC and HUVEC encapsulated GelMA hydrogels (5%) were injected into tooth root segments to regenerate pulp tissue and it was reported that

the cells adhered to the inner dentin surface of tooth root segments (Khayat et al., 2017). Moreover, the infiltration of DPSC into the dentin tubules was detected besides a well-organized neovasculature formation. In another study, injectable DPSC-laden GelMA microspheres were prepared by the electrostatic microdroplet method to induce endodondic regeneration (T. Yang et al., 2021). Regeneration of pulp-like tissue was observed and neovascularization of the pulp-like tissue formed in the DPSC-laden GelMA microsphere group more extensively compared to the DPSC-laden bulk GelMA group 8 weeks after subcutaneous implantation in a nude mouse model.

1.2.4.3   Pectin

Pectin (Pec) is an acidic water soluble, inexpensive, nontoxic heterogenous polysaccharide extracted from citrus peel or apple pomace. It contains linear chains of (1–4) linked α-d-galactouronic acid residues interrupted by some rhamnogalacturonic acid residue and α-l-rhamnopyranose by α-1-2 linkage. The galactouronic acid of backbone is partially methyl esterified (Sriamornsak, Wattanakorn, Nunthanid, & Puttipipatkhachorn, 2008). Pec is widely used in food technology because of its favourable gelling properties. Due to its biocompatibility, biodegradability and non-toxicity, Pec represents an attractive biopolymer for a variety of pharmaceutical and biomedical applications (Sriamornsak, Thirawong, et al., 2008). Pec hydrogels could be easily prepared by using nontoxic crosslinkers such as (i) $CaCl_2$ by adding it into Pec solutions with the molar ratio of Ca^{2+} ions/Pec carboxyl groups: 0.2 (Groult, Buwalda, & Budtova, 2021) or (ii) $CaCO_3$ by internal gelation method (H. R. Moreira et al., 2014). Then, these hydrogels could be converted into cryogels, aerogels, and xerogels by using fast and simple techniques, namely freeze drying, supercritical drying, and evaporation under low vacuum, respectively. In another study, polygalacturonic acid (PGA), i.e. Pec, hydrogels were fabricated with anodic electrophoretic deposition (EPD), which were also combined with bioactive particles such as TiO_2, hydroxyapatite, and bioactive glass to create

Pec hydrogel composites for bone regeneration (Clifford et al., 2020). The results showed that Saos-2 cells were able to proliferate onto the Pec hydrogel films *in vitro*, pointing out that Pec was a suitable natural polymer to achieve rapid surface modification of metallic implants. Moreover, injectable Pec hydrogels could be fabricated containing various other biomaterials. For instance, in a study, injectable chitosan (CS)/Pec hydrogels mimicking ECM were combined with cellulose nanocrystals (CNCs) to improve mechanical properties of the hydrogels for cartilage tissue engineering (Ghorbani, Roshangar, & Rad, 2020). In another study, Pec was utilized as an injectability enhancer of bone substitutes composed of hydroxyapatite/chitosan granules (the aggregate), α-TCP (the setting phase), and Pec solution (the liquid phase) (Dziadek, Zima, Cichoń, Czechowska, & Ślósarczyk, 2020).

Thiol containing ligands can be introduced into polysaccharide chain with the formation of amide or ester bonds. Thiol side chain of thiolated polymers interacts with cysteine rich subdomains of mucus glycoprotein forming stronger disulfide bonds (covalent bonds) between mucoadhesive polymer and mucus layer (Bernkop-Schnürch, 2005). During earlier investigations of thiolated chitosan (Bernkop-Schnürch, Hornof, & Zoidl, 2003), alginate (Bernkop-Schnürch, Kast, & Richter, 2001), gellan (Krauland, Leitner, & Bernkop-Schnürch, 2003), Pec (Perera, Hombach, & Bernkop-Schnürch, 2010; R. Sharma & Ahuja, 2011) have been prepared to improve their mucoadhesive properties.

1.3   Delivery Systems

Controlled release of bioactive agents incorporated into the hydrogel system supports the recovery process (Prasad, Gupta, Devanna, & Jayasurya, 2014; W. Zhang & Yelick, 2010). In order to achieve this goal, other delivery systems such as fibers or microspheres can be added into the hydrogel or the hydrogel itself can be loaded with bioactive agents. Moreover, delivery system of bioactive agents that have been preferred and designed for a tissue-engineered construct remarkably

affects; i) release kinetics (that should be above the optimal level), ii) concentrations (that should be unphysiologically high), and iii) duration time (that should considered according to half-life of a molecule) (Stevens, 2008) (Figure 1.2).
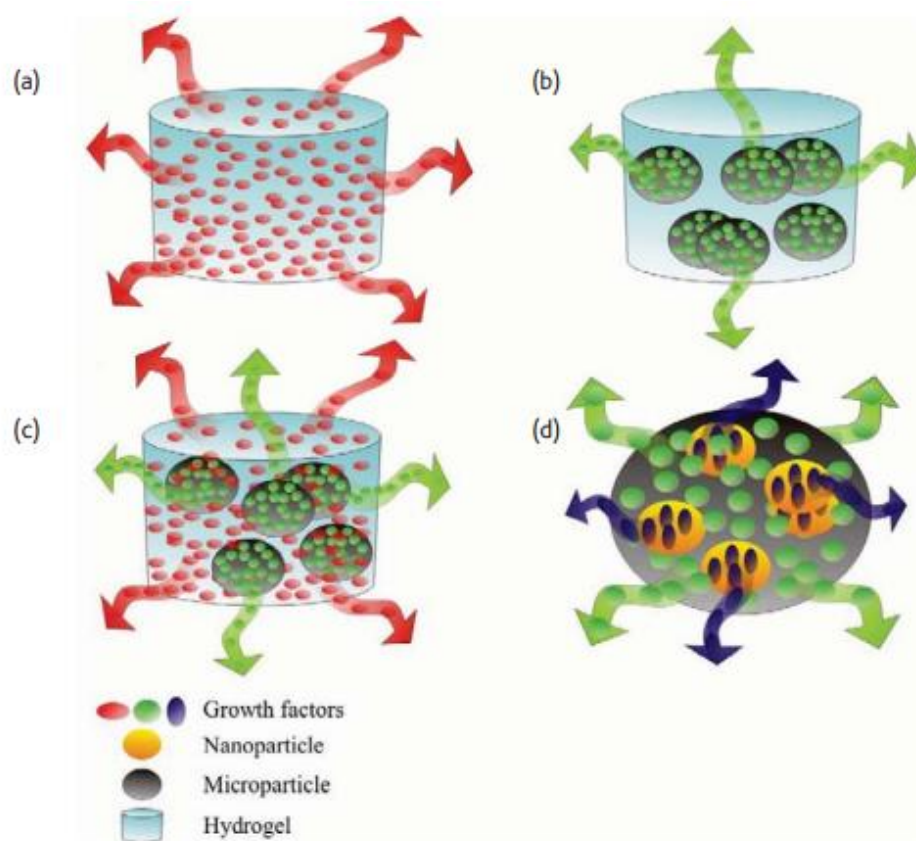
Figure 1.2 Schematic of various potential drug delivery approaches for the delivery of (a, b) a single growth factor or (c, d) multiple growth factors (Lee & Shin, 2007; Stevens, 2008).

1.3.1 Microspheres

When microspheres are introduced into an injectable hydrogel system, they tailor the release behavior of the bioactive agents from the hydrogels and do not hinder the injectability of the overall system due to their spherical shape and small size (Prasad et al., 2014). Microspheres can be prepared by using various techniques such as

electrospraying, water-in-oil-in-water emulsions, solvent evaporation, spray drying, electro-hydrodynamic atomization, etc.

1.3.1.1   Chitosan

Chitosan (CS), namely poly (β-(1→4)-2-amino-2-deoxy-D-glucose), is a natural linear cationic polysaccharide derived from chitin-based exoskeleton of marine crustaceans by alkaline N-deacetylation and can be readily converted into microspheres (Zeng et al., 2011). CS has suitable properties as a drug carrier such as high moisturizing and adsorption capacity (W. Wang et al., 2020) besides its non-toxicity (Yu Yang et al., 2014). CS has been widely used as an effective biopolymer in various fields of medicine and dentistry, e.g. as an anti-inflammatory root canal dressing material for periapical lesions (Cicciù, Fiorillo, & Cervino, 2019; Kmiec, Pighinelli, Tedesco, Silva, & Reis, 2017). It has been proven that CS took role in (i) stimulation of fibroblastic cells to release chemotactic inflammatory cytokines (e.g. interleukin 8), (ii) migration of polymorphonuclear leukocytes and macrophages at the early stage, and (iii) angiogenesis, reorganization of ECM, and granulation at the final stage of wound healing (Mori et al., 1997; Peluso et al., 1994; Ueno et al., 1999). Furthermore, antibacterial action has exhibited by CS against oral bacteria in which electrostatically negatively charged surface of bacterial cells in the interaction with the positively-charged amino groups (NH_3^+) may cause damage to the cell wall, alterations in permeability & barrier properties, and leakage of cell contents, sequentially (Kmiec et al., 2017; J. Li & Zhuang, 2020).

Additionally, the effect of CS monomers (namely D-Glucosamine hydrochloride) on odontogenic differentiation has been demonstrated in a previous study which was conducted by using osteoblastic culture of NOS-1 cells (Matsunaga et al., 2006). It was reported that alkaline phosphatase (ALP) activity significantly increased in the CS group after 3 days. Then, odontoblastic cells were detected at the periphery of the proliferated fibroblasts after 5 days.

1.3.2   Fibers

Micro-/nano-fibers can be incorporated into hydrogel systems in order to mimic native ECM of tissues. However, the injectability of the hydrogel system may not be retained if the fibrous part is not homogeneously distributed within hydrogel structure or the fibrous particulates have large sizes acting as bulk materials within hydrogels. There are many methods to fabricate fibers such as electrospinning, 3D-printing, thermally induced phase separation combined with other methods, etc.

1.3.2.1   Poly(methylmethacrylate)

Poly(methylmethacrylate) (PMMA) is a non-degradable, synthetic, thermoplastic acrylic polymer synthesized by methyl methacrylate monomers having superior properties to metals such as radiolucency, light-weight, lack of thermoconduction, and low cost (Fiaschi et al., 2016; Tihan, Ionita, Popescu, & Iordachescu, 2009). After the first production of hard and transparent PMMA in sheet form called 'Plexiglas', it was replaced with the previous golden standard in dentistry, namely vulcanite which is a hard and opaque rubber; thus it prevents light from inducing gingiva cells for their metabolic activities (Anusavice, Shen, & Rawls, 2013). Also, the toxic effects of mercury-containing amalgam as a dental filler material has forced the researches to replace it with safer biomaterials such as PMMA (Blasiak et al., 2011). Among hard tissue restoratives, PMMA was used in dentistry since 1930s; furthermore, together with stainless steel, PMMA was a common material in total hip replacements (Langer & Tirrell, 2004; Peppas & Langer, 1994; Ratner, Hoffman, Schoen, & Lemons, 2004).

In the medical field, biocompatibility of PMMA was clearly identified and its well-defined chemistry due to its controlled synthesis unlike heterogeneous production of natural polymers with its easy handling makes it reliable during operation and has been increasing its utilization for contact and intraocular lens, bone cements, alloplastic cranioplasty, and screw fixation in bone, etc (Eppley, 2005; Frazer, Byron,

Osborne, & West, 2005). In spite of these excellent properties, PMMA possesses two basic disadvantages mentioned in the literature; i) the heat production during in situ polymerization unless it is polymerized outside the defect region in terms of the shape and size of the defect site and ii) the brittleness under high loads unless it is combined with additive materials that modify mechanical properties (Fiaschi et al., 2016). Although PMMA implants have been examined intensively in dental applications, PMMA scaffolds particularly those in electropun form have not been exemplified excessively in the field of regenerative dentistry. For instance, electrospun PMMA scaffolds were produced to test respiratory epithelium cells *in vitro* (Rabiatul et al., 2015). Furthermore, acceleration of osteoblast differentiation was studied on PMMA/hydroxyapatite scaffolds fabricated via electrospinning; however, the scaffolds were not evaluated specifically for odontogenic response (Xing et al., 2013).

1.3.2.2   Silk Fibroin

Natural biopolymer silk cocoon spun by silkworm species named as *Bombyx Mori* is composed of two types of biocompatible proteins called fibroin and sericin, and silk fibroin (SF) can be removed in fibrous form leaving the rubbery sericin coverage behind in order to be safe in terms of inflammatory response (M. Yang, 2017). Besides low thrombogenicity, excellent biodegradability and non-toxic by-products, high permeability to oxygen and water vapor of SF have attracted researchers (Woloszyk et al., 2014). Furthermore, SF was reported to enhance hard tissue ingrowth by adult human progenitor bone marrow stromal cells while withstanding loads via possessing compressive strength and toughness; hence, it serves bifunctionality as a bone scaffold (K.-H. Kim et al., 2005). In addition, SF-involving scaffolds prepared by using salt leaching technique were successful to provide proliferation of DPSC *in vivo* in the presence of human amniotic fluid, while the same type of cells were stimulated in another study carried out with SF-based scaffolds and enhanced mineralization of DPSC were observed under dynamic

conditions with mechanical loading *in vitro* which is important factor both bone and dental tissue microenvironment (Riccio et al., 2012; Woloszyk et al., 2014). Additionally, basic fibroblast growth factor-incorporated porous SF scaffolds produced by freeze drying method were reported as promoting pulp-like tissue formation after seeding of DPSC (J.-w. Yang, Zhang, Sun, Song, & Chen, 2015). Moreover, the composite films comprised of SF and graphene oxide were tested to detect the response of periodontal ligament stem cells *in vitro* and the cells proliferated on SF-based scaffolds at higher proliferation rates in graphene oxide added-SF films (Rodríguez-Lozano et al., 2014). On the other hand, in a different study conducted with SF-based constructs as a model for guided bone regeneration after dental surgery, degradation rate of the scaffolds was shown to be tailored by the incorporation of hydroxyapatite. SF scaffolds without hydroxyapatite crystals maintained within artificial bone defects on rabbit femur for 8 weeks (Asakura et al., 2011).

1.4   Bioactive Agents for Dental Tissue Engineering

1.4.1   Tideglusib

Tideglusib® (Td), a glycogen synthase-3 (GSK-3) inhibitor molecule, was developed as a candidate drug for Alzheimer's Disease patients, having Phase II clinical trial statute (Lovestone et al., 2015). The molecular structure of Td is given in Figure 1.3. Its therapeutic efficacy has been tested for other diseases such as progressive nuclear palsy (Tolosa et al., 2014) or myotonic dystrophy (Konieczny et al., 2017). Recently, it has been discovered that Td could enhance regeneration of hard tissues e.g. bone or tooth (Alpan, Çalisir, Kizildag, Özdede, & Özmen, 2020; Comeau-Gauthier, Tarchala, Luna, Harvey, & Merle, 2020; Neves, Babb, Chandrasekaran, & Sharpe, 2017a; Zaugg et al., 2020).
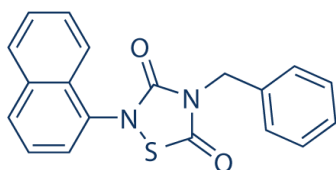
Figure 1.3 Molecular structure of Td.

Td acts as a glycogen synthase kinase 3 (GSK-3) inhibitor which induces cell proliferation in tooth repair process by letting specific cytoplasmic proteins (β-catenin and axin) enter the nucleus which result in a cascade of events (Figure 1.4) (Neves, Babb, Chandrasekaran, & Sharpe, 2017b).
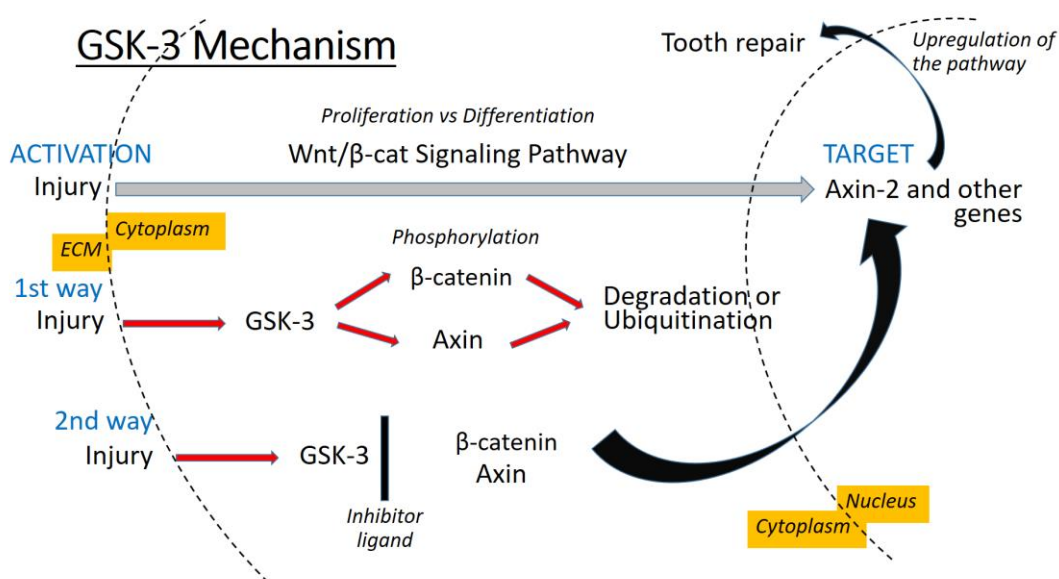
Figure 1.4 GSK-3 mechanism in the case of a tooth injury (Neves et al., 2017a).

Previously, Td-loaded collagen sponges were shown to facilitate dentin-like tissue formation by stimulating natural processes of dentin repair at the defect site of adult CD1 wild-type mouse first molars (Neves et al., 2017a). Furthermore, in another recent study a study was conducted on rat molars demonstrated that GSK-3

antagonists including Td promoted dentin formation and restored an area of dentin damage up to 10 times larger than the initial defect area (Zaugg et al., 2020). Hence, in this thesis study, Td has been incorporated into HAH to fulfill the first requirement of dental pulp regeneration (i.e. triggering odontoblastic differentiation of DPSC residing in the pulp cavity).

1.4.2 Rg1

In China, the root part of *Panax ginseng* plants has been used for thousands of years due to its beneficial biological effects in cardiovascular, endocrine, immune, and many other systems (Attele, Wu, & Yuan, 1999). The active components of ginseng are ginsenosides (~30 in total), of which Rg1 has a pronounced efficacy in enhancing vascularization (Lin, Hsu, & Rajasekaran, 2008). The molecular structure of Rg1 is given in Figure 1.5. In detail, Lin et al. showed that Matrigel plug containing Rg1 significantly promoted angiogenesis in transgenic mice one week after implantation, exhibiting the same effect with basic fibroblast growth factor (bFGF)-containing group (Lin et al., 2008). In another study, gelatin microspheres were loaded with Rg1 and embedded in collagen/CS sponges in which Rg1 release led to a significant increase in vascular endothelial growth factor (VEGF) secretion of human umbilical vein endothelial cells (HUVEC) (Zheng et al., 2013). Moreover, increased proliferation of DPSC, upregulated expression of specific genes including odontogenic ones (DSPP, ALP, OCN, BMP-2, FGF2); and protein expressions of BMP-2 and FGF2 in the presence of Rg1 were reported by the group (Ping Wang et al., 2014). Therefore, Rg1 has been incorporated into CSM in our study, which were added to the injectable hydrogel primarily to enhance vascularization of pulp tissue (i.e. the second requirement of dental pulp regeneration previously mentioned) and to increase the proliferation of DPSC.
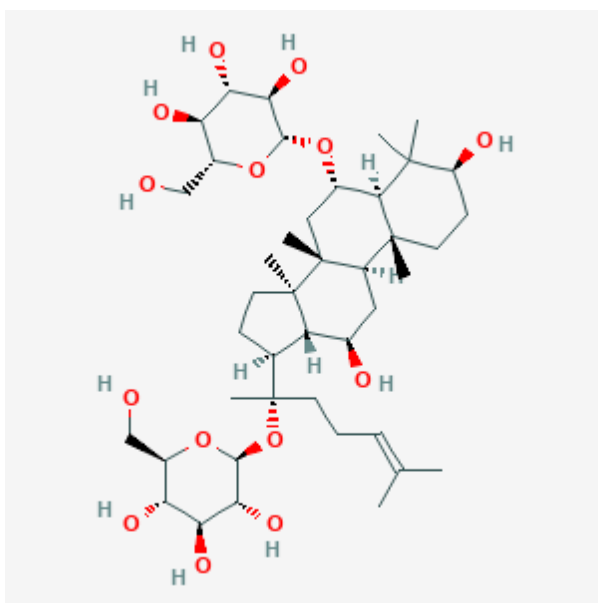
Figure 1.5 Molecular structure of Rg1.

1.4.3   Melatonin

Melatonin (Mel) (N-acetyl-5-methoxytryptamine), a tryptophan-derived naturally produced neuro-hormone (Figure 1.6) of darkness under the control of pineal glands plays a critical role in regulating circadian rhythm & sleep, suppression of tumor growth, activation of immune system, anti-inflammatory & antioxidative effects, and reproduction process (Cho, Noh, Jue, Lee, & Kim, 2015; Dubocovich, Rivera-Bermudez, Gerdin, & Masana, 2003; Fu et al., 2011; Galano, Tan, & Reiter, 2011; Jung-Hynes, Reiter, & Ahmad, 2010). Therefore, incorporation of Mel within a scaffold has the potential of huge benefits as a bioactive agent.
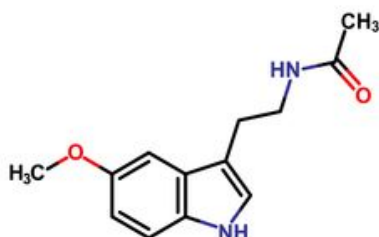
Figure 1.6 Molecular structure of Mel.

Zhang et al. demonstrated the positive effect of Mel loaded into PLGA microspheres on osteogenic differentiation of human mesenchymal stem cells *in vitro* (L. Zhang et al., 2013). Apart from differentiation promotion, Mel has a DNA-protecting capacity which is important to eliminate the damage caused by toxic chemicals which are released as i) excessive monomeric units of dental fillers left in the application site after in situ polymerization such as methyl methacrylate and also ii) degradation by-products of polymethacrylates produced by mechanical loads, involving hydrolysable esters such as methyl acrylic acids in the oral cavity (Blasiak et al., 2011; Y.-J. Jung, Hyun, Kim, & Jang, 2009; D.-X. Tan et al., 1993).

Mel utilization in dental tissue engineering was investigated in a recent study. Effect of Mel on odontogenic differentiation of rat dental papilla cells (rDPC) was investigated *in vitro* and in *in vivo* using twelve 1-day-postnatal SD rats (J. Liu et al., 2013). Proliferation of rDPC decreased in a dose dependent manner (0, 10^{-12}, 10^{-10}, 10^{-8} M) while ALP activity, dentin sialoprotein, and biomineralization increased with the increase in Mel concentration. Moreover, total dentin formation was observed less in the Mel administrated groups than the control groups. It was reported that Mel inhibited proliferation but promoted osteogenic differentiation of rDPC. In another study, human dental papilla cells (hDPC) were used to understand the influence of Mel on odontogenesis (Tachibana, Tatehara, Kumasaka, Tokuyama, & Satomura, 2014). They reported that Mel increased the expression levels of mRNAs for osteopontin, osteocalcin, bone sialoprotein, dentin matrix protein-1 (DMP1), and dentin sialophosphoprotin (DSPP).

Effect of Mel on proliferation and differentiation of DPSC was examined (Q. Liu et al., 2017). Results showed that proliferation of DPSC was negatively affected by the use of Mel in a dose- and time-dependent way. Similar findings were also previously reported for another cell line (rDPC) (J. Liu et al., 2013).

1.5   Aim of the Study

In this thesis study, two different injectable hydrogel systems were developed for vital pulp regeneration.

In the first part of the thesis a hydrogel system containing core/shell fibers that can release the bioactive agents in a controlled manner was developed. The hydrogel was composed of methacrylated gelatin (GelMA) and thiolated pectin (PecTH). Poly methyl methacrylate (PMMA) and silk fibroin (SF) fibers were prepared by coaxial electrospinning. PMMA constituted the core and SF the shell of the fibers. PMMA/SF fibers were loaded with two different bioactive agents; (i) Mel at the PMMA core to trigger odontogenic differentiation and (ii) Td at the SF shell to induce rapid proliferation of DPSC. PMMA/SF fibers whose sizes were lowered by homogenization in the hydrogel not to hinder the injectability of the system. GelMA/PecTH hydrogels of different ratios were prepared and characterized.

In the second part of the thesis, an injectable Td-loaded hyaluronan (HAH) gel incorporated with Rg1-loaded chitosan microspheres (CSM) was developed for vital pulp regeneration. Rg1 loaded cationic CSM were chosen to be incorporated within anionic HAH to constitute a well-integrated and homogeneous architecture owing to electrostatic interaction while providing controlled release of two biomolecules (Td and Rg1).

CHAPTER 2

MATERIALS AND METHODS

2.1   Materials

Low molecular weight HA powder (Hysilk, 150-1300 kDa) was purchased from Contipro (Czech Republic, EU). Td drug (4-Benzyl-2-(naphthalen-1-yl)-1,2,4-thiadiazolidine-3,5-dione) and BDDE (1,4-butanediol diglycidyl ether) were purchased from Sigma-Aldrich (U.S.A.). CS (Highly Viscous) was obtained from Sigma (U.S.A.). Ginsenoside-Rg1 standard was obtained from WAKO (Osaka, Japan). All other chemicals are purchased from Sigma (U.S.A.). The use of DPSC was approved by National Taiwan University Hospital (IRB No: 201103088RC). HUVEC at passage 1 was obtained from ScienCell Research Laboratories (California, U.S.A). PMMA (poly methyl methacrylate, average MW: 120 kDa) was purchased from Aldrich (Missouri, U.S.A.). SF (silk fibroin obtained from silkworm cocoons of *Bombyx mori*) was purchased from Akman İpek Company (Bursa, Turkey). Mel crystalline ($C_{13}H_{16}N_2O_2$ or N-[2-(5-methoxy-1H-indol-3-yl) ethyl]) was purchased from Sigma (Missouri, U.S.A.). HFIP (1,1,1,3,3,3-Hexafluoro-2-propanol) was purchased from Merck (Germany). Irgacure 2959 (2-(Hydroxyl) -4-(2-hydroxyethoxy) -2-methylpropiophenone) and Type A porcine skin gelatin, methacrylic anhydride, were purchased from Sigma-Aldrich (U.S.A.). High methoxyl Pectin was purchased from Benosen Company (Istanbul, Turkey). Thiogylcolic acid used was from Merck (Germany).

2.2 Preparation and Characterization of Hyaluronic Acid (HA)-Based Hydrogels

HA-based hydrogel systems were prepared in order to enhance vital pulp regeneration by inducing (i) odontogenic differentiation of DPSC with the use of Td loaded into HA hydrogel part and (ii) vascularization of pulp with the use of Rg1 loaded into microspheres. Experimental groups constructed to test these hydrogels are given in Table 2.1.

Table 2.1 The HA-based hydrogel groups.

Group Name	*Definition*
HAH	HA hydrogels
HAH+CSM	hydrogels + microspheres
Td@HAH+CSM	Td-loaded hydrogels + microspheres
HAH+Rg1@CSM	hydrogels + Rg1-loaded microspheres
Td@HAH+Rg1@CSM	Td-loaded hydrogel + Rg1-loaded microspheres

2.2.1 Preparation of HAH

HAH were prepared by following the previous protocol (R. Yang, Tan, Cen, & Zhang, 2016). HA solutions were prepared with 14 (w/v) % polymer concentration in 1.0% NaOH. After clear dissolution was obtained, BDDE (0.6 v/v %) was added and stirred at 700 rpm for 5 min. HA solution mixed with BDDE was poured into 24-well plates and incubated at 40°C for 5 h. After gelation was observed, hydrogels

were transferred into d-H2O, incubated for 24 h to remove BDDE and NaOH residues within the hydrogels, and then autoclaved. Sterilized HAH was stored at 4°C until use.

2.2.2 Characterization of HAH

2.2.2.1 Fourier Transform Infrared (FTIR) Spectroscopy

Crosslinking of HAH was verified by FTIR analysis by a spectrometer of PerkinElmer Spectrum 100 series (Massachusetts, U.S.A.) using spectrum 100/100N software program in transmission mode. The analysis was performed within the wavelength range 400–4000 cm^{-1} with a resolution of 8 cm^{-1}. During crosslinking, the ether groups at the edges of BDDE attack O–H groups of HA where the bond formation occurs. Therefore, newly formed ether linkages were examined to verify crosslinking of the hyrogels (Al-Sibani, Al-Harrasi, & Neubert, 2016).

2.2.2.2 Proton Nuclear Magnetic Resonance (^{1}H-NMR) Spectroscopy

HA samples before and after crosslinking were dissolved in deuterium. ^{1}H-NMR spectra were obtained with a Bruker Biospin spectrometer (Varian 400 mHz, U.S.A.) operating at a ^{1}H resonance frequency of 400 mHz. Sixteen scans were made for signal-to-noise averaging. Degree of modification (MoD) or crosslinking degree was calculated by using the equation based on the ratio of the corresponding area under the peaks at 1.7 and 2.1 ppm (Wende, Gohil, Nord, Kenne, & Sandström, 2017).

2.2.2.3 BDDE Removal

The BDDE amount left in the samples was determined according to the previously established method (R. Yang et al., 2016). Briefly, HAH (0.23 g) were soaked in 50 mL of PBS (0.1 M, pH 7.2) at RT. Aliquots (1 mL) from release media were collected

at different time points: 1, 2, 6, 12, 24, 48, and 72 h and fresh PBS (1 mL) was added. The 200 µL of aliquot was mixed with a freshly prepared nicotinamide solution (100 µL, 125 mmol/L). The mixed solution was incubated in a water bath at 37°C for 120 min. Next, acetophenone solution (1 mL, 15 vol% in ethanol) and potassium hydroxide solution (1 mL, 1 mol/L) were added into the above mixture. After 10 min of incubation in an ice bath, formic acid (5 mL) was added into this mixture, which was then heated at 60°C using a water bath for 5 min and subsequently cooled in an ice bath for 10 min. The resulting solution was kept at RT for 15 min and the fluorescence intensity of the solution was measured (excitation wavelength: 370 nm and emission wavelength: 430 nm) using EnSpire® Multimode Plate Reader (PerkinElmer, U.S.A.) and the amount of BDDE removed was calculated using the calibration curve constructed with different concentrations of BDDE (1-20 µg/mL) (Appendix A1).

2.2.2.4   Scanning Electron Microscopy (SEM)

The morphology of HAH was observed using SEM (TM-1000, Hitachi, Japan). HAH were freeze dried (Freeze Dryer, Hitachi, Japan) for 3 days and were sputter-coated with gold before observation.

2.2.3   Preparation of Td-Loaded HAH (Td@HAH)

After BDDE removal, sterile HAH were loaded into the syringes. Td of different concentrations was dissolved in DMSO and added into HAH containing syringes with a volume ratio of solution/HAH (1/100). Afterwards, hydrogels were taken in and out several times. Td@HAH were stored at 4°C until use.

2.2.4   Characterization of Td@HAH

2.2.4.1   Td Release

HAH hydrogels loaded with different amounts of Td (20 g of swollen weight in 50 mL of PBS) were incubated in PBS at 37°C. Aliquots from release media were collected at determined time points (1, 2, 3, 4, 5, 6, 12 h, 1, 2, 3, 6, 12, 18, 24, and 30 d) and fresh PBS in the same volume of the aliquot (1 mL) was added. The absorbance of samples was measured at 285 nm via Nanodrop spectrophotometer (NanoDrop 2000c, Thermo Fisher Scientific, U.S.A.) in the UV-Vis mode. The standard curve was constructed using different concentrations of Td within the interval of 2.25-156.25 µM (Appendix B1). Percent Td release was calculated by using the formula below.

$$Td\ Release\ (\%) = \frac{Amount\ of\ Td\ Released}{Initial\ Td\ Amount\ Loaded} \times 100$$

2.2.5   Preparation of Rg-1 Loaded Chitosan Microspheres (Rg1@CSM)

The optimization studies were initially conducted with empty CSM. CS (20 mg) was dissolved in 10 mL of 2 v/v% aqueous acetic acid solution at RT overnight. Sodium tripolyphosphate (STPP) solution (1 w/v%) was stirred at 300 rpm in a beaker. CS solution was added dropwise into the 100 mL of STPP solution by using a peristaltic pump with a feeding speed of 0.4 rpm. CSM formed were collected by cell strainers and washed with d-H$_2$O. Then, the microspheres were stored at 4°C after lyophilization. CSM were sterilized by UV light exposure for 30 min prior to cell culture studies. Stored CSM (12 mg) were placed in eppendorf tubes and 75 µL of Rg1 solution in 20 mM HEPES containing 150 µg of Rg1 was added onto the CSM dropwise. After air-drying overnight in a sterile laminar hood, Rg1-loaded CSM (Rg1@CSM) were stored at 4°C until use.

2.2.6 Characterization of Rg1@CSM

2.2.6.1 Morphological Analyses

CSM were freeze dried (Hitachi, Japan) and were sputter-coated with gold before observation. The morphology of samples was observed using SEM (TM-1000, Hitachi, Japan). Diameter size distribution histogram of CSM was constructed over 300 measurements obtained from SEM images via ImageJ software (National Institutes of Health, Bethesda, U.S.A.) and the average diameter size of CSM was calculated. Phase contrast microscopy was used to examine the swollen state of CSM in PBS under 20X magnification and images of CSM were taken.

2.2.6.2 Rg1 Release

During optimization studies of Rg1 loading, CSM (8 mg) was loaded with 50, 100, 150, and 200 µg of Rg1 and incubated at 37ºC for 6 days. After the initial loading of 100 µg of Rg1was selected, Rg1@CSM (8 mg) and Rg1@CSM in HAH (8 mg in 600 µL HAH) were placed in dialysis tubing (cut-off = 6000-8000) and incubated in PBS (2 mL) at 37°C. Aliquots from release media were collected at determined time points (1, 2, 3, 4, 5, 6, 12 h, 1, 2, 3, 6, 12, 18, 24, and 30 d) and fresh PBS in same volume of the aliquot was added. The absorbance of samples was measured at 208 nm via Nanodrop micro-spectrophotometer (Nano-100, Allsheng Instruments, China) in the UV-Vis mode and percent Rg1 release was calculated by using the formula below. The standard curve was constructed using different concentrations of Rg1 within the interval of 10-100 µg/mL (Appendix C1).

$$Rg1\ Release\ (\%) = \frac{Amount\ of\ Rg1\ Released}{Initial\ Rg1\ Amount\ Loaded} \times 100$$

2.2.7 Preparation of the Final Td-Loaded HAH Incorporated with Rg1-Loaded CSM (Td@HAH+Rg1@CSM)

Td@HAH placed inside a syringe was combined with Rg1@CSM in a vial bottle by direct mixing (HAH/CSM ratio: 300 µL/4 mg) by pulling in and out of a syringe. After several pulling in and out cycles for less than 2 min, the hydrogels were ready to be applied.

2.2.8 Characterization of Td@HAH+Rg1@CSM

2.2.8.1 Rheological Analyses

Viscosity, storage moduli (G'), and loss moduli (G'') of the hydrogels with or without microspheres (HAH and HAH+CSM) were determined between 0°C and 100°C at a displacement resolution of 10 nrad by using a stress-controlled rheometer (HR-2 system, TA Instruments, U.S.A.). Viscosity equation used was shared below (Barbucci et al., 2002).

$$Complex\ Viscosity\ (\eta^*) = \frac{\sqrt{(G')^2 + (G'')^2}}{Oscillation\ Frequency}$$

2.2.8.2 Morphological Analyses

HAH+CSM were freeze dried (Freeze Dryer, Hitachi, Japan) and were sputter-coated with gold before observation. The morphology of samples was monitored using SEM (TM-1000, Hitachi, Japan) to examine the distribution of CSM in HAH. The swollen state of CSM in HAH was examined by the Fluorescence microscope (Leica DM IRB, Microscope Central, U.S.A.) via cellSence imaging software (Olympus, Japan).

2.2.8.3   *In situ* Degradation in PBS and Enzymatic Degradation

Hydrogels were weighed at initial dry state and then placed in closed bottles (10 mg/mL in PBS), and incubated at 37°C for 2 weeks. The media were refreshed daily. Additionally, collagenase type I solution (5 U/mL) was used to study the enzymatic degradation under the same conditions. At different time intervals, samples were taken from the bottles and washed with deionized water, then excess water was removed by the help of the filter paper, and the samples were freeze-dried for 20 h. Their dry weights were recorded. Their mass losses were calculated by using the equation below where mass loss, W_0 (initial dry weight), and W_t (dry weight at the specific time point of a sample) were used during calculations. Finally, percent cumulative weight loss of the hydrogels was plotted.

$$Mass\ Loss\ (\%) = \frac{W0 - Wt}{W0} \times 100$$

2.2.8.4   Equilibrium Water Content (ECW) and Swelling Measurements

For the ECW measurements, excess liquid on the hydrogels was removed gently with filter paper and wet weights were measured on days 1, 7, and 14. Hydrogels were then rinsed with d-H_2O, lyophilized and weighed. The EWC (amount of water absorbed per weight of the hydrogels × 100) was calculated based on the known equation where Ww and Wd denote wet weight and dry weight of a sample at a specific time point, respectively (Ishihara, Ueda, & Nakabayashi, 1990; Sirousazar, Kokabi, & Hassan, 2012). Moreover, equilibrium degree of weight swelling (EDWS) and equilibrium degree of volume swelling (EDVS) of samples were calculated by using the formulas where Ww, Wd, Vw, and Vd denote swollen weight, dry weight, swollen volume, and dry volume of a sample at a specific time point, respectively (Sirousazar et al., 2012).

$$EWC\ (\%) = \frac{Ww - Wd}{Ww + Wd} \times 100$$

$$EDWS\ (\%) = \frac{Ww - Wd}{Wd} \times 100$$

$$EDVS\ (\%) = \frac{Vw - Vd}{Vd} \times 100$$

2.2.8.5   Co-Release Study of Td and Rg1 from Td@HAH+Rg1@CSM

Td@HAH+Rg1@CSM samples prepared as previously described method in Section 2.2.7 (20 g of swollen weight in 50 mL of PBS) were incubated at 37°C to study the co-release of Td and Rg1 using the formulas given in the Sections 2.2.4.1 and 2.2.6.2. Briefly, aliquots from release media were collected at determined time points (1, 2, 3, 4, 5, 6, 12 h, 1, 2, and 3 d) and fresh PBS in the same volume of the aliquot (1 mL) was added. absorbance of samples was measured at 285 and 208 nm for Td and Rg1, respectively.

2.3   Cell Culture Studies for HA-Based Hydrogels

Human DPSC were cultured in a growth medium consisting of low-glucose DMEM (Dulbecco's Modified Eagle Medium, Gibco, Germany) supplemented with 10% FBS (Fetal Bovine Serum, Gibco, Germany) and 100 U/mL penicillin/streptomycin at 37°C in a humidified atmosphere of 95% air and 5% CO_2 (Thermo Fisher Scientific, U.S.A). HUVEC were cultured in a growth medium consisting of M199 (Gibco, Germany), 30 µg/mL endothelial cell growth supplement (ECGS) from bovine neural tissue (Sigma, U.S.A.), 10% FBS and 100 U/mL Penicillin/Streptomycin.

During odontogenic differentiation study, the growth medium of DPSC was changed with the odontogenic differentiation media (low-glucose DMEM, Gibco, Germany) supplemented with 10% FBS (Gibco, Germany) and 100 U/mL penicillin/streptomycin containing 0.2 mM ascorbic acid, 10 mM β-

glycerophosphate, and 100 nM dexamethasone after one day of incubation (Gong, Wang, Jiang, Lin, & Ling, 2012).

During angiogenic differentiation study for DPSC, the growth medium of DPSC was changed with Endothelial Cell Growth Medium-2 BulletKit CC-3162 (Lonza, Switzerland) (J. Xu et al., 2018) and refreshed once in every 3 days. These cell culture studies were conducted to measure angiogenic potential of DPSC under the exposure of hydrogels when injected in pulp cavity.

2.3.1   Isolation and Expansion of DPSC

Human two and third molars were collected with the patients' consents (19–23-year-old). The use of DPSC was approved by National Taiwan University Hospital (IRB No: 201103088RC). Extracted teeth were taken to the laboratory in containers full of PBS which were on ice. After cleaning the tooth with 70% alcohol and sterile distilled water, it was cut around the cementum-enamel junction by using sterilized diamond disc. Dental pulp was removed with a sterile dentinal excavator and cut into small pieces with sterilized scissors. Enzymatic digestion was done by incubating pulp tissue in a solution of collagenase type I (3 mg/mL) (Sigma, U.S.A.) and dispase (4 mg/mL) (Sigma, U.S.A.) for 60 min at 37°C. In order to stop the enzymatic digestion, DMEM (Dulbecco's Modified Eagle Medium, Gibco, Germany) supplemented with 15% FBS (Fetal Bovine Serum, Gibco, Germany) was added and DPSC isolated were collected by centrifugation at 1800 rpm for 5 min. Cells were washed twice with sterile PBS and centrifuged again for 5 min at 1800 rpm. Cells were then cultured in 10% FBS containing DMEM at 37°C in a carbon dioxide incubator (Atari et al., 2011).

2.3.2   Morphological Analyses

DPSC seeded on the hydrogels and cultivated in odontogenic differentiation medium were fixed on days 1, 7, and 14 with 4% para-formaldehyde for 2 h, and dehydrated

in a graded series of ethanol. The morphology of cells on the hydrogels was observed using SEM (TM-1000, Hitachi, Japan). Energy-dispersive X-ray spectroscopy (EDX) measurements were conducted for elemental analyses of the deposited minerals by the seeded DPSC via SEM-EDX machine (Hitachi S-4700 Type I, Japan). DPSC seeded on HAH+CSM that was previously injected into 24-well plates were cultivated for 7 days. Then, the cells were examined by the Fluorescence microscope (Leica DM IRB, Microscope Central, U.S.A.) via cellSence imaging software (Olympus, Japan). The dose dependent effect of free Td (10, 50, and 90 nM) and Td released from 10, 50, and 90 nM Td-loaded HAH placed in transwell plates on the morphology of DPSC was studied after one week of incubation. The morphology of DPSC was examined by optical microscopy and photographed (Nikon Eclipse Ti, Japan).

2.3.3   Cell Viability Tests

Cell analyses were conducted by using WST-1 Assay Kit (ScienCell Research Laboratories, U.S.A.) according to the manufacturer's instructions. Cells (2000 cells/well) were seeded into 96-well plates and exposed to different concentrations of BDDE (1/64 – 0.8 v/v% for DPSC for 1 day), Td (0 – 100 nM for DPSC for 1 day), Td (0 – 100 nM loaded into HAH for DPSC for 7 days), and Rg1 (0 – 90 μg/mL for DPSC and HUVEC for 1 day) in growth media to study their dose dependent effect on the cells and determine their optimum safe concentration. After the determination of optimum concentrations, the hydrogel groups listed in Table 2.2 were placed in transwell plates and cells (10^4 cells/well) were seeded into 24-well plates including the cell culture inserts. Next, WST-1 tests were performed at the specific time points (day 1, 4, and 7). Briefly, WST-1 dye was mixed with the cell culture medium at 1/10 ratio and cells were incubated with the prepared mixture for 4 h at 37°C in the dark. The solution was transferred to a new 96-well plate and their absorbance was measured at 450 nm. The same amount of WST-1/culture medium solution was added in an empty well as the blank solution. Cells (DPSC or HUVEC)

41

cultured in growth media only were used as the control group. Cell viability was calculated by using the equation below.

$$Cell\ Viability\ (\%) = \frac{OD\ of\ Test\ Well - OD\ of\ Blank}{OD\ of\ Control - OD\ of\ Blank} \times 100$$

Table 2.2 HA-based hydrogel groups used in the cell culture studies.

Group Name	Definition
Control	DPSC or HUVEC
HAH	Neat hydrogel
HAH+CSM	Neat hydrogel + Neat microspheres
Td@HAH+CSM	90 nM Td-loaded hydrogel + Neat microspheres
HAH+Rg1@CSM	Neat hydrogel + 50 µg/mL Rg1-loaded microspheres
Td@HAH+Rg1@CSM	90 nM Td-loaded hydrogel + 50 µg/mL Rg1-loaded microspheres

2.3.4   Live/Dead Staining

To understand the effect of Td concentration (10, 50, and 90 nM) on cells, DPSC in transwell plates (initial seeding density: 2000 cells/well) incubated with Td-loaded hydrogels for 7 days were fixed with 4% para-formaldehyde for 30 min. The samples were stained for 30 min with 4 µM of (green) calcein AM (Life Technologies Inc., CA, U.S.A.) for live cells, and with 4 µM of (red) propidium iodide (Life Technologies, Inc., U.S.A..) for dead cells. Live cells stained by calcein AM showed

green fluorescence (Ex/Em 495 nm/515 nm), whereas dead cells stained by PI showed red fluorescence (Ex/Em 540 nm/615 nm). Cells were examined by the Fluorescence microscope (Leica DM IRB, Microscope Central, U.S.A.) via cellSence imaging software (Olympus, Japan).

2.3.5   Confocal Laser Scanning Microscopy

For the examination of biomineralization, DPSC in transwell plates (initial seeding density: 1000 cells/well) incubated with Td-loaded hydrogels ([Td] = 10, 50, and 90 nM) for 14 days were fixed with 4% para-formaldehyde for 30 min. The cells were incubated with 20 µM xylenol orange (Sigma-Aldrich, U.S.A.) for 15 min, and counterstained with 1 µg/mL Hoechst 33342 (Sigma-Aldrich, U.S.A.) for 5 min, and observed by Confocal Laser Scanning Microscopy (Leica TCS SP5, Germany). The biomineralized area of the cell clusters displayed bright orange-red color (Ex/Em 440 nm/610 nm), whereas the nuclei were stained blue. The 3-dimensional images were reconstructed using Imaris x 64, 9.6.0 software (Oxford Instruments, U.K.).

DPSC and HUVEC were seeded on coverslips in a 24-well plate with an initial seeding density of 5×10^4 cells/well and incubated in the release media obtained from the previously defined HAH-based hydrogel groups for 7 days. The cells were fixed with 4% para-formaldehyde for 30 min. The samples were stained with DRAQ5 (Invitrogen, USA) for nuclei and fluorescein isothiocyanate (FITC) (Invitrogen, USA) for actin. Images were obtained using a confocal laser scanning microscope (CLSM) (Leica TCS SPE, Germany).

2.3.6   Gene Expression Studies

Odontogenic gene expression (DSPP, DMP1, Axin-2, ALP, COL1A1, and OCN) levels of DPSC seeded in 6-well plates at an initial seeding density of 5×10^5 cells/well was studied after incubating these cells in the release media obtained from the previously defined HAH-based hydrogel groups for 1 and 7 days (Table 2.2). At

the end of each incubation period, total RNA of the cells was extracted using TRIzol™ Reagent (Life Technologies, CA, U.S.A.) and Direct-zol™ RNA MiniPrep Kit (Zymo Research, U.S.A.). DPSC cultured in odontogenic differentiation medium were used as the control group. Total RNA was subjected to RT-PCR to generate complimentary DNAs. qRT-PCR was performed using KAPA SYBR® FAST One-Step Universal Kit (KAPA Biosystems Inc., Roche, Switzerland). The primers used are listed in Table 2.3. Agarose gel electrophoresis of DNA obtained from qPCR reaction products of GAPDH calibration study was conducted to double-check the reliability of the data (Appendix D1).

Angiogenic gene expression (VEGFA and eNOS) levels of DPSC seeded in 6-well plates at an initial seeding density of 2×10^5 cells/well was studied after incubating these cells in the release media obtained from the previously defined HAH-based hydrogel groups (Table 2.2) for 1 and 7 days. At the end of each incubation period, total RNA of the cells was extracted using High Pure RNA Isolation Kit (Roche Molecular Systems, Switzerland). Complimentary DNAs were generated using Revertaid First Strand cDNA Synthesis Kit (Thermo Fisher Scientific, U.S.A.). Then, qRT-PCR was performed using GoTaq® qPCR Master Mix (Promega Corporation, U.S.A.). The primers used are listed in Table 2.3. Angiogenic gene expression levels of HUVEC was studied by using the same protocol used for DPSC.

Table 2.3 Primer list of the genes used during the gene expression studies.

Genes	*Sequences from 5' to 3' ends*	
DSPP	Forward	CAACCATAGAGAAAGCAAACGCG
(Dentin	Reverse	TTTCTGTTGCCACTGCTGGGAC
sialophosphoprotein)		
DMP1	Forward	CAACTGGCTTTTCTGTGGCAA
(Dentin matrix protein 1)	Reverse	TGGGTGCGCTGATGTTTGCT
Axin-2	Forward	TAGGCGGAATGAAGATGGAC
(Axin-2 protein)	Reverse	CTGGTCACCCAACAAGGAGT

ALP	Forward	CCACAAGCCCGTGACAGA
(Alkaline phosphatase)	Reverse	GCGGCAGACTTTGGTTTC
COL1A1	Forward	GCCCTGTCTGCTTCCTGTA
(Collagen type I)	Reverse	TTTGGGTTGGTTGTCTGTTT
OCN	Forward	ACTGTGACGAGTTGGCTGAC
(Osteocalcin)	Reverse	CAAGGGCAAGAGGAAAGAAG
VEGFA	Forward	TCACCAAGGCCAGCACATAG
(Vascular endothelial	Reverse	CCGGATTTCTTTGCGCTTTC
growth factor-A)		
VEGFR2	Forward	CTCCCTGCCGTGTTGAAGAG
(Vascular endothelial	Reverse	TGAACCTCCCGCATTCAGTC
growth factor-Receptor 2)		
eNOS	Forward	GAAGGCGACAATCCTGTATGGC
(Endothelial nitric oxide	Reverse	TGTTCGAGGGACACCACGTCAT
synthase)		
GAPDH	Forward	ACAGTCAGCCGCATCTTCTT
(Housekeeping control)	Reverse	ACGACCAAATCCGTTGACTC

2.3.7   *In vitro* Angiogenesis Test on Matrigel

To evaluate the angiogenic potential of the Rg1-containing hydrogels, tube formation capacity of HUVEC was examined. Tube formation capacity of cells was assessed by using BD Matrigel™ Basement Membrane Matrix (BD Biosciences, U.S.A.) according to previously utilized method (Kayabolen et al., 2017; I.-H. Yang

et al., 2021). Briefly, Matrigel (50 µL) was added into into 96-well plate to coat the wells prior to the cell seeding. HUVEC (2000 cells/well) at passage 3 were seeded on Matrigel and cultured in 150 µL of media collected from the previously defined HAH-based hydrogel groups (Table 2.2) for 5 days. HUVEC cultured in the previously defined angiogenic differentiation media was used as the control group. Then, the cells were observed by microscopic examinations and photographed (Nikon Eclipse Ti, Japan). Tube length percentages of the samples were determined via ImageJ software (n=6) by setting the total tube length of the control group as 100% (Carpentier et al., 2020).

2.3.8 Fluorescence Microscopy

DPSC and HUVEC were seeded on coverslips in a 24-well plate with an initial seeding density of 5×10^4 cells/well and incubated in the release media obtained from the previously defined HAH-based hydrogel groups (Table 2.2) for 7 days. The cells were fixed with 4% para-formaldehyde for 30 min. The samples were stained with DRAQ5 (Invitrogen, USA) for nuclei and fluorescein isothiocyanate (FITC) (Invitrogen, USA) for actin. Fluorescence images were obtained to examine the morphology of the cells using a fluorescence microscope (Zeiss Axio Imager 2, Germany).

2.4 Preparation and Characterization of Methacrylated Gelatin (GelMA)-Based Hydrogels

GelMA-based hydrogel systems were prepared in order to enhance vital pulp regeneration by inducing proliferation and odontogenic differentiation of DPSC with the use of Td and Mel loaded into core (PMMA) and shell (SF) regions of electrospun fibers incorporated into the hydrogel part. Experimental groups constructed to test these hydrogels are given in Table 2.4.

Table 2.4 The GelMA-based hydrogel groups.

Group Name	Definition
Control	DPSC
GelMA	GelMA hydrogel
GelMA/PecTH	GelMA hydrogel + PecTH
GelMA/PecTH+PMMA/SF	Hydrogel + Electrospun fibers
GelMA/PecTH+Mel@PMMA/SF	Hydrogel + Mel-loaded PMMA / SF fibers
GelMA/PecTH+PMMA/Td@SF	Hydrogel + PMMA/Td-loaded SF fibers
GelMA/PecTH+Mel@PMMA/Td@SF	Hydrogel + Mel-loaded PMMA / Td-loaded SF fibers

2.4.1   Preparation of GelMA Hydrogels

Synthesis of GelMA (Figure 2.1) was achieved according to the previously described protocol (Nichol et al., 2010). Briefly, Type A porcine skin Gel was dissolved in PBS at 60°C to create a 10% (w/v) solution. Methacrylic anhydride (MA) was added to this Gel solution at a rate of 0.5 mL/min at 50°C to prepare 20 (w/v) % MA solution. The reaction was stopped after 1 h and 3 h (2 experimental groups) by 5X dilution with warm (40°C) PBS, and the solution was dialyzed against distilled water for 1 week at 40°C to remove the excess methacrylic acid and salts. Distilled water

was changed once in a day. The solution was lyophilized for 1 week to generate a white porous foam and stored at −80°C until further use.

After optimization studies, 10 (w/v) % solutions of GelMA in PBS containing 0.5 (w/v) % photoinitiator (Irgacure 2959) were poured into 24-well plates and exposed to UV light (365 nm, 0.120 J/cm^2) for 1 min in a dark hood. After 1 min, the reverse side of the hydrogel was exposed to UV for 1 min.
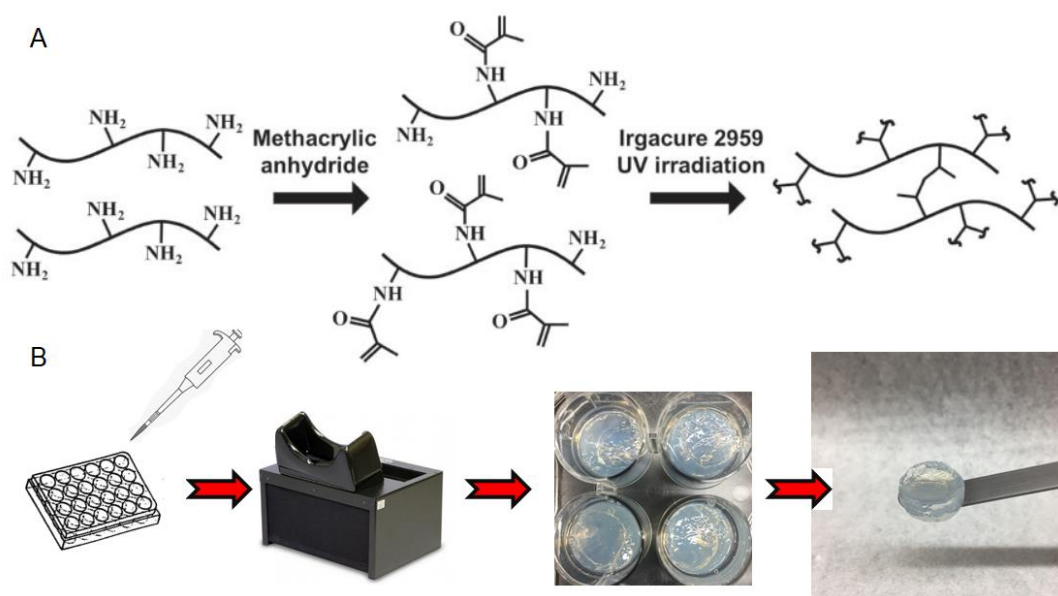
Figure 2.1 Schematic representation of GelMA synthesis and formation of GelMA hydrogel after UV exposure (A) (J. Jung & Oh, 2014) and illustration of experimental steps for crosslinking of GelMA (B).

2.4.2 Characterization of GelMA

2.4.2.1 Proton Nuclear Magnetic Resonance (^{1}H-NMR) Spectroscopy

Gel and GelMA polymers before hydrogel formation were dissolved in d-H_2O (20 mg/mL) at 40°C. ^{1}H-NMR spectra were obtained with a Bruker Biospin spectrometer (Bruker AVANCE, U.S.A.) operating at a ^{1}H resonance frequency of

300 MHz. Sixteen scans were made for signal-to-noise averaging. Degree of methacrylation was calculated by integrating the area under the lysine methylene signals of Gel and Gel-MA spectra according to the previously established method (Hoch, Schuh, Hirth, Tovar, & Borchers, 2012).

$$MoD\ (\%) = \left(1 - \frac{Area\ (lysine\ methylene\ of\ GelMA)}{Area\ (lysine\ methylene\ of\ Gel)}\right) \times 100$$

2.4.3   Preparation of Thiolated Pectin (PecTH)

Synthesis of PecTH (Figure 2.2) was done according to the previously described protocol (R. Sharma & Ahuja, 2011). It was synthesized by the esterification of Pec with thioglycolic acid in the presence of hydrochloric acid. The reaction was carried out with 2 moles of thioglycolic acid for every 1 mole of hydroxyl group in Pec (Dicharry et al., 2006). Pec (16 g) was dissolved in 70 mL of hot water and 7.59 g of 80% thioglycolic acid and 2 mL of 7 N HCl were then added. These were allowed to react for 150 min at 80°C. The reaction mixture was poured in 500 mL of methanol. White precipitates of PecTH obtained were washed twice with methanol and dried at RT.
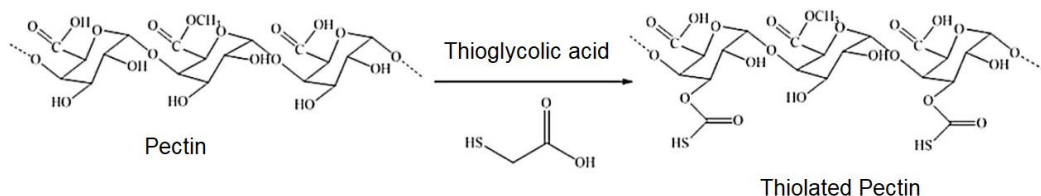
Figure 2.2 Schematic representation of thiolation of Pec (Cheewatanakornkool, Niratisai, Manchun, Dass, & Sriamornsak, 2017).

2.4.4 Characterization of PecTH

2.4.4.1 Fourier Transform Infrared (FTIR) Spectroscopy

FTIR analysis was also performed to verify the specific peaks of Pec and PecTH as KBr pellets via a spectrometer of PerkinElmer L1050002 series (PerkinElmer, Inc., UK) using spectrum 100/100N software program in transmission mode. The analysis was performed within the wavelength range 400–4000 cm^{-1}, with a resolution of 4 cm^{-1}, and a total of 50 scans per sample were done. The spectra of all samples were corrected with respect to background and atmosphere inside the FTIR device.

2.4.5 Preparation of PMMA/SF Core/Shell Fibers

2.4.5.1 Isolation of SF

SF isolation from cocoons of *Bombyx mori* was performed as described previously (Rockwood et al., 2011). Briefly, cocoons were cut into small pieces and boiled with 0.02 M Na_2CO_3 for 30 min and washed with deionized water several times for 60 min to remove the glue-like sericin proteins from the silk fibers. Degummed silk fibers were then dried overnight at 37°C. Dried fibers were dissolved in 9.3 M LiBr at 60°C for 4 h and was dialyzed against deionized water for 48 h with several water changes to remove the lithium bromide. Final concentration of the SF solution was about 8-9% (w/v), which was determined gravimetrically after drying SF solution at 60°C.

2.4.5.2 Coaxial Electrospinning of PMMA/SF Fibers

During the optimization studies, PMMA and SF fibers were electrospun separetaly by conventional electrospinning methods and the effect of parameter alterations on fiber formation was assessed (e.g. flow rate, electrical voltage, collector type and/or

distance, and polymer concentration). After smooth fibers were obtained, coaxial electrospinning of PMMA/SF core/shell fibers was optimized. Electrospinning set-up was composed of NE-1000 syringe pump (New Era Pump Systems, Inc., New York, USA), Gamma High Voltage Source ES30 (Gamma High Voltage Research, Inc., Florida, USA), and a static metal collector. Coaxial electrospinning of the PMMA and SF solutions was performed by using a bicomponent apparatus consisting of a combined two-syringe-system one in other (Figure 2.3). This enabled the PMMA solution to flow through the inner path while the SF solution could flow from the outer region surrounding the inner tube. Thus, core-shell (PMMA/SF) structures were obtained in fibrous form. After optimization studies, coaxial electrospinning was applied with the parameters of 3 and 1 mL/h of flow rates for SF (9 w/v %) and PMMA (15 w/v %) solutions, respectively. The other parameters were set to 13 cm of nozzle-to-bath distance and 20 kV of electric potential difference. Then, PMMA/SF fibrous mats were obtained. Finally, mats were immersed in methanol for 2 h at RT in order to trigger crosslinking of SF surface of the fibers.
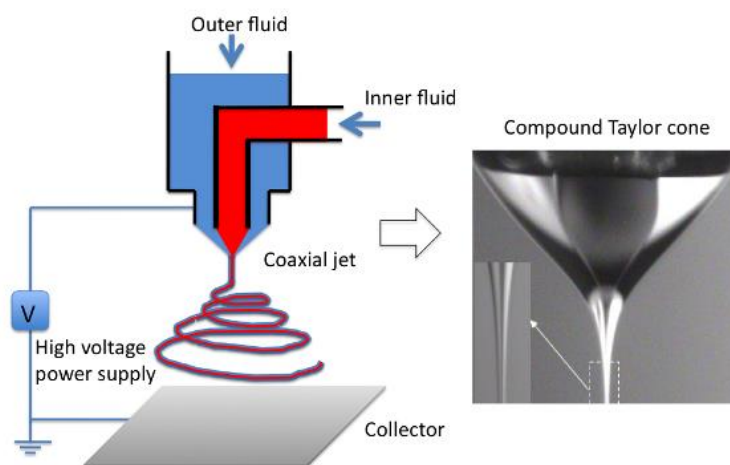
Figure 2.3 Illustration of coaxial electrospinning set-up (F. Li et al., 2010).

2.4.5.3   Preparation of Mel-Loaded PMMA and Td-Loaded SF Fibers

Coaxial electrospinning of the PMMA and SF solutions containing Mel and Td, respectively were performed and removed from the dry collector. PMMA solution was loaded with different concentrations of Mel (10, 30, 50, and 70 µg/mL). SF solution was loaded with different concentrations of Td (100, 200, 300, and 400 nM). The fibers in PMMA/SF meshes was tried to be lowered in size using different methods to create hydrogels containing homogenously distributed fibers so that it can be injectable. Firstly, mats were pulverized by cryo-mill (Retsch, Germany) for 30 s with 3 cycles. Secondly, fiber suspensions in PBS were homogenized with a homogenizator device (Ultraturrax T-25, IKA, Germany) at 12000 rpm for 2 min with 2 cycles. The size of the mats were also tried to be made smaller by cutting with scissors into size of 5 mm × 1 mm. Next, the cut fibers were blended with the hydrogels by using a blender which will be explained in the final hydrogel preparation.

2.4.6   Characterization of PMMA/SF Core/Shell Fibers

2.4.6.1   X-Ray Photoelectron Spectroscopy (XPS)

XPS analyses were conducted to study the chemical composition on the surface of neat SF, neat PMMA, and PMMA/SF coaxially electrospun samples by using PHI 5000 VersaProbe scanning XPS system (Ulvac-phi, Inc., Japan). Besides the neat forms, two types of mats, that were coaxially electrospun with the flow rate ratios of 2/1 and 3/1, were compared with this technique to detect whether PMMA and SF were present at the same spot of PMMA/SF. Otherwise, it could be interpreted that phase separation might occur between PMMA and SF which might be a sign of improper coaxial electrospinning of PMMA/SF.

2.4.6.2 Thermo-Gravimetric Analyses (TGA)

Thermal properties of neat SF, neat PMMA, and PMMA/SF coaxially electrospun samples were studied by TGA by heating the samples from RT up to 1000°C at a heating rate of 20°C/min under air atmosphere (PerkinElmer Pyris 1, PerkinElmer Inc., UK).

2.4.6.3 Scanning Electron Microscopy (SEM)

Morphology of the fibers and hydrogels was investigated by nano SEM device (FEI, Nova Nano SEM 430, U.S.A.) and by mini SEM device (Nano Eye, Portland, U.S.A.). Prior to SEM examination, the samples were coated with ultrafine (10 nm) gold layer by precision etching coating system (682 PECS, Gatan, Inc., U.S.A.). Diameter size distribution histograms of SF, PMMA, and PMMA/SF fibers were constructed over 300 measurements obtained from SEM images via ImageJ software.

2.4.6.4 Mechanical Tests

Tensile properties of electrospun neat SF, neat PMMA, and PMMA/SF mats in dry state were evaluated using uniaxial tensile testing method (Univert, Cellscale, Canada) using 10 N load cell and speed of 1 mm/min at room temperature. The samples were cut into rectangular samples (20 mm × 5 mm) (n=4) with a gauge length of 10 mm and average values of the data were reported with standard deviation (±SD). Ultimate tensile strength, percent strain, and tensile modulus of the samples were calculated.

2.4.6.5 *In situ* Degradation in PBS and Enzymatic Degradation

The electrospun meshes were incubated in 3 mL of phosphate-buffered saline (PBS, pH 7.2, 0.1 M) at 37°C. Then, the samples were removed from the liquid environment and freeze-dried at specific time points. Their mass losses were calculated by using the equation given in the Section 2.2.8.3. The degradation profile of scaffolds (n=3) was further studied by utilizing 1 mg/mL lysozyme from chicken egg white (L6876, Sigma) and lipase from porcine pancreas (L3126, Sigma) at 37°C in a CO_2 incubator (Panasonic Healthcare Co., Ltd., Japan). Samples of (4 mm x 4 mm) scaffolds were immersed in 4 mL of the solution for 1, 7, and 14 d. At defined time points, scaffolds were carefully removed, washed several times with PBS, and freeze-dried.

2.4.6.6 Water Uptake Capacity

For water uptake capacity measurements, the electrospun meshes were incubated in 3 mL of phosphate-buffered saline (PBS, 0.1 M, pH 7.2) at 37°C. Dry and wet weights of electrospun meshes were measured on days 1, 7, and 14 besides their initial weights. The meshes were then rinsed with d-H_2O, lyophilized and weighed. Their water uptake capacity was calculated based on the known equation below, where W_W and W_D stand for wet and dry weights of the sample, respectively

$$Water\ Uptake\ (\%) = \frac{W_W - W_D}{W_D} x\ 100$$

2.4.6.7 Td Release from the Core/Shell Fibers

Td-loaded electrospun mats (10 mm x 6 mm rolled up in 2 mL of PBS) were incubated at 37°C. Aliquots from release media were collected at determined time points (1, 2, 3, 4, 5, 6, 12 h, 1, 2, 3, 6, 12, 18, 24, and 30 d) and fresh PBS in same volume of the aliquot was added. The absorbance of samples was measured at 285

nm via Nanodrop spectrophotometer (NanoDrop 2000c, Thermo Fisher Scientific, U.S.A.) in the UV-Vis mode. The standard curve was constructed using different concentrations of Td within the interval of 2.25 156.25 μM (Appendix B1). Percent Td release was calculated by using the formula as described in the Section 2.2.4.1.

2.4.6.8 Mel Release from the Core/Shell Fibers

Mel-loaded electrospun mats (10 mm x 6 mm rolled up) were incubated in PBS (2 mL) at 37°C. Aliquots from release media were collected at determined time points (1, 2, 3, 4, 5, 6, 12 h, 1, 2, 3, 6, 12, 18, 24, and 30 d) and fresh PBS in same volume of the aliquot was added. The absorbance of the aliquots was measured at 222 nm via UV spectrophotometry (UV-VIS U2800 Hitachi, Japan). A standard curve was constructed using different concentrations of Mel (0 and 125 μg/mL) in PBS and methanol to determine the amount of Mel released into the release media (Appendix E). Percent Mel release was calculated by using the formula below.

$$Mel\ Release\ (\%) = \frac{Amount\ of\ Mel\ Released}{Initial\ Mel\ Amount\ Loaded} \times 100$$

2.4.7 Preparation of the Final Hydrogel (GelMA/PecTH+PMMA/SF)

Previously sized PMMA/SF electrospun mats were immersed in PecTH solution (8%) containing $CaCl_2$ (1%). The prepared PecTH+PMMA/SF was sterilized by UV exposure for 20 min in a laminar flow hood. Next, GelMA component was poured into 24-well plates and crosslinked by UV as described in the Section 2.4.1 and autoclaved. The autoclaved GelMA hydrogel and the previously prepared PecTH+PMMA/SF mixture were mixed to obtain a hydrogel composition of GelMA/PecTH (w/w) with the ratio of 10/1. Finally, GelMA/PecTH+PMMA/SF hydrogel systems were pulverized together for 10 min using Luxell Blender (LX-9310, Turkey) in order to generate an injectable form of the hydrogels.

2.4.8 Characterization of the Final Hydrogel (GelMA/PecTH+PMMA/SF)

2.4.8.1 Td Release from GelMA/PecTH+PMMA/Td@SF

Td release from the GelMA/PecTH+PMMA/Td@SF hydrogels (20 g of swollen hydrogel in 50 mL of PBS) was studied by incubating the hydrogels at 37°C. Aliquots from release media were collected at determined time points (1, 2, 3, 4, 5, 6, 12 h, 1, 2, 3, 6, 12, 18, 24, and 30 d) and fresh PBS in the same volume of the aliquot (1 mL) was added. The absorbance of aliquots was measured and calculated as described in the Section 2.2.4.1.

2.4.8.2 Mel Release from GelMA/PecTH+Mel@PMMA/SF

Mel release from the GelMA/PecTH+Mel@PMMA/SF hydrogels (20 g of swollen weight in 50 mL of PBS) was studied by incubating the hydrogels at 37°C. Aliquots from release media were collected at determined time points (1, 2, 3, 4, 5, 6, 12 h, 1, 2, 3, 6, 12, 18, 24, and 30 d) and fresh PBS in the same volume of the aliquot (1 mL) was added. The absorbance of samples was measured and calculated as described in the Section 2.4.6.7.

2.4.8.3 *In situ* Degradation in PBS and Enzymatic Degradation

The hydrogels were incubated in 5 mL of phosphate-buffered saline (PBS, 0.1 M, pH 7.2) at 37°C. Then, the samples were removed from the liquid environment and freeze-dried at specific time points. The degradation profile of scaffolds (n=3) was further studied by utilizing 1 mg/mL lysozyme from chicken egg white (L6876, Sigma) at 37°C in a CO_2 incubator (Panasonic Healthcare Co., Ltd., Japan). Samples of (4 mm x 4 mm) scaffolds were immersed in 4 mL of the solution for 1, 3, 6, 12, 18, and 24 h. At defined time points, scaffolds were carefully removed, washed

several times with PBS, and freeze-dried. Their mass losses were calculated by using the equation given in the Section 2.2.8.3.

2.4.8.4 Water Uptake Capacity

For water uptake capacity measurements, the hydrogels were incubated in 5 mL of phosphate-buffered saline (PBS, pH 7.2, 0.1 M) at 37°C. Dry and wet weights of the hydrogels were measured on days 1, 7, and 14 besides their initial weights. The meshes were then rinsed with d-H_2O, lyophilized and weighed. Their water retention capacity was calculated based on the equation given in the Section 2.4.6.6.

2.5 Cell Culture Studies for GelMA-Based Hydrogels

Human DPSC were cultured in a growth medium consisting of low-glucose DMEM (Dulbecco's Modified Eagle Medium, Gibco, Germany) supplemented with 10% FBS (Fetal Bovine Serum, Gibco, Germany) and 100 U/mL penicillin/streptomycin at 37°C in a humidified atmosphere of 95% air and 5% CO_2 (Thermo Fisher Scientific, U.S.A).

2.5.1 Isolation and Expansion of DPSC

DPSC were isolated as described in the Section 2.3.1. Human two and third molars were collected with the patients' consents (21–24-year-old) under the guidelines approved by the Ethic Committee of Middle East Technical University.

2.5.2 Morphological Analyses

Morphology of DPSC on the electrospun mats was examined with SEM (Quanta 200 FEG, Netherlands) after 7 days. At the end of each period, cells were fixed in 4% paraformaldehyde solution in PBS and washed with PBS, then dehydrated with

increasing ethanol concentration series (20–100%), and hexamethyldisilazane for 20 min prior to storage in desiccator. Before SEM analysis, scaffolds were coated with ultrafine (10 nm) gold layer by precision etching coating system (682 PECS, Gatan, Inc., USA) and then imaged via micro- and nanoscanning electron microscopy (FEI, Nova Nano SEM 430, U.S.A.).

2.5.3 Cell Viability Tests

Alamar Blue cell viability assay (Invitrogen, USA) was conducted to study the attachment and proliferation of DPSC on the electrospun fibers and the hydrogels groups (Table 2.5) at specific time points. After ethanol (70%, 2 h) and UV (30 min) sterilization, the samples (n=4) were placed in 24-well-plates and their extraction media were collected. DPSC seeded at an initial seeding density of 25×10^3/well were cultured in a growth medium, DMEM (Dulbecco's Modified Eagle Medium, Gibco, Germany) supplemented with 10% FBS (Fetal Bovine Serum, Gibco, Germany) and 100 U penicillin/streptomycin at 37°C in a humidified atmosphere of 95% air and 5% CO_2 (5215 Shel Lab., Cornelius, OR, USA). The media were refreshed with the collected release media 1 day after the initial cell seeding. Alamar Blue assay was performed after 1, 4, and 7 days of incubation according to the manufacturer's instructions. The results are presented as % reduction using the formula below. The wells containing only media and scaffolds without cells served as controls and viability of cells on meshes were expressed as percent reduction. Increase in cell viability was interpreted as cell proliferation.

$$Alamar\ Blue\ Reduction\ (\%)$$
$$= \frac{(\varepsilon_{ox})\lambda_2 A\lambda_1 - (\varepsilon_{ox})\lambda_1 A\lambda_2\ of\ test\ dilution}{(\varepsilon_{red})\lambda_1 A'\lambda_2 - (\varepsilon_{ox})\lambda_2 A'\lambda_1\ of\ untreated\ positive\ control}$$
$$\times 100$$

ε_{ox}; Molar extinction coefficient of Alamar Blue oxidized form (blue)

ε_{red}; Molar extinction coefficient of Alamar Blue reduced form (red)

A; Absorbance of test well

A'; Absorbance of negative control well

(The negative control well contained media + Alamar Blue without cells.)

λ_1; 570nm

λ_2; 600nm

Table 2.5 GelMA-based hydrogel groups used in the cell culture studies.

Group Name	Definition
Control	DPSC
GelMA	10% GelMA
GelMA/PecTH	10% GelMA + 1% PecTH
GelMA/PecTH+PMMA/SF	Hydrogel + 1% Electrospun fibers
GelMA/PecTH+Mel@PMMA/SF	Hydrogel + 50 µg/mL Mel-loaded PMMA/SF fibers
GelMA/PecTH+PMMA/Td@SF	Hydrogel + PMMA/ 200 nM Td-loaded SF fibers
GelMA/PecTH+Mel@PMMA/Td@SF	Hydrogel + 50 µg/mL Mel-loaded PMMA/200 nM Td-loaded SF fibers

2.5.4 Alkaline Phosphatase (ALP) Enzyme Activity Test

Odontogenic differentiation level of DPSC treated with GelMA-based hydrogel groups (Table 2.6) was tested by measuring the ALP enzyme activity of cells since ALP is a biomarker of osteo/odontogenic differentiation of cells (Tang, Chen, He, & Ma, 2019). During the preliminary studies, ALP activity of DPSC treated with culture media containing different concentrations of Mel was measured to determine which concentration of Mel that should be released from Mel-loaded hydrogel samples to induce odontogenic differentiation of DPSC in pulp tissue. Moreover, the effect of different loading ratios of Mel/Td (i.e. 3/1, 1/1, and 1/3) into PMMA/SF core/shell fibers on ALP activity of DPSC was studied by culturing the cells in the release media collected from hydrogels (Table 2.6). DPSC at passage-4 were seeded on 96-well-plates at an initial density of 1000 cells/well during these studies. ALP activity of DPSC was measured after 7 and 14 days of incubation.

Table 2.6 GelMA-based hydrogel groups used in the preliminary ALP activity tests.

Group Name	Mel/Td Ratio
GelMA	-
GelMA/PecTH	-
GelMA+PMMA/SF	-
GelMA/PecTH+PMMA/SF	-
GelMA+PMMA/SF with Mel/Td : 3/1	3/1
GelMA/PecTH+PMMA/SF with Mel/Td : 3/1	3/1
GelMA+PMMA/SF with Mel/Td : 1/1	1/1

GelMA/PecTH+PMMA/SF with Mel/Td : 1/1	1/1
GelMA+PMMA/SF with Mel/Td : 1/3	1/3
GelMA/PecTH+PMMA/SF with Mel/Td : 1/3	1/3

Briefly, the standard cell culture medium was changed with odontogenic differentiation medium a day after cell seeding. ALP activity of cells incubated in the released media obtained from the hydrogel groups was measured after 7 and 14 days of incubation. In order to obtain cell lysates, media were removed and membranes were placed at -80°C for 10 min followed by 10 min incubation at 37°C. The same steps were repeated after adding PBS on the membranes. 75 µl of p-nitrophenyl phosphate (pNPP) substrate solution and 25 µl of $MgCl_2$ (10 mM) solution were added to 75 µl of the lysate in a 96 well-plate, and were incubated at 37°C while shaking at 150 rpm for 1 h. A calibration curve was constructed using pNPP to measure the ALP activity of cells (Appendix F1). Absorbance measurements were done with a plate reader (µOuantTM microplate spectrophotometer, Biotek Instruments Inc., USA) at 405 nm. Protein contents of the lysates were determined with the calibration curve obtained with bovine serum albumin (BSA) via bicinchoninic acid (BCA) assay according to the manufacturer's instructions (Appendix G1). The enzyme activity of cells was given in terms of specific enzyme activity (nmol/µg protein/min) (Toker, Tezcaner, & Evis, 2011).

2.5.5 Fluorescence Microscopy

DPSC and HUVEC were seeded on coverslips with an initial seeding density of 5×10^4 cells/well which were then placed in a well of 24-well plate and incubated in the release media obtained from the previously defined GelMA-based hydrogel groups (Table 2.2) for 7 days. The cells were then fixed with 4% para-formaldehyde for 30 min. The samples were stained with DRAQ5 (Invitrogen, USA) for nuclei and fluorescein isothiocyanate (FITC) (Invitrogen, USA) for actin. Fluorescence images

were obtained to examine the morphology of the cells using a fluorescence microscope (Zeiss Axio Imager 2, Germany).

2.5.6   Gene Expression Studies

To determine gene expression levels of cells seeded in 6-well plates with the initial seeding density of 15×10^4 cells/well, DPSC were incubated in the release media obtained from the previously defined GelMA-based hydrogel groups (Table 2.5). Total RNA of cells was isolated using High Pure RNA Isolation Kit (Roche Molecular Systems, Switzerland). Complimentary DNAs were generated using Revertaid First Strand cDNA Synthesis Kit (Thermo Fisher Scientific, U.S.A.). Then, qRT-PCR was performed using GoTaq® qPCR Master Mix (Promega Corporation, U.S.A.). The primers used are listed in Table 2.3.

2.6   Statistical Analyses

All experiments were conducted in quadruplet replicates (n=4). One-way analyses of variance (ANOVA) and post hoc Tukey tests for multiple comparisons were done to assess the statistical significance of the results using SPSS Statistics and the difference was considered statistically significant at $p < 0.05$.

CHAPTER 3

RESULTS AND DISCUSSIONS

3.1 HA-Based Hydrogels

3.1.1 Material Characterizations of HA-Based Hydrogels

During HAH preparetion by using BDDE, HA and BDDE concentrations are determinative factors to tune viscoelastic properties of the hydrogel. BDDE concentrations to crosslink HA (10 wt% solutions) varied from 0.4 to 1.0 (v/v)% in a previous report (R. Yang et al., 2016). In our study, 0.6 (v/v)% of BDDE was chosen to crosslink HA (14 wt% solutions) by considering the toxicity of BDDE and stiffness level of hydrogel that should be match with pulp tissue. BDDE was found cytotoxic above 100 μm/mL concentrations for normal keratinocyte cell line and human dermal fibroblast cell line (Jeong et al., 2021). Moreover, HA gel crosslinked by BDDE caused alterations in cell morphology and negative influence on cell viability in mouse fibroblasts at 0.5 mg/mL concentration (Xue et al., 2020). Therefore, an injectable HAH was aimed to be constructed possesing suitable mechanical properties for dental pulp by using an adaquate amount of BDDE in our study, while BDDE was intended to completely be removed from HAH after proper crosslinking. These properties of HAH was characterized in the following sections.

3.1.1.1 Crosslinking Confirmation of HA

HA was crosslinked by BDDE to prepare HAH. Functional groups of BDDE and HA taking role in crosslinking are namely (i) the ether groups at the edges of BDDE shown in dashed circles and (ii) the attacked O–H groups of HA where the bond formation occurs (Figure 3.1A). FTIR (Figure 3.1B) and ^{1}H-NMR spectra (Figure

3.2) of HA and HAH confirmed the crosslinking of the hydrogels by BDDE. Area under all the specific bands at 3343 cm^{-1}, 2900 cm^{-1}, 1300 cm^{-1} increased in the HAH spectrum (Figure 3.1B), which were assigned to O–H stretching, C–H stretching, and ether linkage, respectively (Al-Sibani et al., 2016). The first broad band seen in the HAH spectrum at 3343 cm^{-1} might be related with the moisture holding capacity of HAH which was superior to that of HA powder (Scatena, Brown, & Richmond, 2001) due to the interconnected network structure of HAH. Moreover, additional O–H groups of BDDE incorporated into the hydrogel structure contributed to this band at 3343 cm^{-1}. The area under the other specified bands increased in the HAH spectrum which confirmed newly emerged C–H bonds at the crosslinking sites of HA and newly formed C–O–C (ether) bonds at crosslinking sites of BDDE (Figure 3.1 A&B).
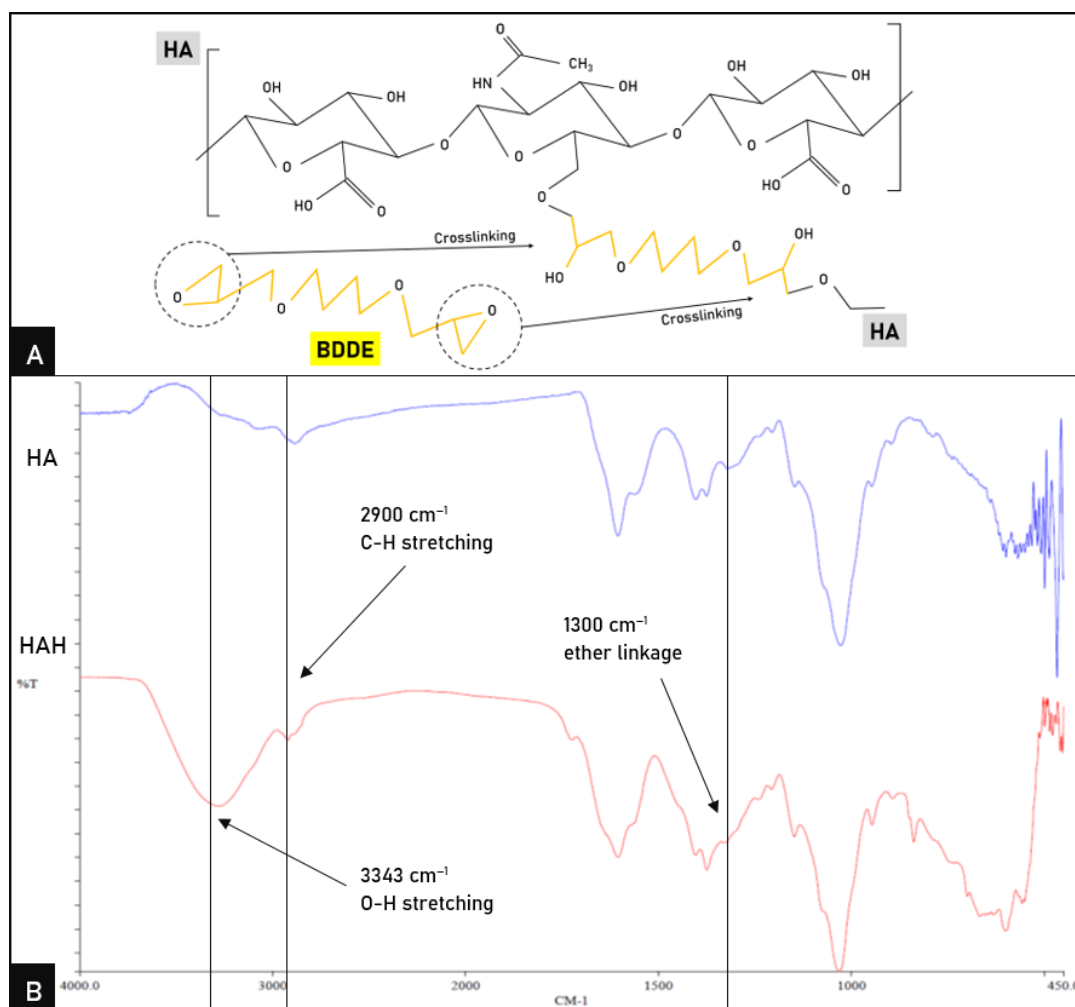
Figure 3.1 Chemical structures of HA, BDDE, and crosslinking sites (A) and FTIR spectra of HA and HAH (B).

The degree of modification (MoD) of HAH was determined using the characteristic peaks formed for cross-linked HA at 1.66 and 2.05 ppm (Wende et al., 2017) in the ^{1}H-NMR spectrum of HAH (Figure 3.2). The MoD value was calculated as 27.32% which demonstrated that the crosslinking efficiency was comparable to the BDDE-crosslinked HA hydrogels previously reported in the literature (Wende et al., 2017).
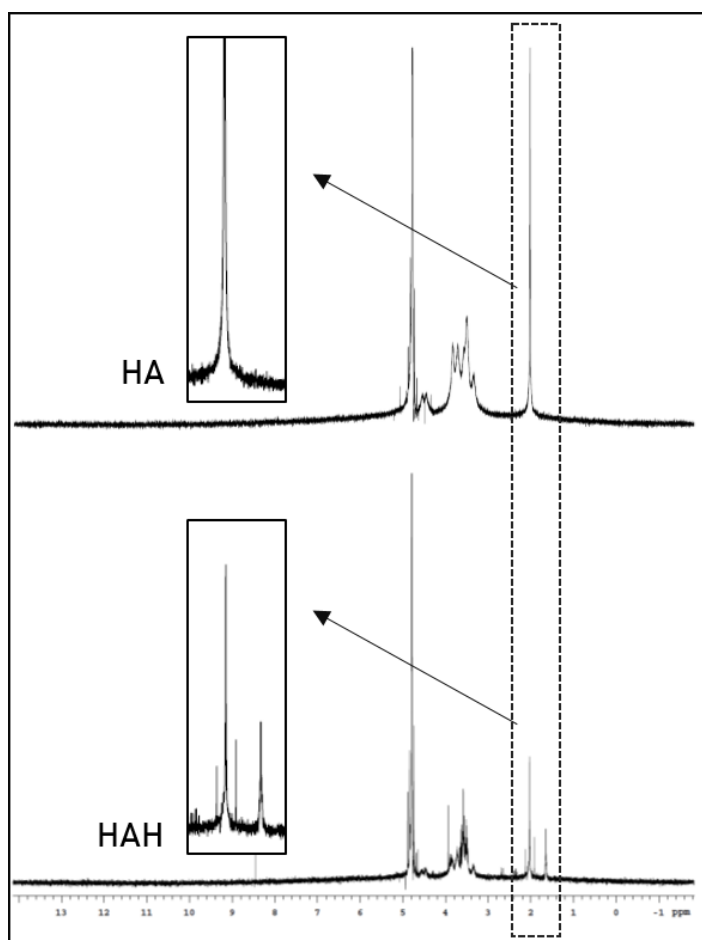
Figure 3.2 ^{1}H-NMR spectra of HA and HAH (Arrows represent the specific bands and peaks of HA before and after crosslinking, respectively).

3.1.1.2   Confirmation of BDDE Removal

Generally, crosslinkers including BDDE can have toxic effects and unreacted crosslinkers should be removed to minimize toxic effect to protect the cells and the surrounding tissue (Jeong et al., 2021). Therefore, BDDE removal was monitored. Initial burst release of BDDE from the hydrogels was observed in the first 6 h (Figure 3.3). Almost all BDDE content (97.98%) was released from HAH after 24 h. The amount of BDDE residues in HAH measured was within the non-toxic range for DPSC according to the cytotoxicity study conducted (Figure 3.12). Therefore, HAH was ready for use after 1-day of incubation in water, which in turn eases and shortens

the preparation process concerning time and cost-effectiveness of the product (L. A. Sharma & Love, 2019).
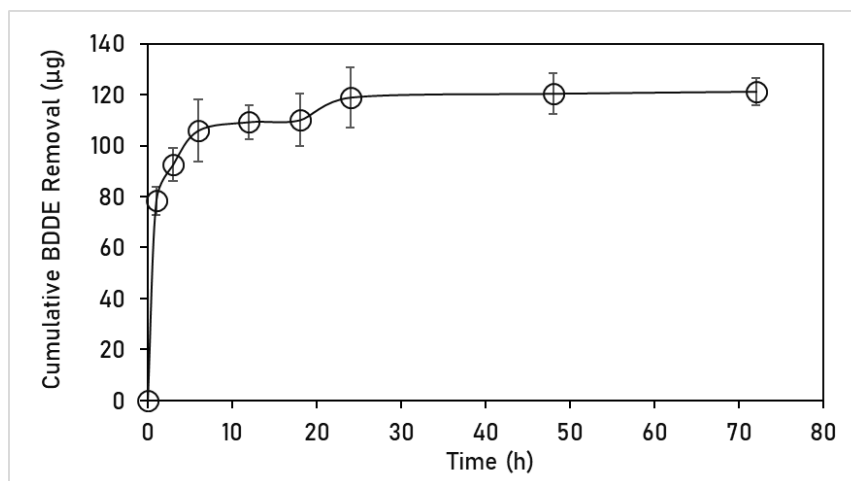
Figure 3.3 Cumulative BDDE removal profile from HAH in PBS (0.1 M, pH 7.2) at RT (n=4).

3.1.1.3 Rheological Analyses of HAH and HAH+CSM

Rheological analyses revealed that G' and G'' values of HAH were higher than that of HAH+CSM (Figure 3.4A) until the oscillation strain reached to 10%. The G' values of HAH (135-466 Pa) and HAH+CSM (165-372 Pa) were slightly higher than that of native pulp tissue (~110 Pa) obtained from the mandibular canine of a 28-month-old miniature pig within the interval of 1-10% of oscillation strain (Erisken, Kalyon, Zhou, Kim, & Mao, 2015). Similarly, the G'' values of HAH (104-155 Pa) and HAH+CSM (55-109 Pa) were 2-3 fold higher than the native tissue counterparts (~40 Pa) (Erisken et al., 2015). Hence, both moduli were suitable for implantation since they can be considered as favorable to sustain cell migration soon after implantation and also eventual biodegradation will lead to a decline in G' and G'' by time.

Moreover, CSM addition caused a decrease in the viscosity of HAH below 80°C, although both exhibited similar trend above this temperature (Figure 3.4B).

Viscosities of HAH (28.3 Pa.s) and HAH+CSM (21.9 Pa.s) at body temperature were similar with the CS hydrogels prepared as an injectable formulation for drug delivery purposes (Dang et al., 2016).
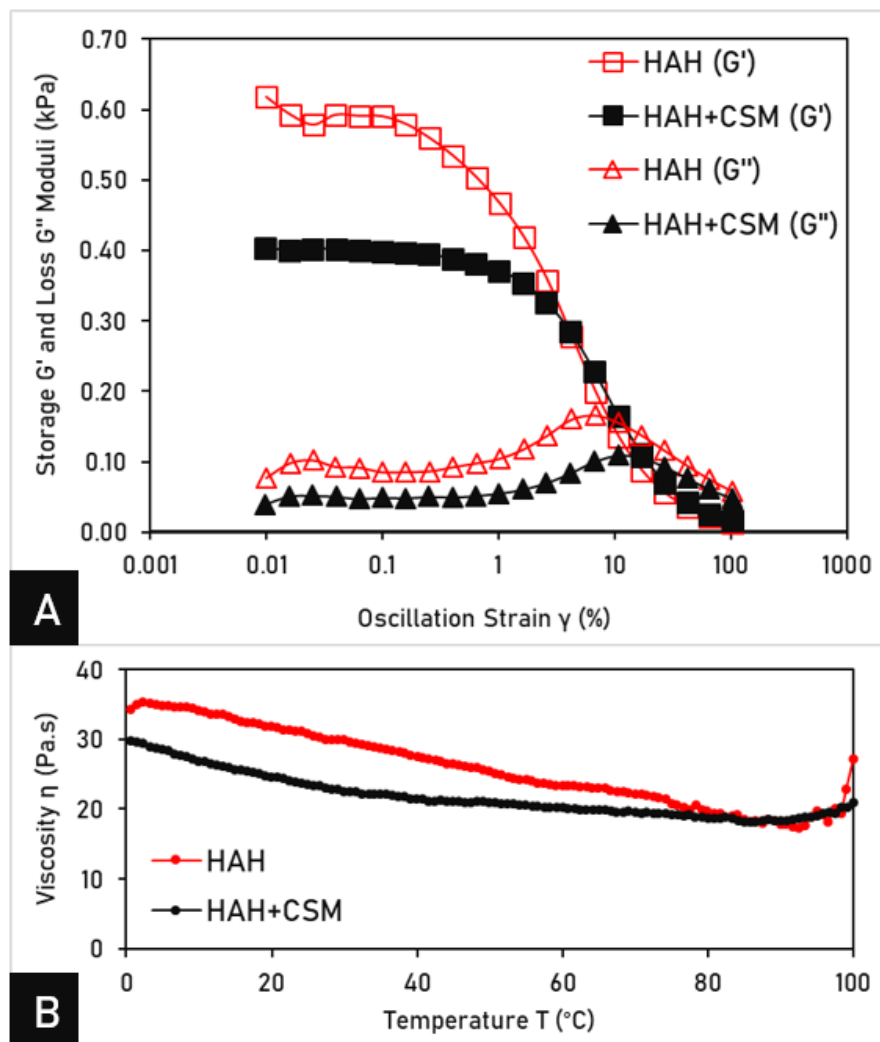
Figure 3.4 Rheological properties of HAH and HAH+CSM with respect to G' and G'' (A) and viscosity measurements (B).

3.1.1.4   Morphological Analyses of HAH and CSM

HAH turned into yellowish color after crosslinking with BDDE (Figure 3.5A). However, they became colorless and transparent after BDDE-removal and autoclave

steps (Figure 3.5B). The disappearance of yellow color of the hydrogels after autoclaving also confirmed the BDDE removal. Macroscopic image of the dry CSM in its powder form is given (Figure 3.5C). The CSM were homogeneously distributed in HAH after injection (Figure 3.5D). Furthermore, injectability of the hydrogels did not change after the incorporation of CSM due to their roundness and tininess (Prasad et al., 2014).
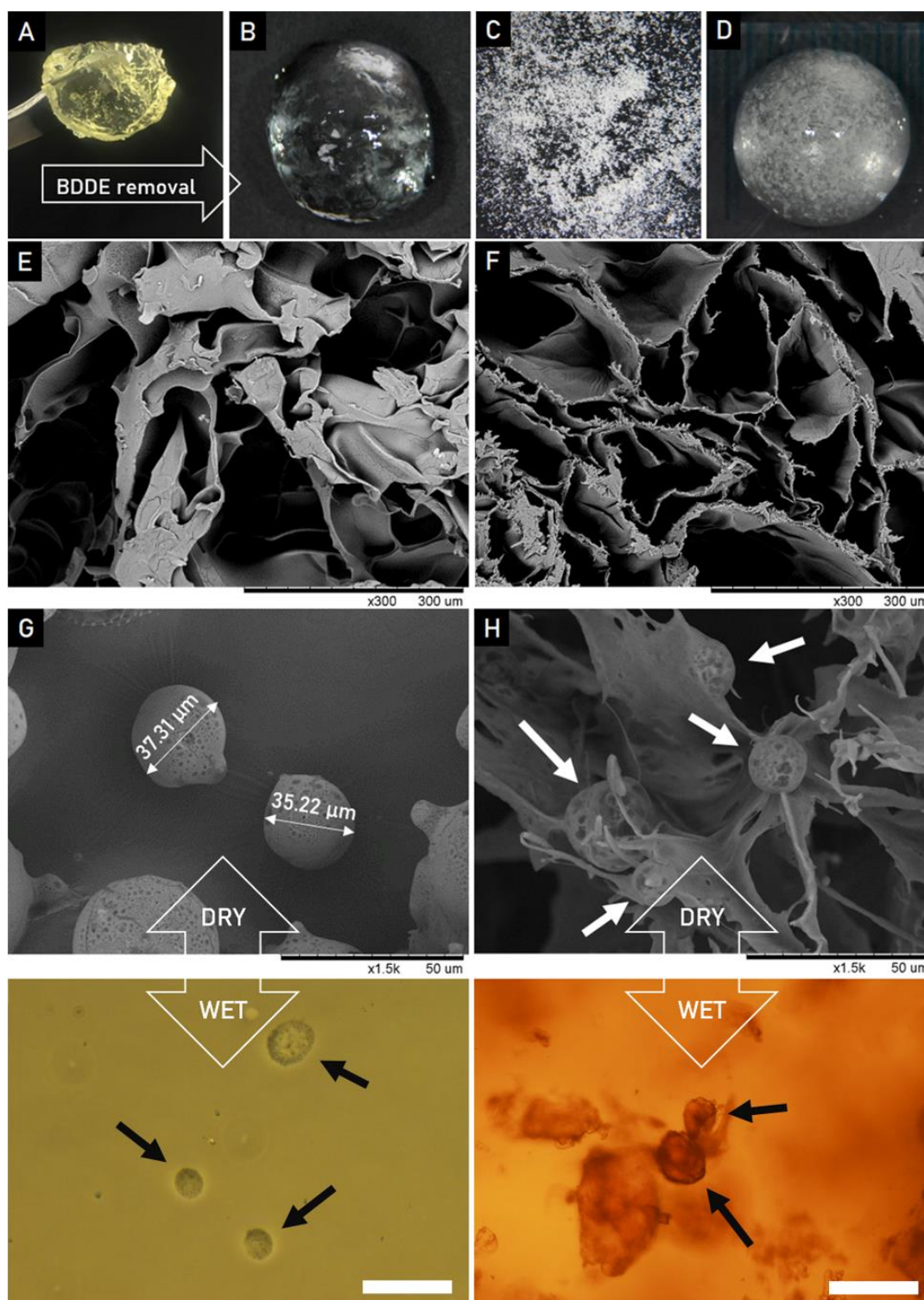
Figure 3.5 Macroscopic images of HAH before (A) and after (B) BDDE removal; CSM powder (C); HAH+CSM injected on a ruler (D). SEM images of the surface

(E) and cross-section (F) of HAH. SEM images of CSM and their wet forms in PBS captured by optical microscope with 20X magnification (G). SEM images of HAH+CSM and their wet forms captured by fluorescence microscope with 20X magnification (H). (White arrows: CSM incorporated in the HAH structure. Black arrows: wet CSM and wet CSM incorporated in the HAH structure. White Scale Bars: 50 µm.)

SEM examinations showed that HAH had open porous structure both on the surface (Figure 3.5E) and in the cross-section (Figure 3.5F). Thus, HAH architecture was suitable for new tissue formation owing to its pronounced porosity at surface and cross-section. Morphology of CSM and their incorporation into HAH were monitored by SEM (Figure 3.5G&H). When CSM were mixed with the hydrogels (Figure 3.5H), a coherent hydrogel structure was formed, owing to oppositely charged groups of CS and HA (Ahmadian et al., 2019; Zeng et al., 2011). CSM were also observed within the transparent HAH hydrogels in their swollen state, suspended in the water phase in HAH (Figure 3.5H).

3.1.1.5   Diameter Size Distribution of CSM

Diameter size distribution analysis demonstrated that 90% of CSM had a diameter within the range of 30-150 µm and 50% of the CSM was below 60 µm with an average diameter size of 105.6 µm (Figure 3.6). CSM in the swollen state was observed in the round shape (Figure 3.5G). Particle size distribution (half of the CSM was < 60 µm) pointed out that these microspheres can be considered as 'smaller-sized' among injectable particles (Qutachi et al., 2014). Thus, CSM might have a potential effect on Rg1 release profile. In other words, they might lead to a delay in Rg1 release, since drug release is directly proportional to microparticle size (Siepmann, Faisant, Akiki, Richard, & Benoit, 2004).
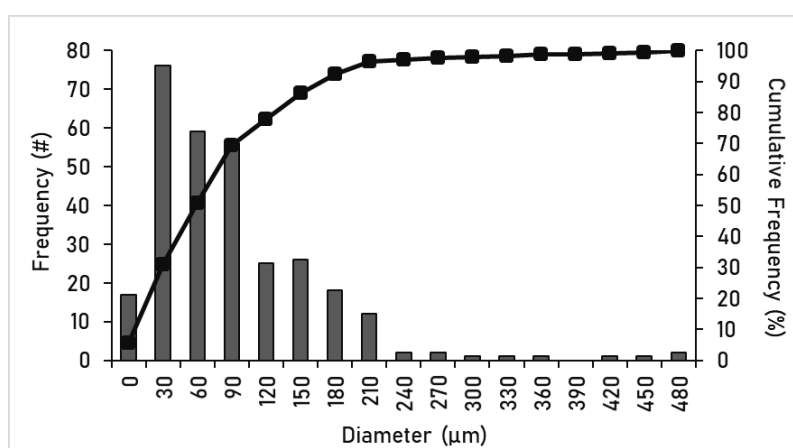
Figure 3.6 Diameter size distribution histogram of CSM.

3.1.1.6   Degradation and Swelling Measurements

Degradation profiles of HAH were studied in PBS and collagenase solution in PBS since dental tissue acquires collagenases within mineralized dentine that degrade native triple helix type 1 collagen fibrils to organize the dentine matrix prior to mineralization (Lovász et al., 2021). Cumulative weight loss of the hydrogels was 26.9% in PBS and 35.85% in collagenase type I solution after 2 weeks (Figure 3.7). The results were similar with the degradation profile of the injectable HA gels in PBS in which maleimide-functionalized-HA and furan-modified HA derivatives were combined in various ratios (Fan et al., 2015). The group of 2/1: maleimide/furan HA lost approximately 20% of its weight after 14 days. The slow degradation of hydrogels in PBS was a marker of controlled drug delivery (Patterson et al., 2010). Besides, HAH preserved 70-60% of their initial weights in collagenase type I solution which was similar to that of matrix metalloproteinase-insensitive HA hydrogels (J. Kim et al., 2008). Thus, HAH is a candidate to be able to support new tissue formation over the course of tissue regeneration.
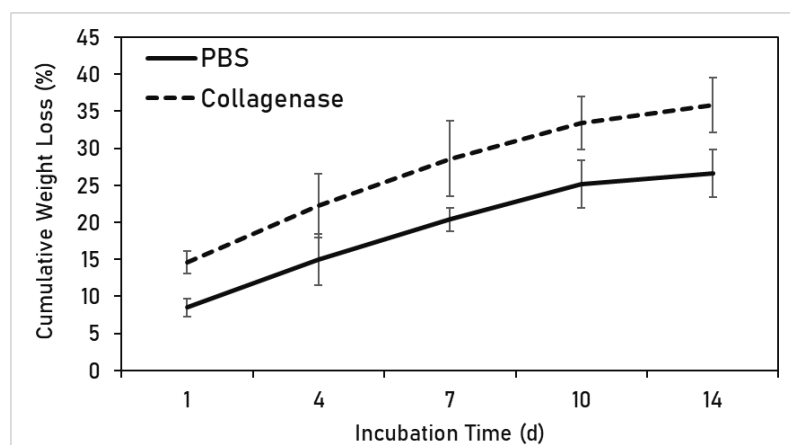
Figure 3.7 Cumulative weight loss of HAH in PBS and PBS containing Collagenase Type I (5 U/mL) at 37ºC.

EWC studies demonstrated that both HAH and HAH+CSM could hold water up to 80-100% (Figure 3.8A). In the literature, BDDE-crosslinked HA hydrogels having the same BDDE concentration with ours (0.6 v/v%) had EWC value above 80% (R. Yang et al., 2016) which was similar to our results. After 14 days, EWC of the HAH+CSM group was lower than that of EWC of the neat HAH group. However, EWCs of HAH and HAH+CSM were still above 70% which can sustain effective nutrient/waste transfer even CSM addition can form a physical barrier inside the hydrogel network (Sirousazar et al., 2012). EDVS and EDWS of the hydrogels reached to their maxima within 5 h (Figure 3.8B) and their initial and final forms are given in the representative images (Figure 3.8B-inserts). Swelling properties of hydrogels generally vary remarkably with respect to crosslinking degree, leading to alterations of solute diffusion (Peppas, Hilt, Khademhosseini, & Langer, 2006). Hence, stabilization of swelling is critical for generating reliable properties for a biomaterial. In this case, since HAH swelling was stabilized, the hydrogels were ready to use after 5 h (Figure 3.8B).
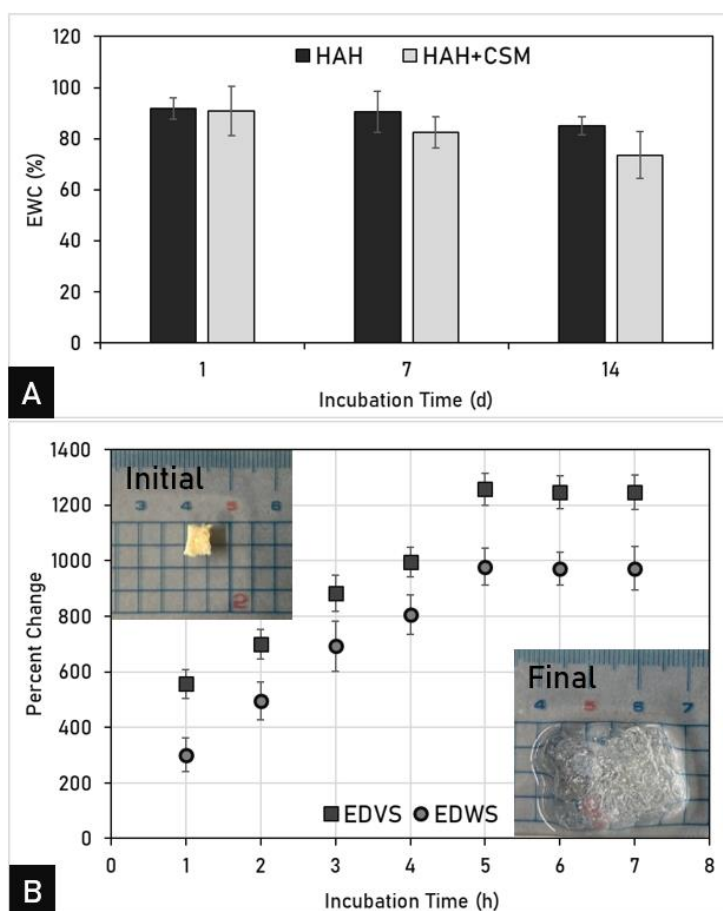
Figure 3.8 EWC of HAH and HAH+CSM on days 1, 7, and 14 (A); EDVS and EDWS of HAH (B). Inserts are the representative images of initial and final forms of HAH during swelling.

3.1.1.7   Td Release from HAH

Cumulative Td release profiles of HAH samples loaded with different amounts of Td are given in Figure 3.9. It was revealed that as the loading content increased, the amount of Td released increased while the Td percent release remained the same or slightly decreased. All hydrogels had a burst release above 80% within 1 day of incubation in PBS and then released above 90% of their Td content within 2 days (Figure 3.9-insert). This means that 90 nM Td-loaded HAH injected pulp cavity would be affected by all of the Td content of HAH. Since there is no similar study in

the literature about Td release from the hydrogels, it could not be compared; however, cell culture studies in the following sections gave an insight.
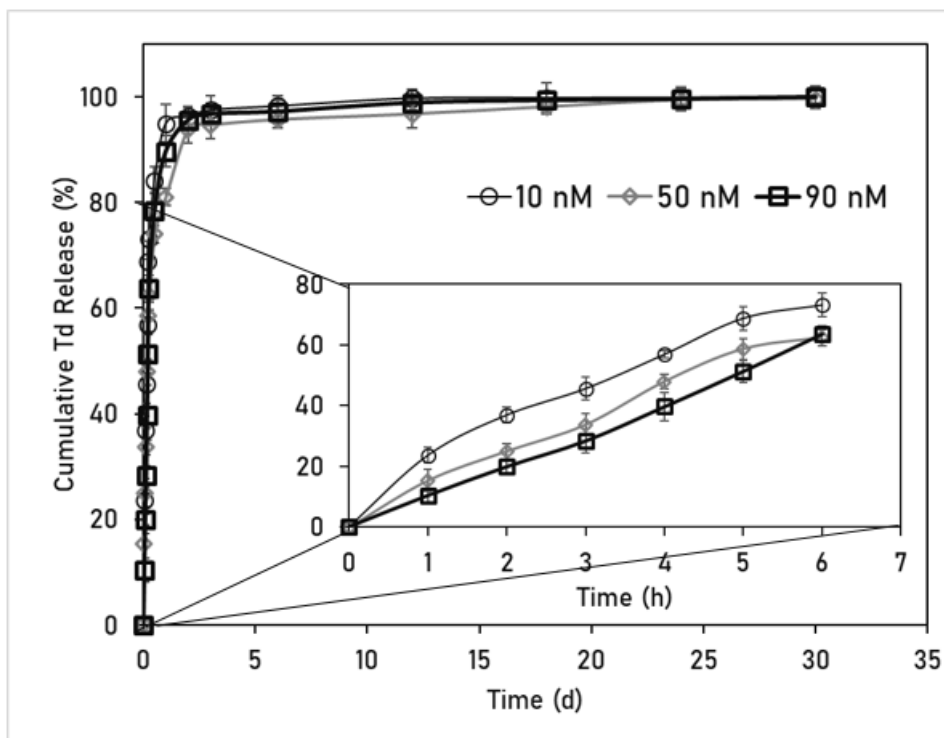
Figure 3.9 Cumulative Td release from 10, 50, and 90 nM Td-loaded HAH in PBS (0.1 M, pH 7.2) at 37ºC for 30 days (n=4).

3.1.1.8 Rg1 Release

Presence of HAH delayed the Rg1 release when compared to the neat CSM group (Figure 3.11). The differences in the initial loading of Rg1 did not alter the release profile remarkably (Figure 3.10) and 100 µg of Rg1 was selected since it matched to the desired amount to be released that was shown to be effective on the cells.
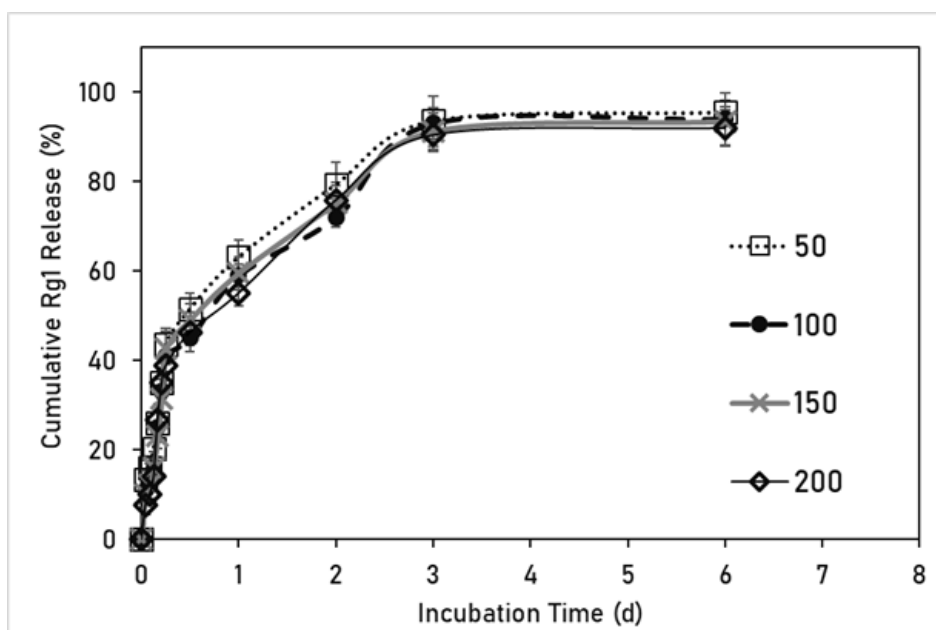
Figure 3.10 Cumulative Rg1 release profiles of CSM loaded with different amounts of Rg1 (50, 100, 150, and 200 µg) in PBS (0.1 M, pH 7.4) at 37ºC for 6 days (n=4).

It was observed that 41% of Rg1 was released from the CSM within 6 h as an initial burst which was comparable to the examples in the literature. Collagen/chitosan-gelatin microspheres were loaded with Rg1 (50, 100, and 200 µg) and their Rg1 release on day 1 were 46.00, 46.26, and 46.50%, respectively. They showed that as the loading content decreased, the release rate reduced correspondingly; however, the burst release percent was similar. On the other hand, the Rg1 release from HAH+CSM was determined 20% within 6 h while it was 41% from the CSM (Figure 3.11-insert). Delayed release of Rg1 from CSM in HAH resulted in a prolonged release compared to the release from CSM. Indeed, it is an expected result since solid carriers (e.g. microspheres) in hydrogels were shown to sustain prolonged release and thus effective local concentrations (Gaihre et al., 2017; X.-Z. Zhang, Lewis, & Chu, 2005), so that to create local Rg1 concentrations within the HAH was aimed to attract vessel buds/ends and to promote vascularization of newly-formed pulp. Since the optimal concentration of Rg1 was determined as 50 µg/mL during cell culture studies conducted by DPSC and HUVEC (Figure 3.16B), reaching 47 µg/mL of Rg1

76

concentration within 2 days in HAH+CSM groups by a burst release, was considered as suitable.
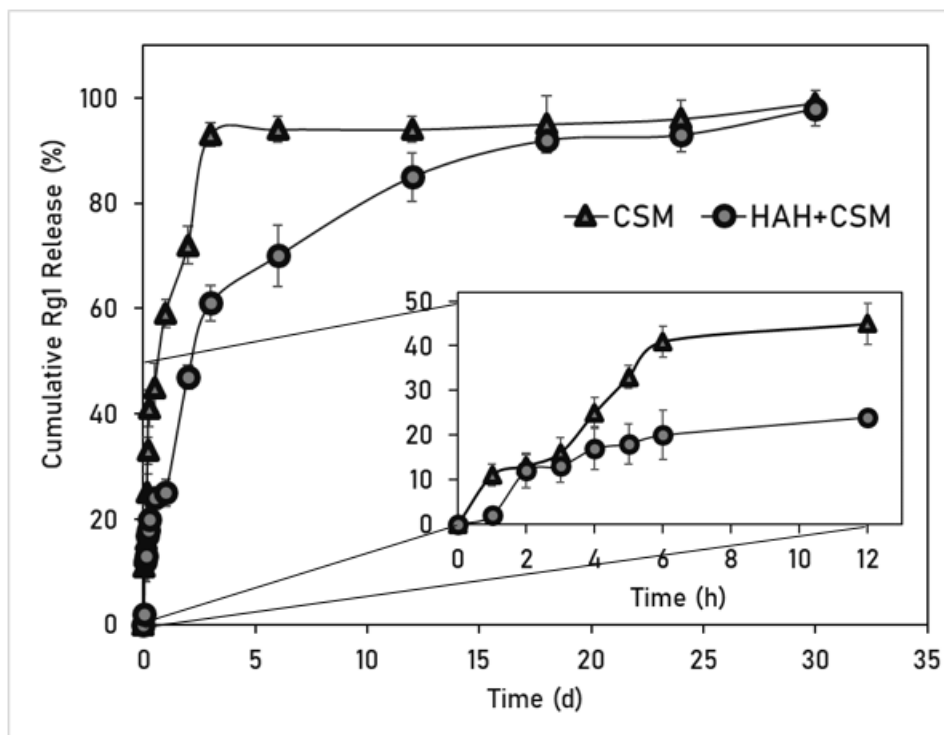
Figure 3.11 Cumulative Rg1 release from CSM and HAH+CSM in PBS (0.1 M, pH 7.2) at 37ºC for 30 days (n=4).

3.1.1.9   Co-Release of Td and Rg1 Td@HAH+Rg1@CSM

Co-release profiles of Td and Rg1 from Td@HAH+Rg1@CSM (Figure 3.12) demonstrated that Td was released slightly faster than that of Td@HAH whereas Rg1 was released slightly slower than that of HAH+Rg1@CSM counterparts. However, no statistical difference was detected between bare and co-release rates.
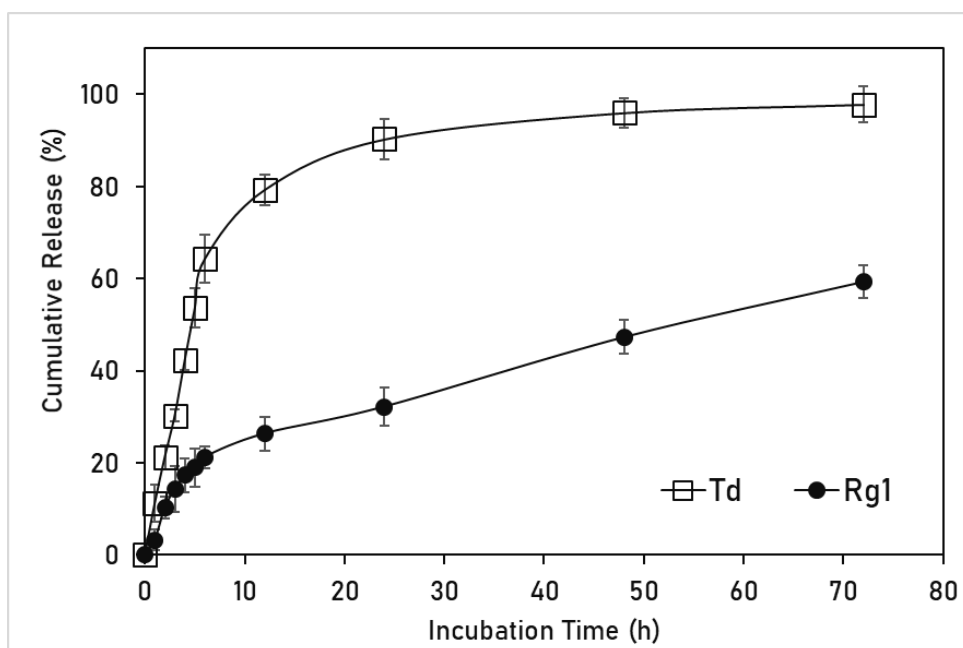
Figure 3.12 Cumulative co-release of Td and Rg1 from Td@HAH+Rg1@CSM in PBS (0.1 M, pH 7.4) at 37ºC for 3 days (n=4).

3.1.2 Cell Culture Studies for HA-Based Hydrogels

3.1.2.1 Morphological Analyses

SEM examination of the DPSC-seeded hydrogels exhibited that cells were able to attach on the hydrogels on day 1 (Figure 3.13A) and cell lawns and nucleation sites of biomineralization were observed after 7 days of incubation (Figure 3.13B). DPSC attachment (Figure 3.13A), spreading, proliferation, and initiation of biomineralization (Figure 3.13B) indicated that HAH served as a dental pulp-like extracellular environment. Minerals deposited on HAH were observed on day 14 (Figure 3.13C&D). Moreover, Ca and P elements in the biomineralized area were detected by EDX analyses (Figure 3.13D-insert). Those formations might be attributed to two reasons; (i) mineral precipitation on HAH in cell culture media (Figure 3.13C&D) due to strong ability of HA (negatively charged) to bind ions in aqueous environment and to bind cations protruding from the crystal lattice (Z.-H.

78

Chen, Ren, Zhou, & Li, 2012) or (ii) mineral deposition by cells (Figure 3.13B&C) due to odontoblastic differentiation (Bakopoulou et al., 2011). Although Ca/P ratio of the deposited minerals (Figure 3.13D-insert) did not exactly match to that of stoichiometric apatite (1.67), the apatite-like formation might still correspond to odontogenic differentiation since dental tissue has different phases of apatite deposited by odontoblasts (Wöltgens, Vingerling, & Witjes, 1980). DPSC were also seeded on HAH+CSM after injected into well plates and their attachment, spread, and proliferation were observed on day 1 and 7 (Figure 3.13E&F).
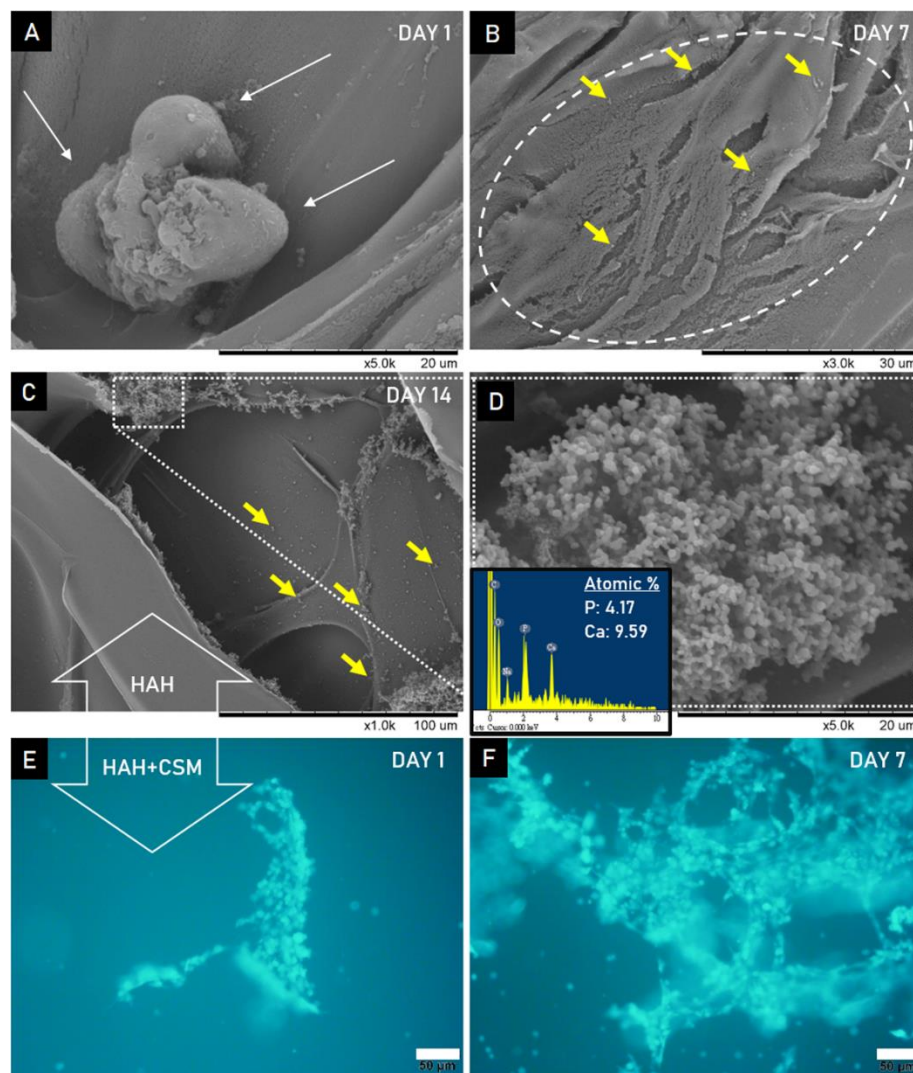
Figure 3.13 Images of DPSC seeded on HAH on day 1 (A), 7 (B), and 14 (C) and magnified image of the mineralized region is shown in the dashed square (D). EDX

analysis result of mineralized area (D-insert) (White Arrows: Cells adhered to the HAH surface. Dashed Circle: Cell lawns on HAH. Yellow Arrows: Biominerals deposited by DPSC). Fluorescence microscopy images of DPSC seeded on the injected HAH+CSM on day 1 (E) and day 7 (F) (Scale Bars: 50 µm).

3.1.2.2 Cytotoxicity Tests

3.1.2.2.1 Dose-dependent Study of BDDE

BDDE can have toxic effects that should be removed from the biomaterials to protect the surrounding tissue (Jeong et al., 2021). The cytotoxicity of HAH on DPSC were conducted after BDDE removal was studied (Figure 3.14). The amount of BDDE residues in HAH measured after 24 h of incubation in d-H_2O was 0.14 µg/mL (Figure 3.3). Therefore, BDDE residues within HAH after 24 h of removal process was in the non-toxic range (0.00-0.63 µg/mL) for DPSC according to the cytotoxicity study conducted (Figure 3.14).
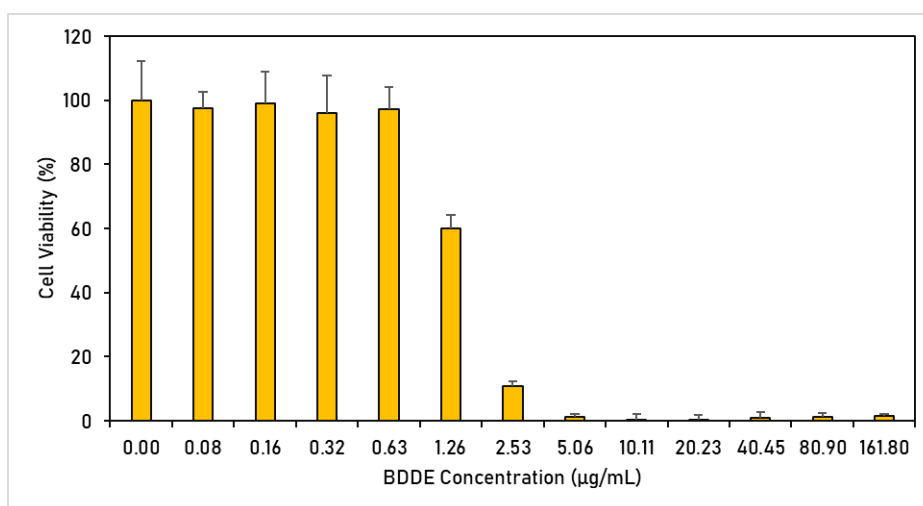
Figure 3.14 Dose-dependent cytotoxicity test results of BDDE on DPSC (n=4).

3.1.2.2.2   Dose-dependent Study of Td

The cytotoxicity test of Td on DPSC showed that free Td in the cell culture media was cytotoxic for DPSC (Figure 3.15). In the literature, the highest Td concentration (200 nM) was shown to be non-toxic for 17IA4 mouse dental pulp cells (Neves et al., 2017a); however, there was no dose-dependent cytotoxicity study for Td concentrations below 50 nM. Further studies conducted by microscopy also confirmed that Td precipitates were present in the cell culture media in the free Td group and will be discussed in the following section.
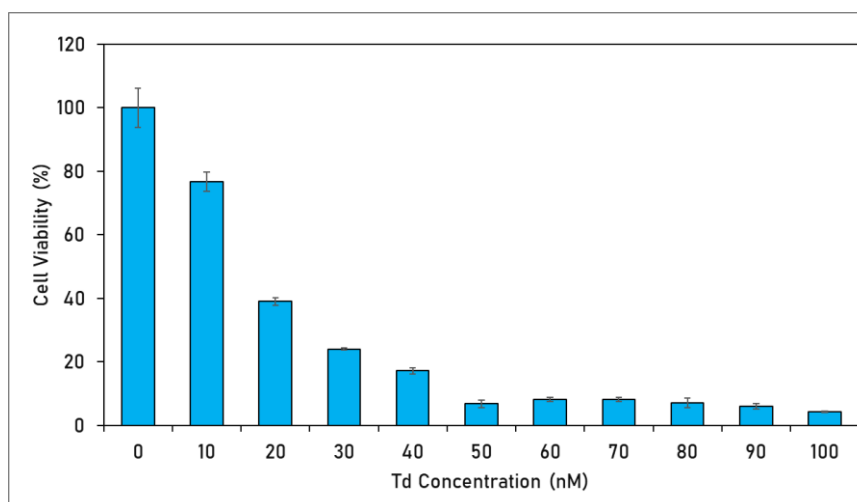
Figure 3.15 Dose-dependent cytotoxicity study of Td on DPSC (n=3).

3.1.2.3   Cell Viability Tests

During optimization studies, cell viability tests showed that Td at all concentrations increased the viability of DPSC compared to the control, and 90 nM resulted in statistically the highest cell viability than all other concentrations on day 1 (Figure 3.16A). Td concentration of 50-100 nM resulted in higher cell viability on days 4 and 7. This finding was also in agreement with the previous reports in which the researchers selected 50 nM as the optimum concentration for 17IA4 cells (Neves et

al., 2017a). In our study, 90 nM was selected as the optimum Td concentration for the further experiments.

Dose dependent study of Rg1 showed that 50-80 μg/mL and 50 μg/mL were favorable for DPSC and HUVEC proliferation, respectively (Figure 3.16B). None of the Rg1 concentrations had toxic effect on DPSC. In the literature, 30 μg/mL of Rg1 concentration was reported as the dose to stimulate HUVEC proliferation (Lin et al., 2008); however, 50 μg/mL of Rg1 had a maximum effect on HUVEC migration and it did not change when it was increased up to 100 μg/mL (Zheng et al., 2013). Similarly, 50 μg/mL was found favorable for HUVEC viability in our study (Figure 3.16B). Once the optimum concentrations of Td and Rg1 were determined as 90 nM and 50 μg/mL respectively, these doses were used for the further studies conducted with the hydrogels (Figure 3.16C&D). Both types of cells were able to proliferate in the presence of hydrogels and microspheres (HAH and HAH+CSM) without bioactive agents and had a higher cell viability than the control groups. After a week of incubation, Td@HAH+Rg1@CSM group had the highest cell viability compared to all the other groups (Figure 3.16C).

Viability of HUVEC was higher for the Td and Rg1-containing groups (Td@HAH+CSM, HAH+Rg1@CSM and Td@HAH+Rg1@CSM) on day 7 (Figure 3.16D). Rg1-containing groups (HAH+Rg1@CSM and Td@HAH+Rg1@CSM) exhibited numerically higher level of HUVEC viability on day 7. Therefore, the highest cell viability was observed in the Td and Rg1-loaded hydrogel groups (Td@HAH+Rg1@CSM) (Figure 3.16C&D).
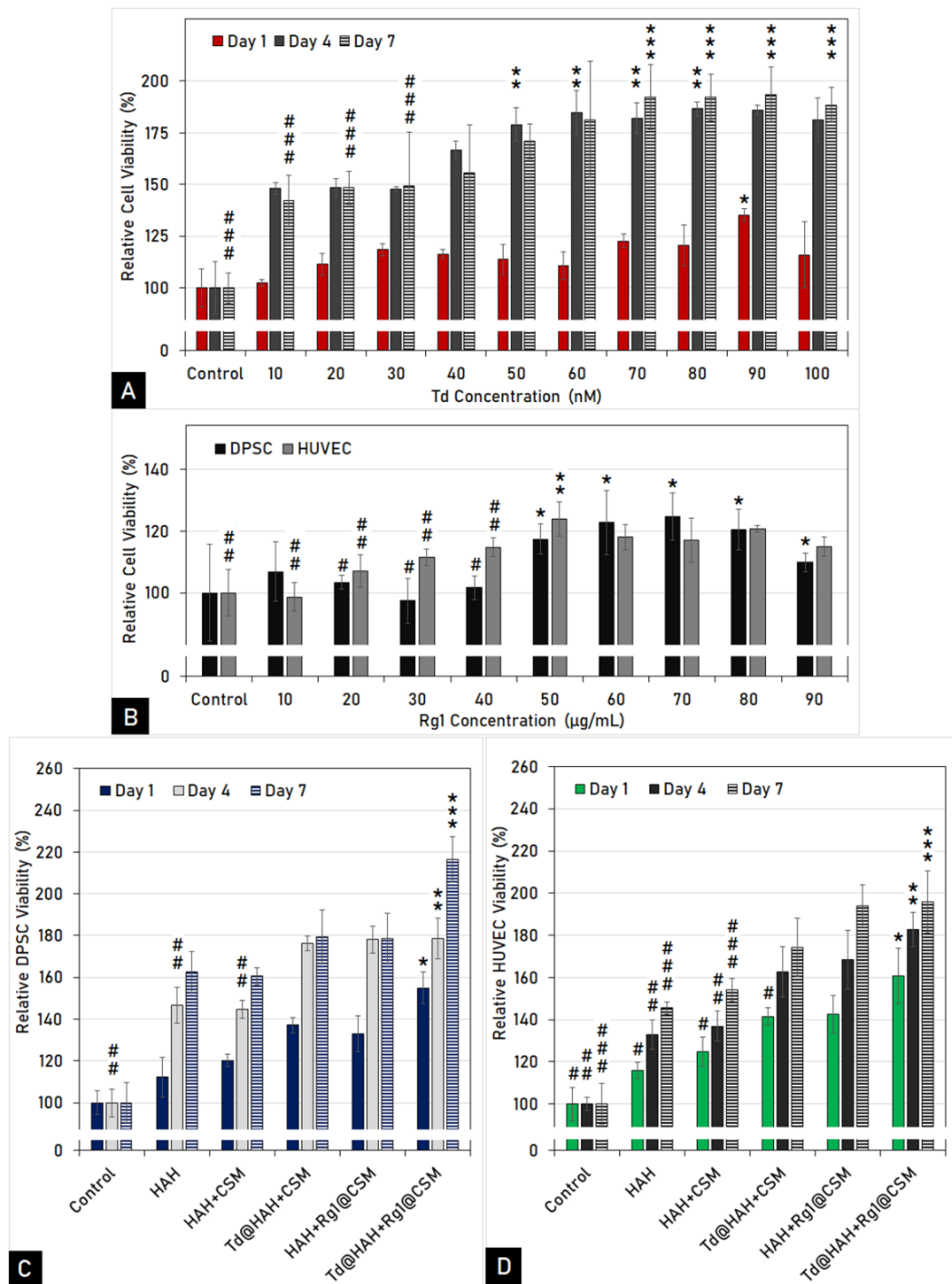
Figure 3.16 Relative viability of DPSC (A) in response to various concentrations of Td in transwell plates. * denotes the significantly highest group on day 1; ** denote the significantly highest groups on day 4; *** denote significantly higher groups than

groups on day 7 ($p < 0.05$). Relative viability of DPSC and HUVEC (B) in response to various concentrations of Rg1. * denote significantly higher groups than # groups for DPSC; ** denote significantly higher groups than ## groups for HUVEC ($p < 0.05$). Relative viability of DPSC (C). * denotes the significantly highest group on day 1; ** denotes significantly higher group than ## groups on day 4; *** denotes the significantly highest group on day 7 ($p < 0.05$). Relative viability of HUVEC (D). * denotes significantly higher group than # groups on day 1; ** denotes significantly higher group than ## groups on day 4; *** denotes significantly higher group than ### groups on day 7 ($p < 0.05$). Untreated cells were used as the control group (n=4).

3.1.2.4   Microscopic Evaluations

Microscopic evaluations showed that DPSC proliferation was negatively affected by Td addition into the cell culture media (Figure 3.17A). When Td in DMSO was added into the cell culture media, Td precipitates were observed (Figure 3.17A-black circles). Cells could only be labeled in the group with the lowest Td concentration because Td precipitations interfered imaging the cells at higher Td concentrations (Figure 3.17A1-white circles). Moreover, these precipitations had cytotoxic effect which was also observed in the dose-dependent study of Td (Figure 3.15).
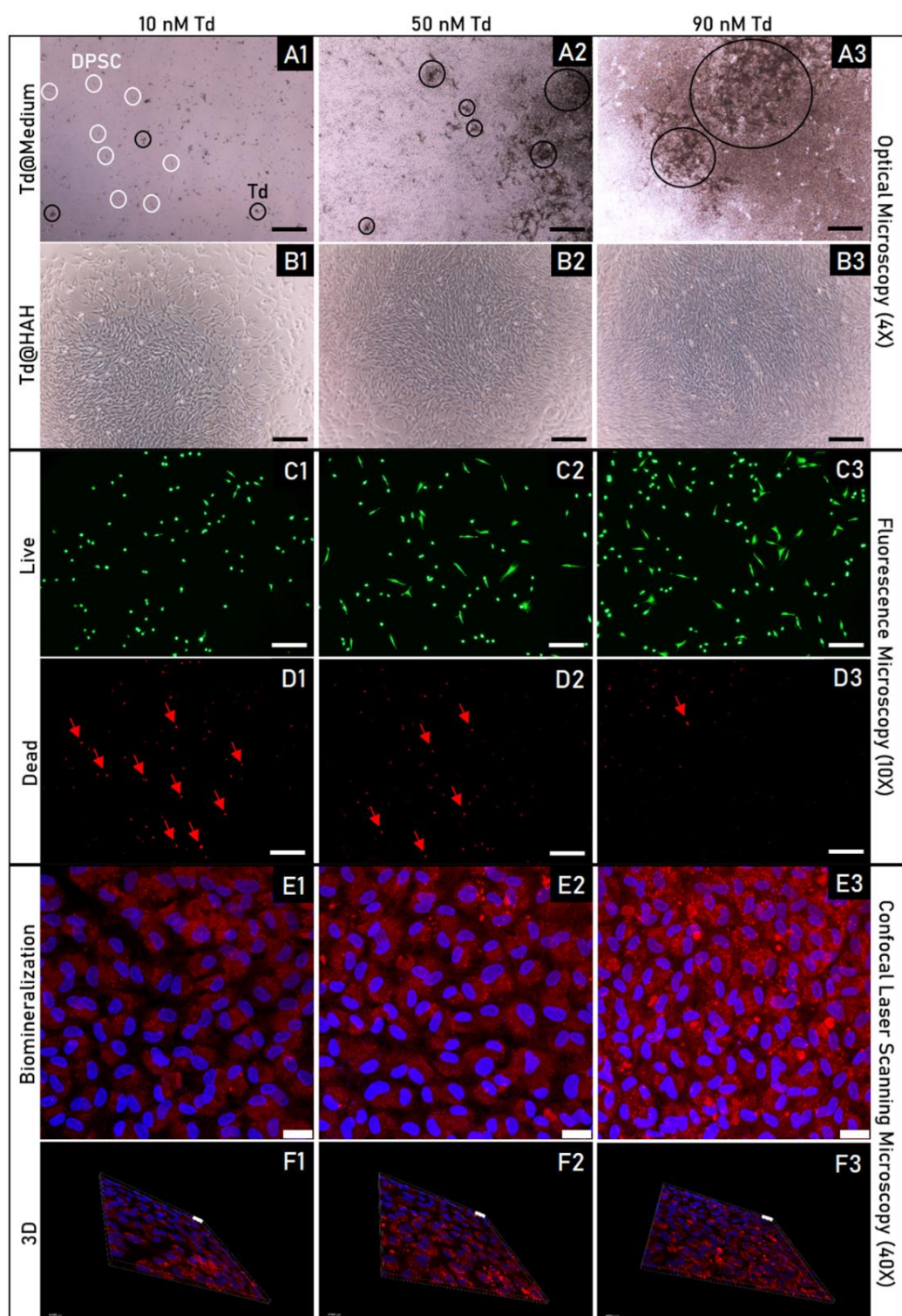
Figure 3.17 Optical microscopy images of DPSC exposed to different concentrations of Td (10, 50, and 90 nM) in cell culture medium (A) and released from the hydrogels

(Td@HAH) in the transwells (B); Scale bars: 50 µm; White circles: DPSC; Black circles: Td precipitates. Fluorescence microscopy images of live (C) and dead (D) DPSC (stained with Calcein AM-green and PI-red) exposed to Td@HAH in transwell plates; Scale bars: 100 µm; Red arrows: Dead cells. CLSM images of DPSC; nuclei (DAPI-blue) and biomineralized area (xylenol orange-reddish orange) on day 14 (E) and their 3D stacking (F); Scale bars: 25 µm.

When Td was incorporated into the hydrogels, no precipitation of Td released was detected and the cells were able to proliferate remarkably (Figure 3.17B). Cell density was slightly higher in the groups of 50 and 90 nM (Figure 3.17B2&3) compared to 10 nM (Figure 3.17B1). Thus, Td delivery in a controlled manner from a carrier (e.g. Td@HAH) can be considered crucial since local concentration variations caused by precipitation (Td and also the solvent, i.e. DMSO) might lead to cytotoxicity (Birjandi, Suzano, & Sharpe, 2020; Prasad et al., 2014).

Live/Dead cell assay conducted in trans-wells revealed that DPSC spreading was enhanced in 50 and 90 nM concentrations of Td (Figure 3.17C2&3) whereas round morphology of DPSC was observed in 10 nM group (Figure 3.17C1). Dead cells at the same spots were counted and more dead cells were observed in the lowest Td concentration (Figure 3.17D). Live/Dead Assay also confirmed that 50 and 90 nM of Td concentrations were more favorable for the spreading of DPSC (Figure 3.17C).

Biomineralization by DPSC exposed to the hydrogels was examined after xylenol orange staining as reddish orange color among blue cell nuclei (Figure 3.17E&F). The amount of accumulation was higher when the Td concentration was increased to 90 nM (Figure 3.17E3&F3). Furthermore, similar to SEM results (Figure 3.75B-D), CLSM findings exhibited that DPSC deposited minerals under Td exposure (Figure 3.17E&F), which is a major sign of odontogenic differentiation of DPSC (Bakopoulou et al., 2011).

3.1.2.5 Gene Expression Studies

Preliminary gene expression studies by using different amounts of Td-loaded HAH groups only were conducted prior to gene expression studies for the hydrogel groups to understand which Td concentration upregulated the expressions of odontogenic genes more effectively. It has been demonstrated that especially Axin-2 gene is upregulated within 1st day of Td exposure (Neves et al., 2017a). It was shown that 90 nM Td-loaded HAH significantly upregulated the expressions of Axin-2, DSPP, and DMP1 on day 1 compared to 50 nM Td-loaded counterparts (Figure 3.18). The effect of Td diminished as time passed. RT-PCR studies demonstrated that 90 nM was not only favorable for proliferation of DPSC but also their odontogenic differentiation. After the preliminary findings, the effect of 90 nM Td on the expression of osteo/odontogenic (COL1A1, ALP, and OCN) and odontogenic (Axin-2, DSPP, and DMP1) markers was studied (Figure 3.19).
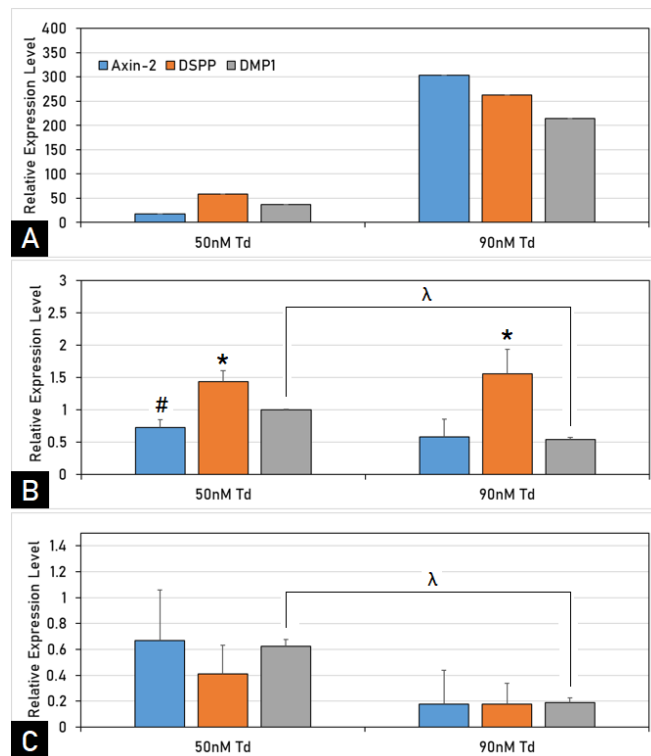
Figure 3.18 Relative gene (Axin-2, DSPP, and DMP1) expression levels of DPSC treated with 50 and 90 nM Td-loaded HAH in transwell plates (n=4) on day 1 (A), 4

(B), and 7 (C). Neat HAH was set as control. Statistical analyses showed that all groups were significantly different at day 1; * denotes significantly the highest gene expression level for the given Td concentration; # denotes the significantly the lowest gene expression level for 50 nM Td; and λ denotes statistically different groups ($p < 0.05$).

HAH group had the highest level of COL1A1 gene expression level (Figure 3.19A) which was in consistent with the positive HA effect on COL1A1 gene expression of DPSC (Ferroni et al., 2015), which is a ligand for receptor CD44 involved in early mineralization processes of odontoblasts (K.-L. Chen, Yeh, Lung, Yang, & Yuan, 2016). Relative expression levels of ALP (Figure 3.19B) and OCN (Figure 3.19C) were statistically higher in the HAH+Rg1@CSM group than any other group since it has been reported that Rg1 stimulated osteo/odontogenic differentiation of DPSC (Ping Wang et al., 2014). Moreover, ALP and OCN gene expression levels of DPSC in the Td-containing groups were higher than the control groups', yet still lower than that of HAH+Rg1@CSM on day 7. This result might be due to usual late expression of those genes (i.e. after 14 days) (Asgary, Nazarian, Khojasteh, & Shokouhinejad, 2014). On the other hand, the expression of Axin-2 was significantly higher in the Td@HAH+Rg1@CSM group than all other groups (Figure 3.19D). This means that Td and Rg1 incorporation together resulted in remarkable upregulation of Axin-2 expression, demonstrating Rg1 had an impact on GSK-3 pathway similar to the previously mentioned influence of Td (Neves et al., 2017a). Moreover, only Td could upregulate Axin-2 expression significantly on day 1, then this effect faded out on day 4 and 7 (Figure 3.16). Concordantly, the positive effect of neat Td on Axin-2 expression was reported up to day 1 in the previous studies (Neves et al., 2017a; Zaugg et al., 2020). However, the collective delivery of Td and Rg1 prolonged the expression of Axin-2 up to day 7 which could be a sign of synergistic impact of them (Figure 3.19D).
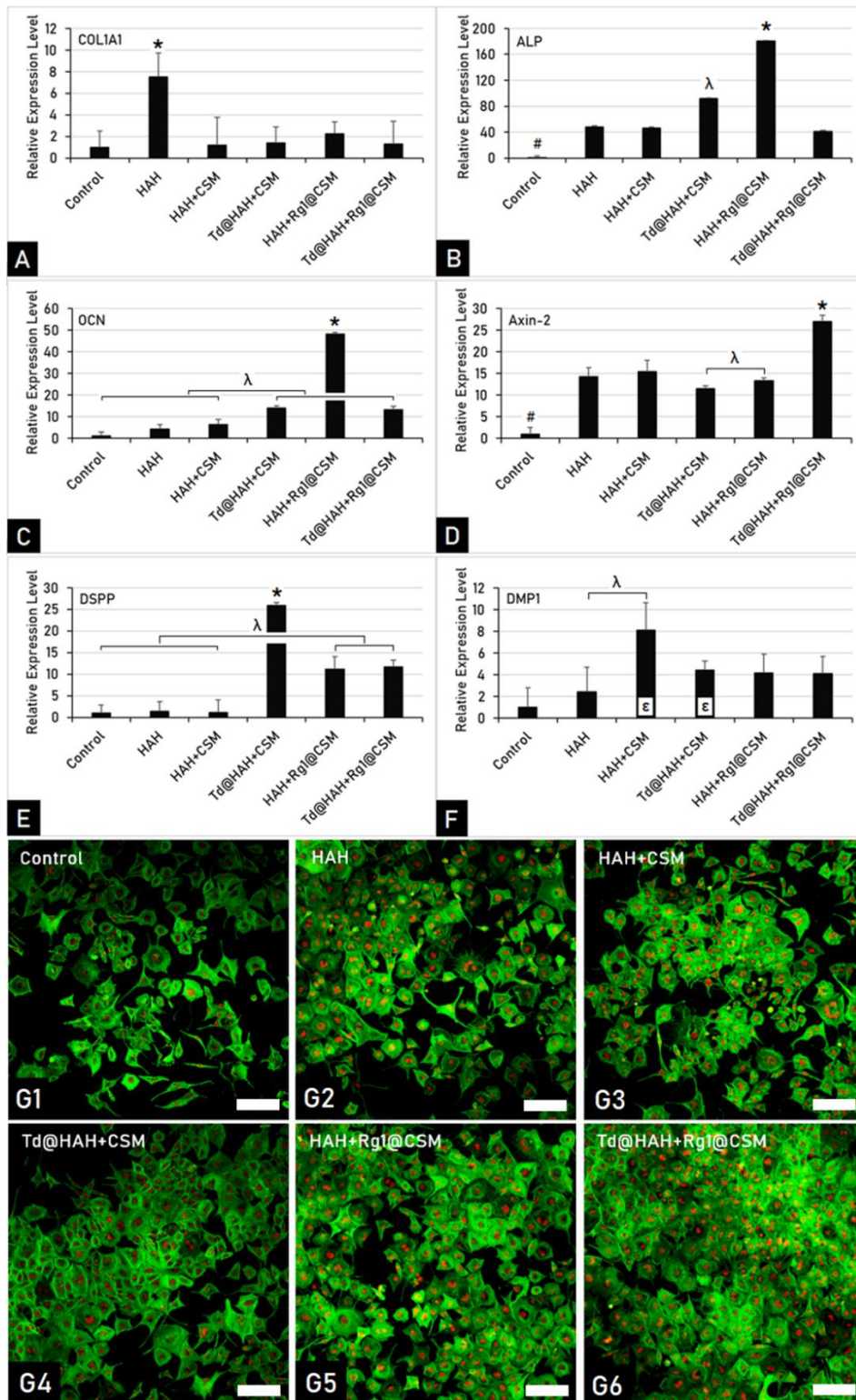
Figure 3.19 Relative gene [COL1A1 (A), ALP (B), OCN (C), Axin-2 (D), DSPP (E), and DMP1 (F)] expression levels of DPSC treated with previously defined test

groups on day 7. * denotes the significantly highest group; # denotes the significantly lowest group; λ denotes statistically difference between the groups; ε denotes statistically different groups than the control ($p < 0.05$). CLSM images of DPSC on day 7 (G). Scale Bars: 30 μm.

DSPP expression levels significantly increased by Td so that the Td@HAH+CSM group had the highest DSPP expression (Figure 3.19E). Besides, this level was ~10 fold higher in Rg1-containing groups (HAH+Rg1@CSM and Td@HAH+Rg1@CSM) than control and also higher than the literature findings reported in a study showing Rg1-effect on DSPP expression of DPSC on day 7 in the presence of Rg1 (Ping Wang et al., 2014). The gene expression of other odontogenic differentiation marker, DMP1, measured in the HAH+CSM and the Td@HAH+CSM groups was significantly higher than that observed in the control group (Figure 3.19F). The highest DMP1 expression observed in the HAH+CSM group could be attributed to the effect of CS monomers on dental regeneration (Matsunaga et al., 2006), which were released during biodegradation of the polymers in the cell culture environment. The reason that Rg1-contaning groups did not have the highest DSPP and DMP1 expression might be associated with the previous reports demonstrating that DSPP and DMP1 could only reach ~3 fold and ~2 fold higher gene expression levels than that of controls after 7 days (P Wang et al., 2012). During morphological analyses for the experimental groups, the highest cell density was observed in Td@HAH+Rg1@CSM group (Figure 3.19G), in parallel with the cell viability results (Figure 3.16C).

VEGFA expression of DPSC on day 7 was the highest for Td@HAH+Rg1@CSM group among all DPSC groups whereas for HUVEC the highest expression was observed for both of the Rg1-containing groups (HAH+Rg1@CSM and Td@HAH+Rg1@CSM), meaning that VEGFA expression of both of the cell types was enhanced at most in the presence of Td@HAH+Rg1@CSM (Figure 3.20A). These results showed that the angiogenic differentiation of DPSC and HUVEC was significantly promoted by the use of Td@HAH+Rg1@CSM hydrogels, since

VEGFA is the primary pro-angiogenic growth factor possessing many regulatory functions, e.g. survival, proliferation, migration, and sprouting of capillary vessels (Saghiri, Asatourian, Sorenson, & Sheibani, 2015). Furthermore, VEGFR2 was stated as the major receptor type of VEGFA that allows angiogenesis (Gomez-Sosa, Caviedes-Bucheli, Diaz-Barrera, & Munoz, 2019) affecting endothelial cell differentiation, proliferation, migration, and formation of the vascular tube (Kawamura et al., 2008). Therefore, VEGFR2 expression levels of DPSC and HUVEC were also determined (Figure 3.20B). Similarly, Rg1-containing hydrogels stimulated the VEGFR2 expression of DPSC and HUVEC at most. HUVEC in all of the hydrogel groups of had higher gene expression levels compared to their control, which might be attributed to the presence of HAH (Seidlits et al., 2011) or HAH+CSM (M. Li et al., 2021).
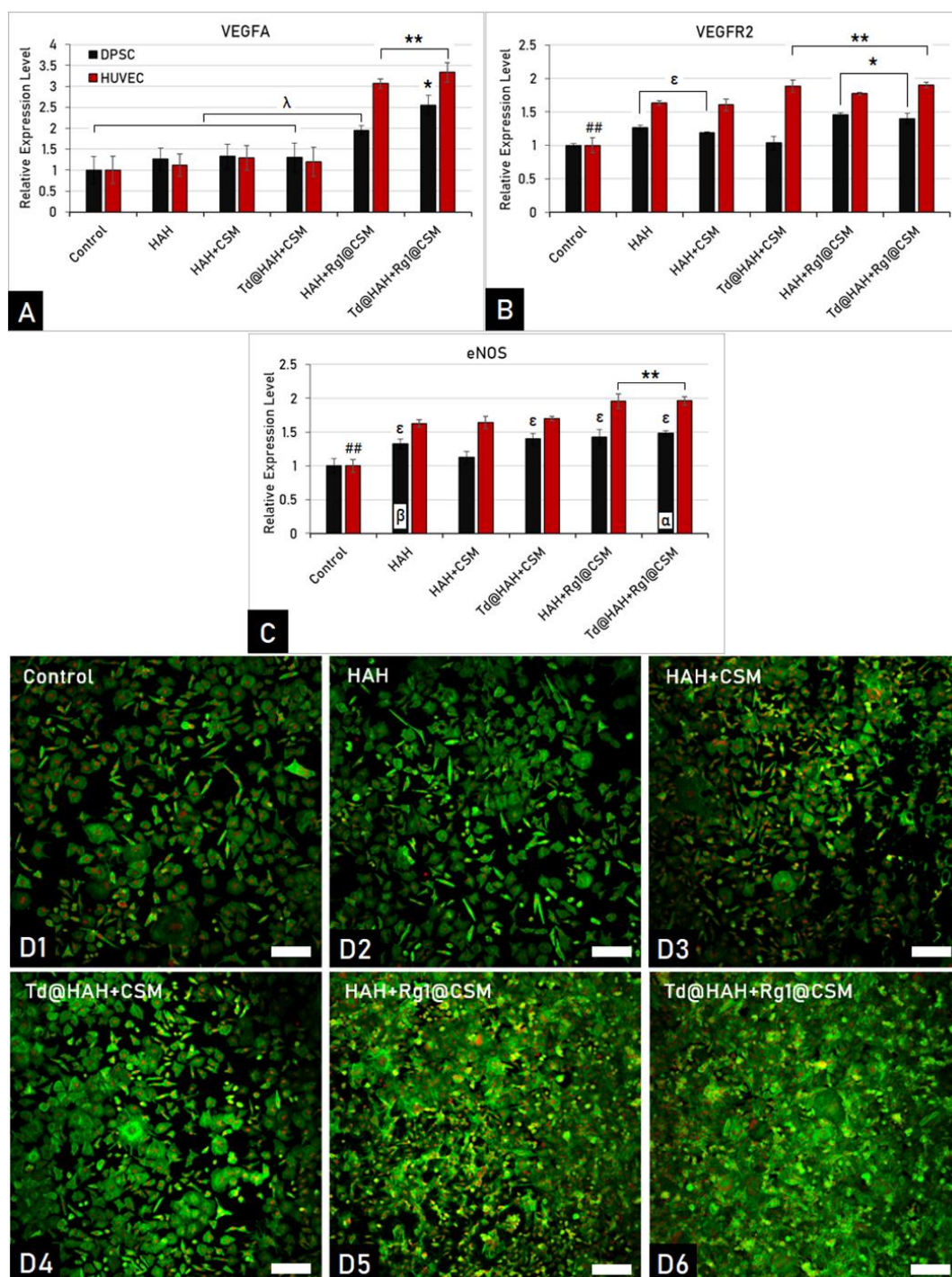
Figure 3.20 Relative gene [VEGFA (A), VEGFR2 (B), and eNOS (C)] expression levels of DPSC and HUVEC treated with previously defined hydrogel groups on day 7. * and # denote significantly the highest and the lowest groups of DPSC, respectively; ** and ## denote significantly the highest and the lowest groups of

HUVEC, respectively; λ denotes the groups statistically different from each other; ε denote the groups statistically different than the control; α denotes the group which is significantly different than β ($p < 0.05$). CLSM images of HUVEC on day 7 (D). Scale Bars: 30 μm.

Another angiogenic marker eNOS acts as one of the key regulator enzyme in formation of vasculature which was vital for tissue growth (S. C. Huang et al., 2015). In a previous study, localization of eNOS in dental pulp tissue was observed in the cells at the de novo matrix-pulp interface after tooth restoration procedures (Mei et al., 2007), showing that eNOS was secreted in pulp to enhance vascularization. The significant upregulation of eNOS expression in DPSC and HUVEC was detected among the hydrogel groups (Figure 3.20C). In detail, Rg1-containing groups of HUVEC exhibited the highest levels of gene expression, confirming the angiogenic effect of Rg1 released from the hydrogels. Similarly, it was reported that Rg1 activated eNOS in HUVEC up to a plateau level (150 nM of Rg1) (Leung et al., 2006). Expression of eNOS in DPSC cultured in the presence of Td@HAH+Rg1@CSM was statistically higher than observed in HAH, HAH+CSM, and the control groups. Such finding showed the angiogenic potential of Td@HAH+Rg1@CSM, since it was demonstrated that eNOS expression of pulp and microvessel density had a positive correlation (Degidi et al., 2006).

During morphological analyses for the experimental groups, the highest cell density was observed in Td@HAH+Rg1@CSM group (Figure 3.20D), in parallel with the cell viability results (Figure 3.16C).

In vitro angiogenesis studies confirmed the angiogenic effect of Rg1 released from the hydrogels on HUVEC seeded on Matrigel (Figure 3.21), which was in agreement with the literature (I.-H. Yang et al., 2021). Microscopic evaluations showed that the tube patterns formed by HUVEC were visually thicker in the groups of HAH+Rg1@CSM (Figure 3.18E) and Td@HAH+Rg1@CSM (Figure 3.21F) than the others'. The quantified results exhibited that tube formation significantly increased in the presence of Td comparing to control and further increased in the

presence of Rg1 comparing to the groups without Rg1 (Figure 3.21G). Furthermore, Td@HAH+CSM group having higher level of tube length formation comparing to the control group might be explained by the stimulatory effect of GSK-3 inhibitors on angiogenesis (Baruah et al., 2017).
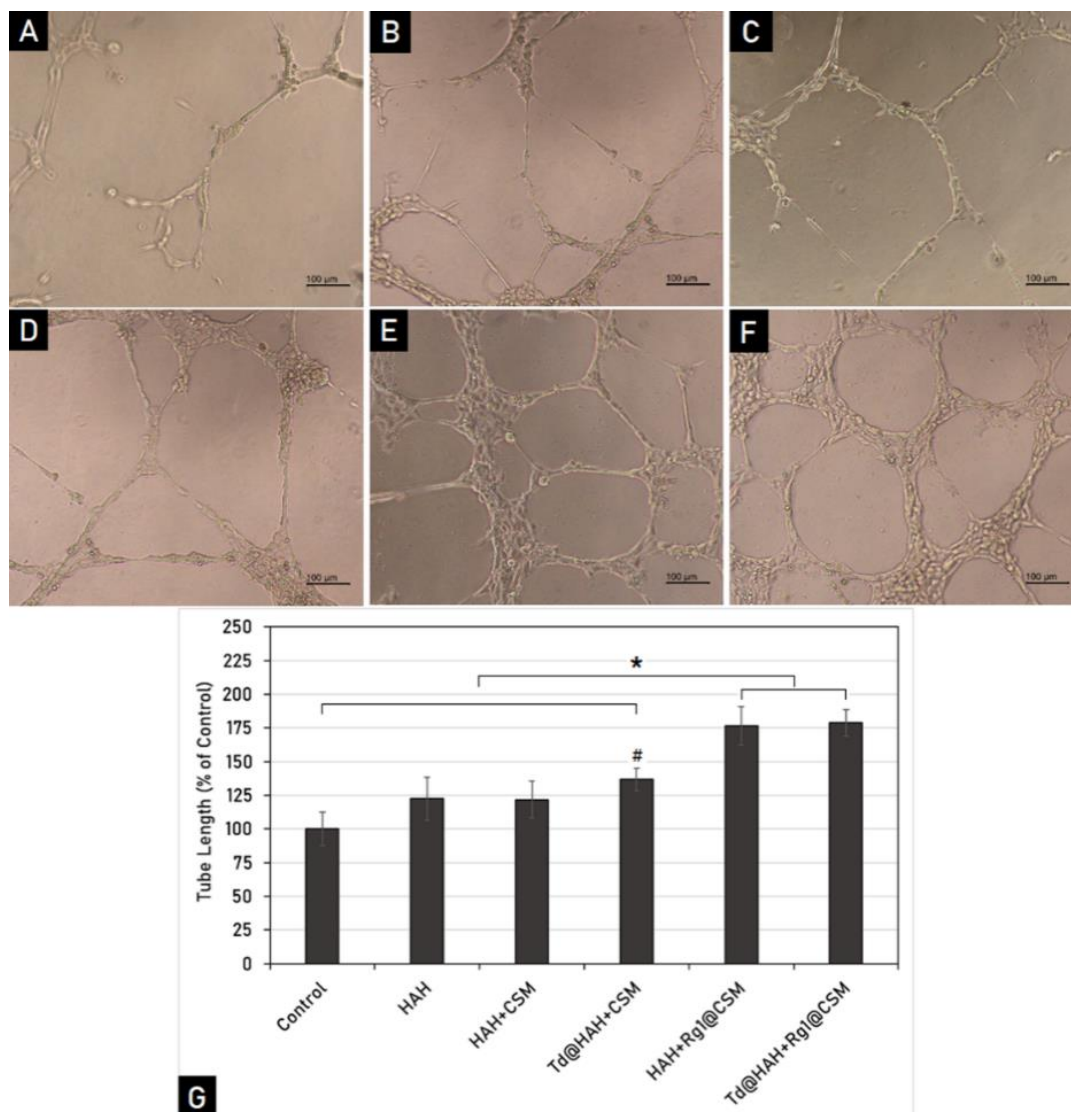
Figure 3.21 *In vitro* angiogenesis monitoring of HUVEC on Matrigel (n=4) under phase-contrast microscopy for the groups: control (A), HAH (B), HAH+CSM (C), Td@HAH+CSM (D), HAH+Rg1@CSM (E), Td@HAH+Rg1@CSM (F), and tube length measurements of these groups (G). * denote for statistically different groups from each other; # denotes the statistically different group than the control ($p < 0.05$).

3.2   GelMA-Based Hydrogels

3.2.1   Material Characterizations of GelMA-Based Hydrogels

3.2.1.1   Characterizations of Electrospun Fibers

Electrospinning was initially performed separately for PMMA and SF solutions in order to identify their specific parameters suitable for electrospinning.

3.2.1.1.1   Optimization of Electrospinning Parameters for PMMA

PMMA solutions were electrospun in different concentrations under various electrospinning process parameters and electrospun PMMA fibers were analyzed via SEM. Beaded fibers were observed when PMMA solutions of 5% (w/v) were electrospun (Figure 3.22). PMMA spheres were observed when a flow rate of 2 mL/h and voltage of 12 kV were used, thus such settings with a lower polymer concentrations such as 5% were similar to those used for electrospraying process (Bhushani & Anandharamakrishnan, 2014) rather than electrospinning (Figure 3.22A). Fibers became much apparent when the voltage was decreased (Figure 3.22B). Bead formation was tried to be eliminated by increasing the flow rate and applied voltages accordingly in order to form a stable jet (Figure 3.22C&D). Bead formation decreased; however, complete removal of beads could not be achieved.
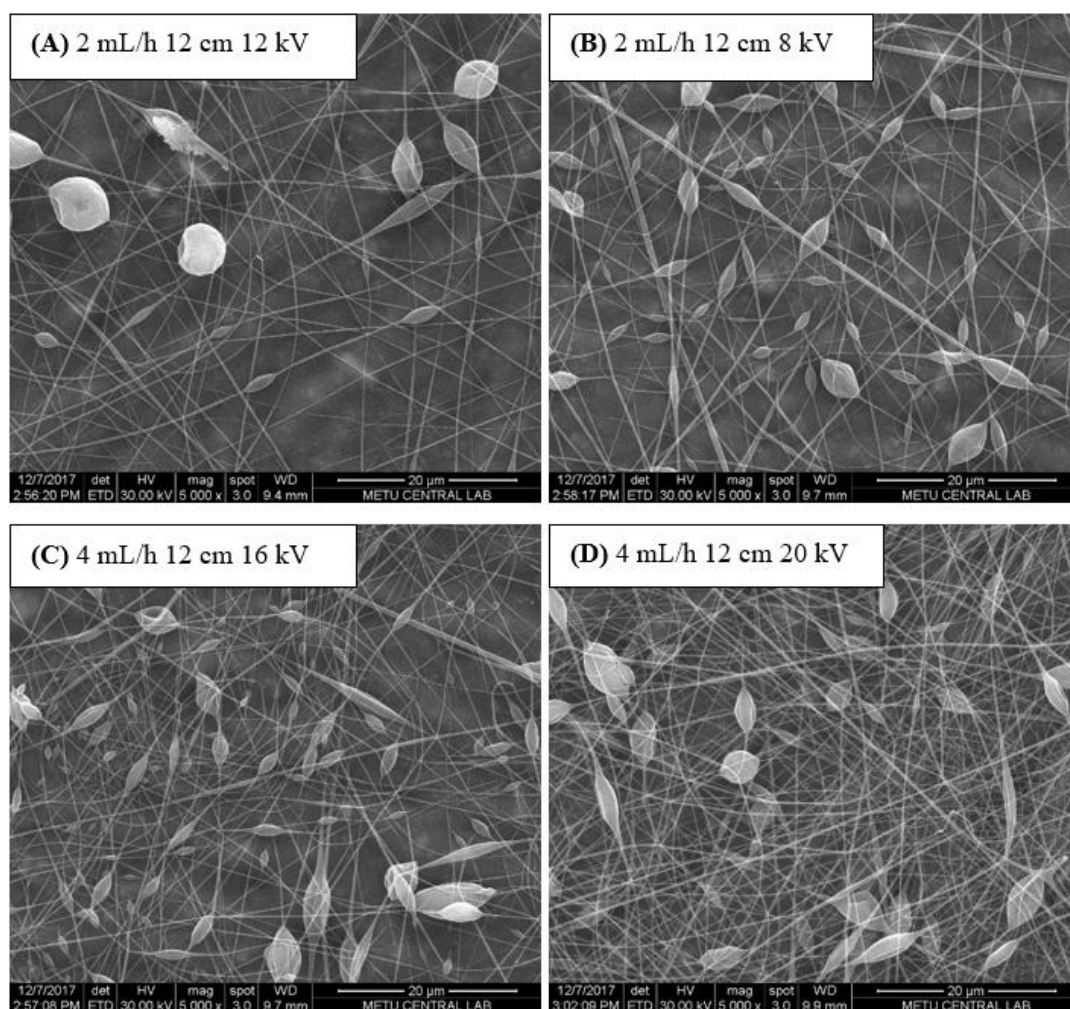
Figure 3.22 SEM images of electrospun PMMA solutions of 5% (w/v) polymer concentration.

In order to eliminate beaded morphology, polymer concentration was increased to 10% (w/v) and bead density was further decreased (Figure 3.23). Moreover, stable jet formation was still observed when the flow rate was increased up to 8 mL/h (Figure 3.23D). Such observations pointed out that the polymer concentration should not be exceeded its specific viscosity level suitable for electrospinning.
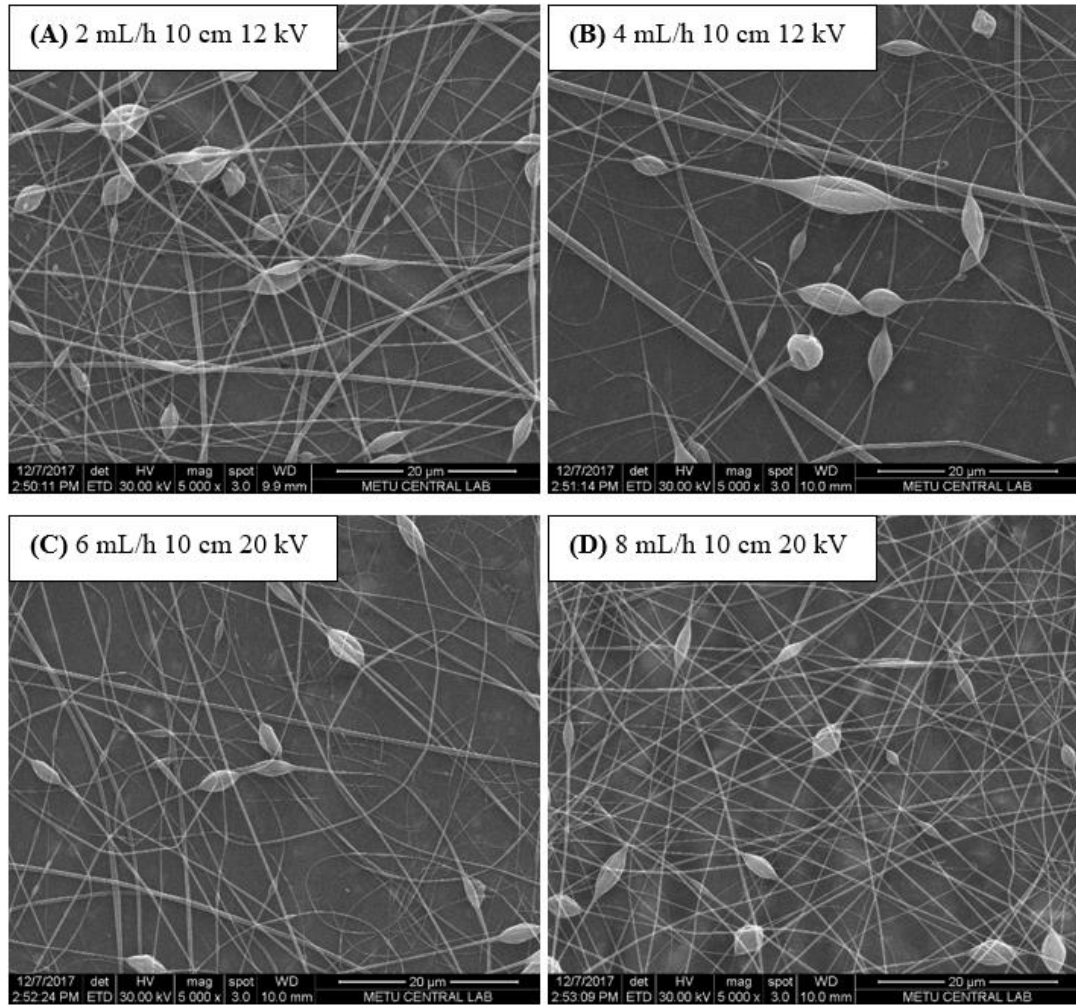
Figure 3.23 SEM images of electrospun PMMA solutions of 10% (w/v) polymer concentration.

More concentrated solutions were prepared (15%) and fibers were obtained without bead deformities (Figure 3.24) and homogeneous fibrous mesh was formed (Figure 3.24A). Moreover, fusion of fibers at the intersection point was detected at certain regions (Figure 3.24D). It could be claimed that PMMA utilization for core part was a suitable choice to keep fibers apart from each other. SEM images also showed that the diameter of PMMA fibers ranged between 4-7 μm (Figure 3.24C) while it was reduced below 2 μm when lower polymer concentrations were used (Figures 3.22&23) since thicker fibers are formed as the initial polymer concentration increases during electrospinning (Thompson, Chase, Yarin, & Reneker, 2007).
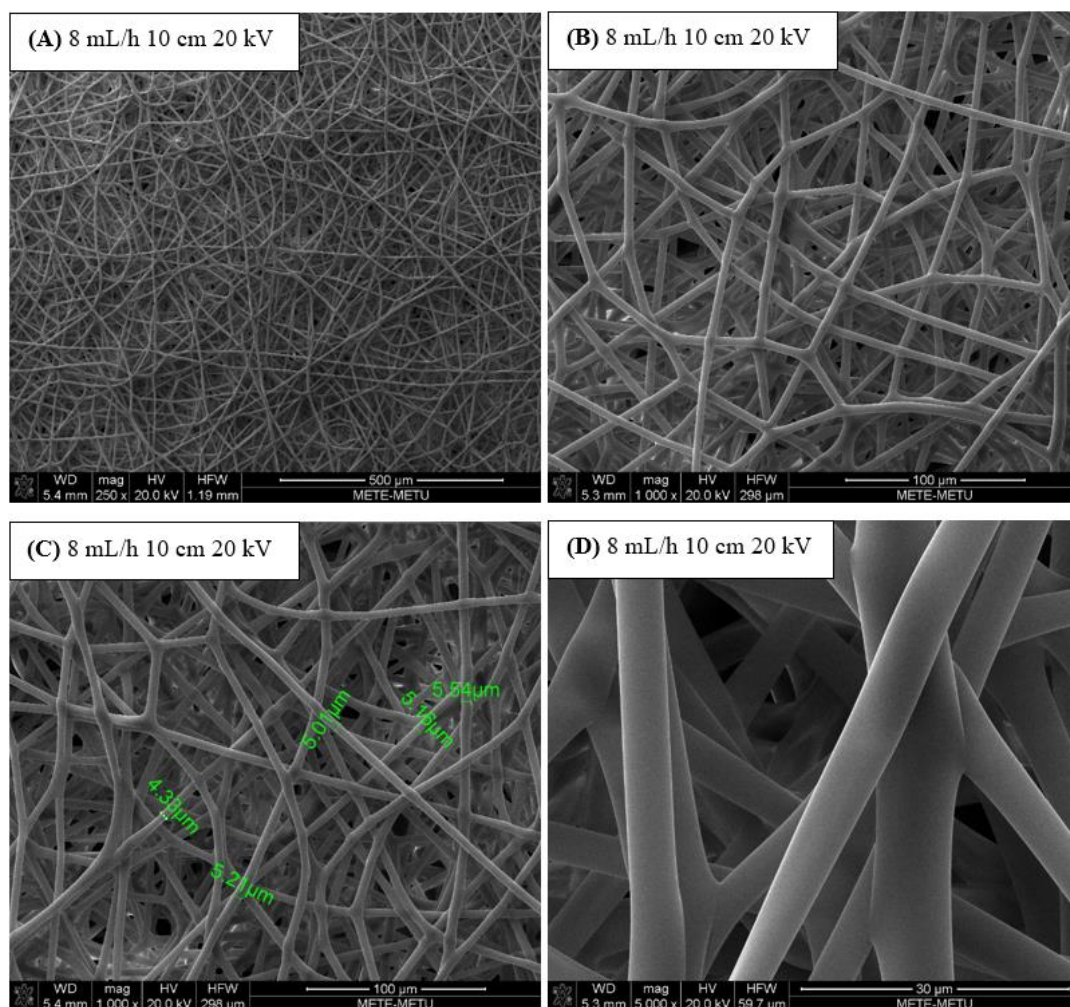
Figure 3.24 SEM images of electrospun PMMA solutions of 15% (w/v) polymer concentration in different magnifications 250X (A), 1000X (B&C), and 5000X (D) magnifications.

3.2.1.1.2 Optimization of Electrospinning Parameters for SF

Electrospun SF fibers formed had ribbon-like structures (Figure 3.25). It has been reported that there might be two reasons of resulting with the ribbon-like morphology of SF fibers; (i) high polymer concentration that makes the viscosity of the solution too high and instable so that SF was electrospun unevenly or/and (ii) high voltage causing faster arrival of fibers to the collector screen without complete evaporation

of the solvent, thus SF was drying on the collector becoming ribbon-shaped (H. Wang, Zhang, Shao, & Hu, 2005). The fiber diameter distribution of SF became wider when the flow rate was increased from 2 mL/h (Figure 3.25A&B) to 4 mL/h (Figure 3.25C&D) since thicker fibers are produced as the flow rate increases during electrospinning (Thompson et al., 2007). The polymer concentrations were then set to 9 and 10% and the solution viscosity increased accordingly. As a result, SF solutions could not be electrospun at any higher concentrations.
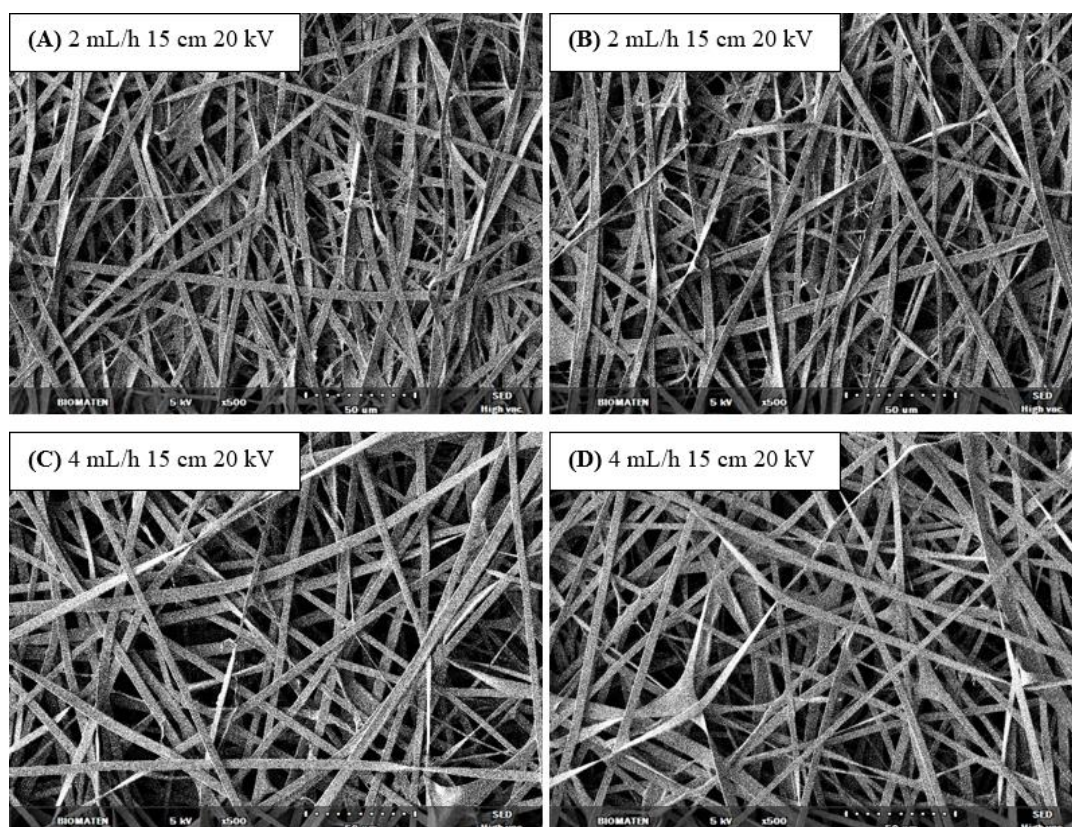
Figure 3.25 SEM images of electrospun fibers using SF solutions of different polymer concentrations; 10 (w/v) % (A&C) and 9 (w/v) % (B&D).

3.2.1.1.3 Optimization of Electrospinning Parameters for PMMA/SF Core/Shell Fibers

Optimization studies were conducted to determine the concentration range for PMMA and SF for coaxial electrospinning. The characteristic differences in SF and PMMA fibers created a need of a further optimization to produce PMMA/SF core/shell fibers. The SF fibers were observed as ribbon-like structure (Figure 3.26 A&B) whereas electrospinning of PMMA resulted with a smooth cylindrical structure (Figure 3.26C&D). The difference between the morphologies of the SF and PMMA might be due to difference of the evaporation of the solvent in two systems. Incomplete evaporation of HFIP during SF electrospinning caused flattened fibers (K. Zhang et al., 2010). This occasion was altered with the use of PMMA which could be due to higher evaporation of HFIP. During coaxial electrospinning in the following steps, the ribbon-like structures of SF fibers would have contributed to the asymmetric diameter distribution of PMMA/SF core/shell fibers when utilized in combination.

Furthermore, broken fibers were seen in PMMA meshes due to the brittleness of PMMA (Shioya, Koga, Fujimoto, & Ishida, 1988) which should be tailored to be used as a stable scaffold (Figure 3.26D). On the other hand, SF fibers were intact owing to its flexible nature. The diameter distribution of PMMA fibers was narrower when compared to that of SF (Figure 3.27).
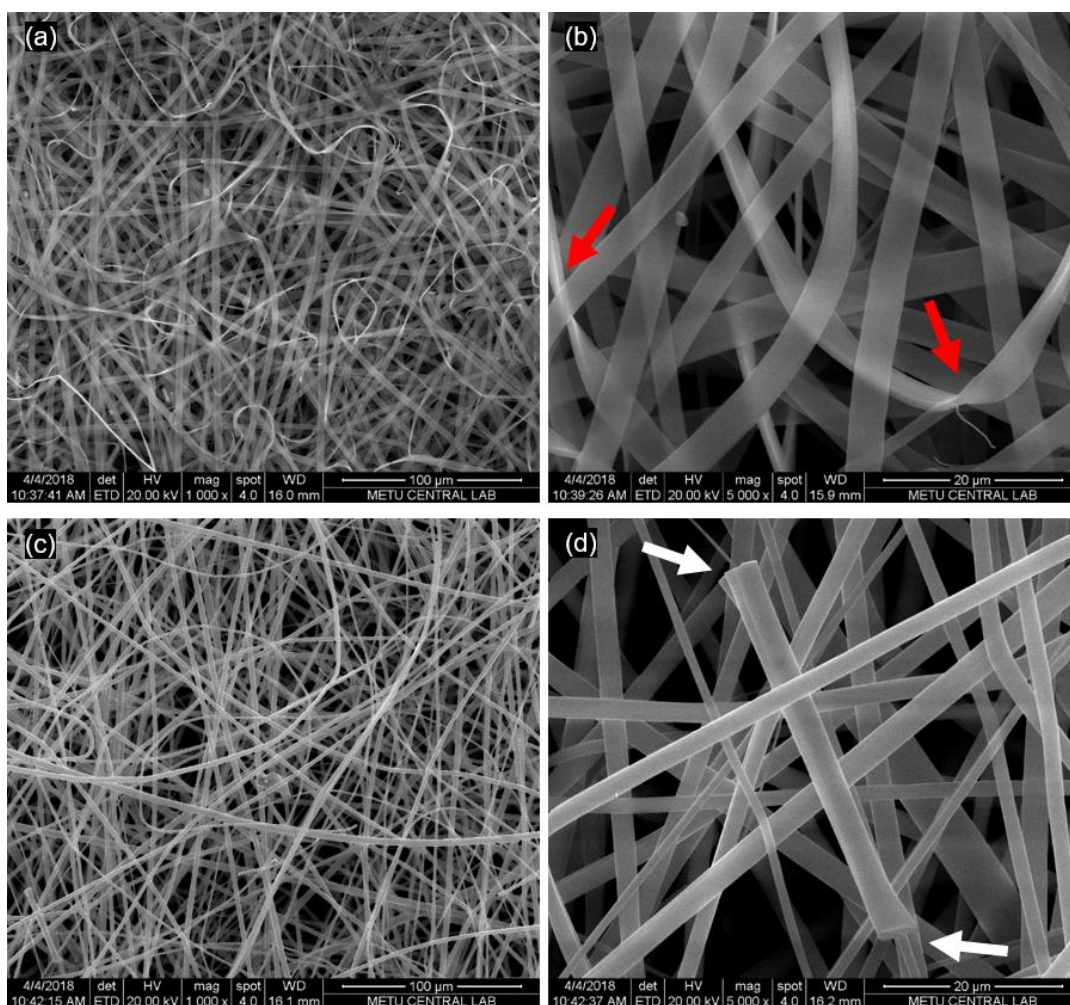
Figure 3.26 SEM images of neat SF (a and b) and neat PMMA (c and d). Red Arrows: Ribbon-like fibers of SF. White Arrows: Broken fiber ends of PMMA.
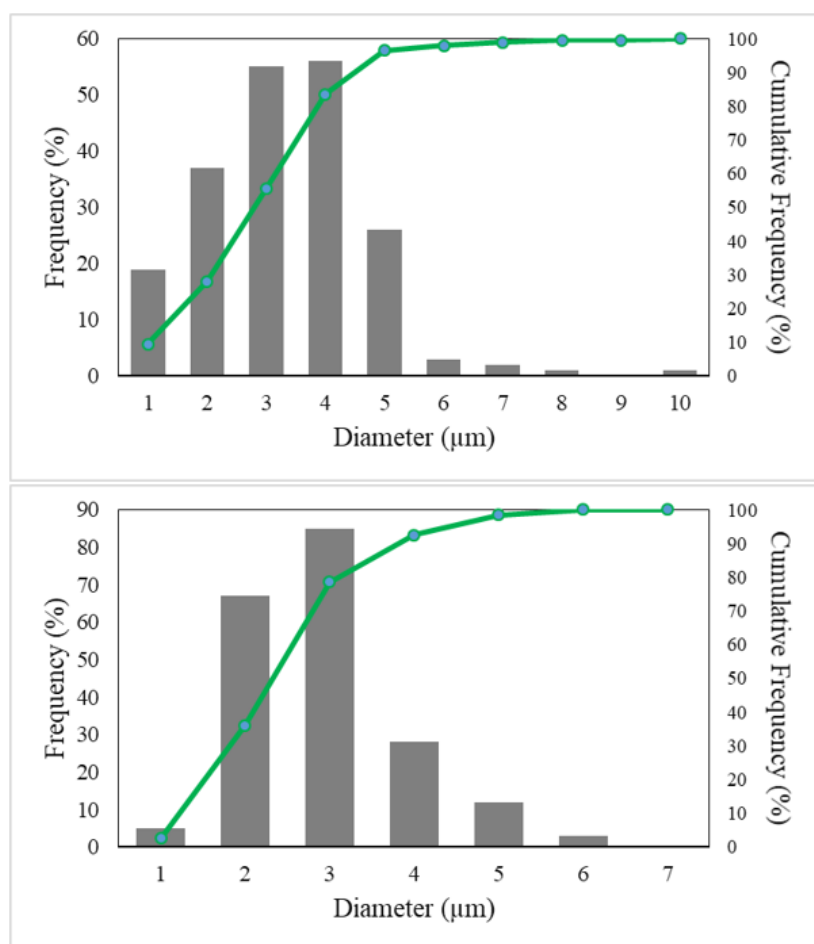
Figure 3.27 Diameter size distribution histograms of SF (top) and PMMA (bottom) fibers with an average diameter size of 2.84 µm ± 1.34 and 2.40 µm ± 0.94, respectively.

Coaxial electrospinning of PMMA (15 w/v %) and SF (9 w/v %) solutions was performed (parameters: 8 mL/h, 10 cm, 20 kV). PMMA/SF core-shell fibers composed of SF (shell) and PMMA (core) were analyzed via SEM. SEM images showed that there was a phase separation between different polymer types with different concentrations (Figure 3.28-top). This might be caused by differences between solutions in terms of concentration and electrical conductivity. Therefore, coaxial electrospinning of PMMA (10 w/v %) and SF (10 w/v %) solutions was performed to test whether concentration difference had any effect on phase

separation. SEM images exhibited that phase separation of solutions were eliminated by this way; however, the bead formation remained (Figure 3.28-bottom).
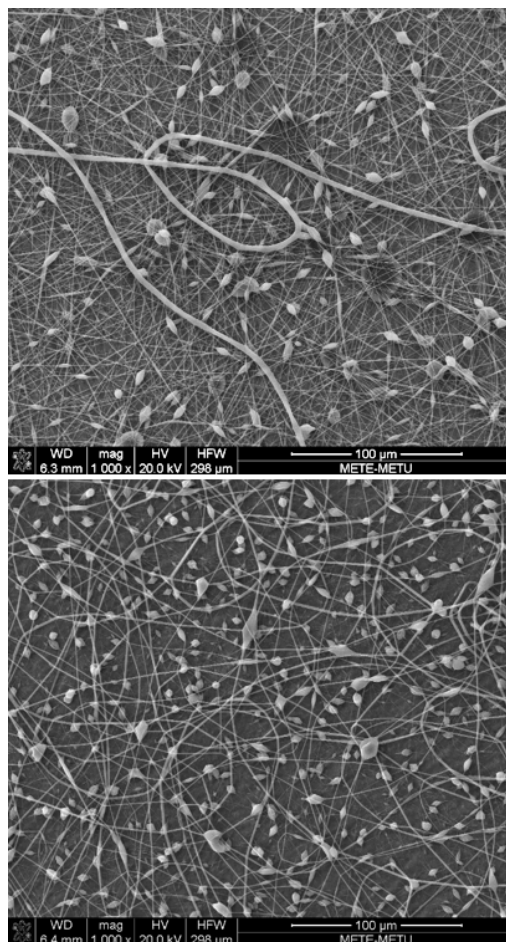
Figure 3.28 SEM images of electrospun PMMA/SF by coaxial electrospinning technique using polymer concentrations of 15% & 9% (top) and (bottom) 10% & 10%, respectively.

The core/shell PMMA/SF fiber formation was optimized by changing two parameters i) the flow rates of PMMA and SF solutions with respect to each other (i.e. 1/2 or 1/3) and ii) the concentrations of PMMA and SF solutions (i.e. 10 & 20 or 9 & 5 wt% respectively) (Figures 3.29&30).

When SF (10 wt%) and PMMA (20 wt%) were used for co-axial spinning, SF and PMMA fibers were observed almost separately instead of uniform core-shell form

(Figure 3.29). PMMA core could not be effectively covered by SF shell for both flow rate ratios, namely 1/2 (Figure 3.29A&B) and 1/3 (Figure 3.29C&D). This phenomenon might be associated with the high viscosity of solutions. Therefore, their concentrations were lowered to 9 and 15 wt% in the following experiments (Figure 3.30). Moreover, the greater difference between the concentrations of PMMA and SF solutions might lead to distinct electrospinning behavior. Thus, the joint action of fibers might not occur under the same electrical field applied. In order to achieve the conflux of the solutions, this gap between PMMA and SF concentrations was tried to be minimized.
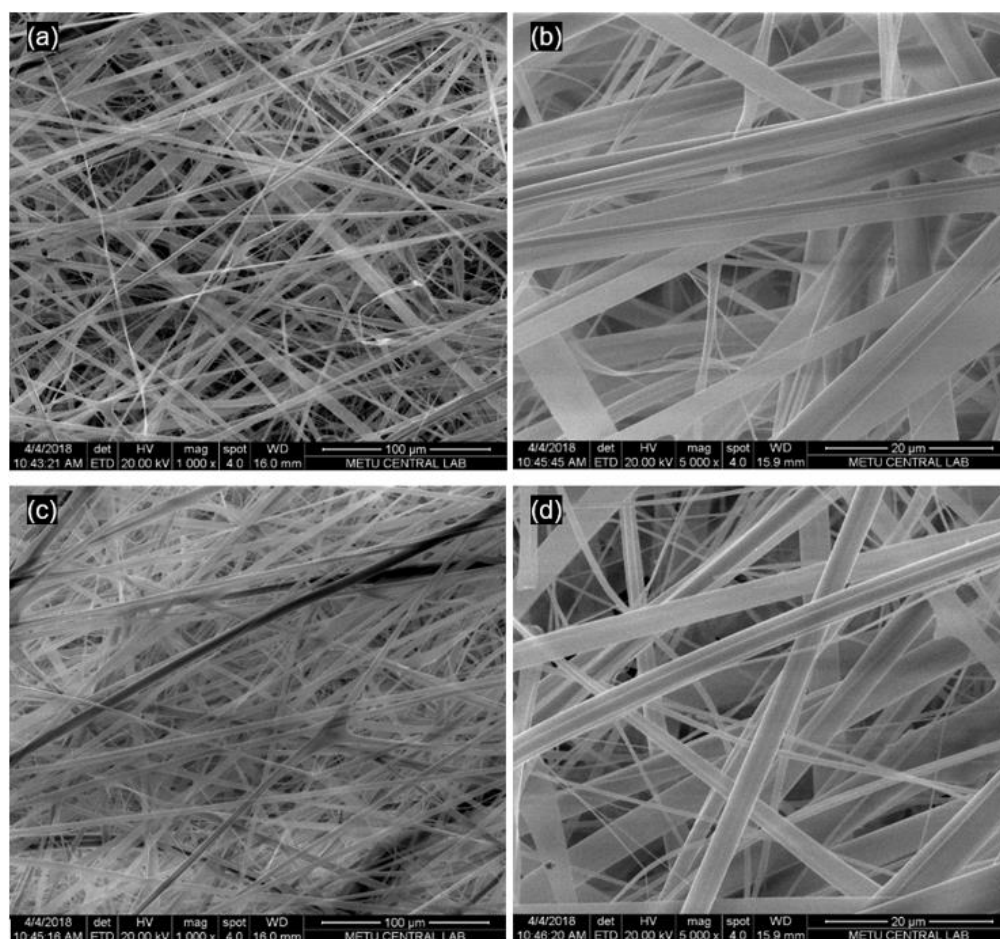
Figure 3.29 SEM images of coaxially electrospun PMMA/SF using SF and PMMA solutions having 10 and 20 wt% concentrations, respectively. The flow rate ratios of SF/PMMA solutions were 2/1 (A&B) and 3/1 (C&D).

When 9 wt% SF and 15 wt% PMMA were used, homogeneity of diameter size distribution and shape of the fibers were improved. However, PMMA core still could not be effectively covered by SF shell when the flow rate ratio of PMMA/SF was 1/2 (Figure 3.30A&B). Finally, uniform morphology was observed when a ratio of 1/3 for PMMA/SF was applied during coaxial electrospinning process (Figure 3.30C&D). Fiber diameter size distribution demonstrated that the average thickness of the core/shell fibers was in between average fiber size of PMMA and SF (Figure 3.31).
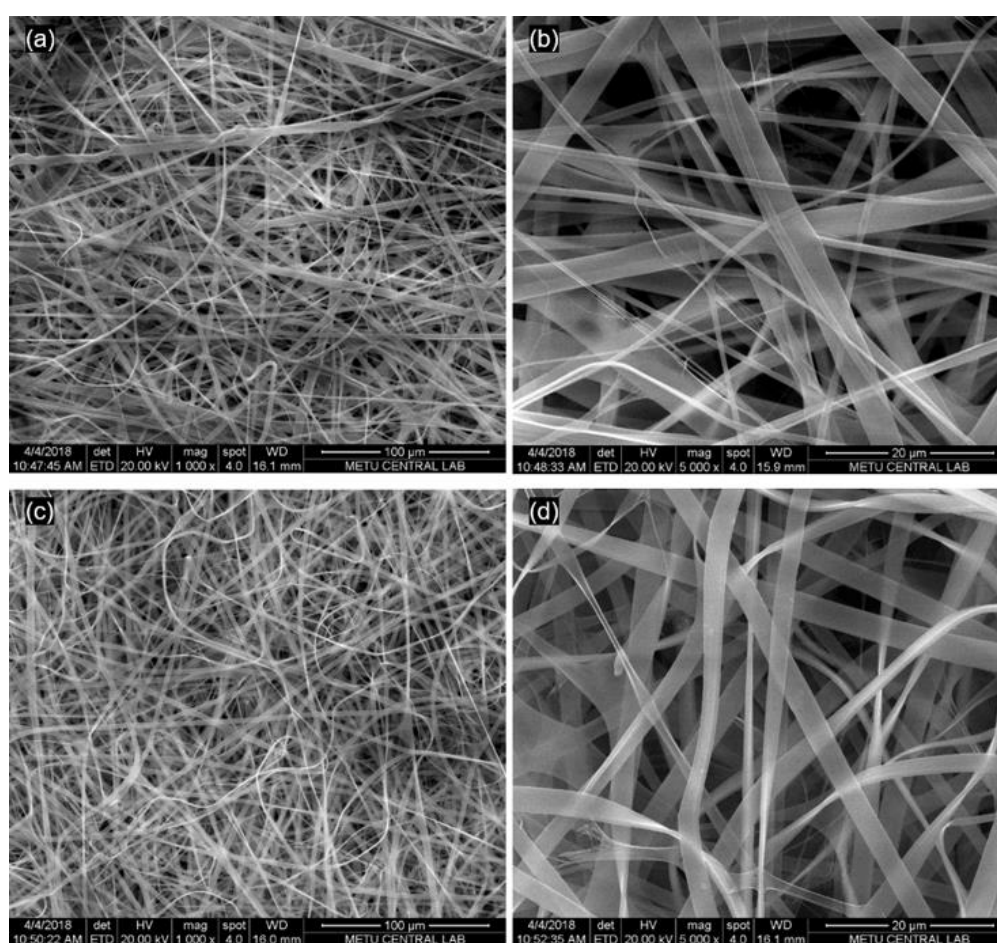
Figure 3.30 SEM images of coaxially electrospun PMMA/SF fibrous meshes using 9 wt% SF and 15 wt% PMMA solutions. The flow rate ratios of PMMA/SF solutions were 1/2 (A&B) and 1/3 (C&D).
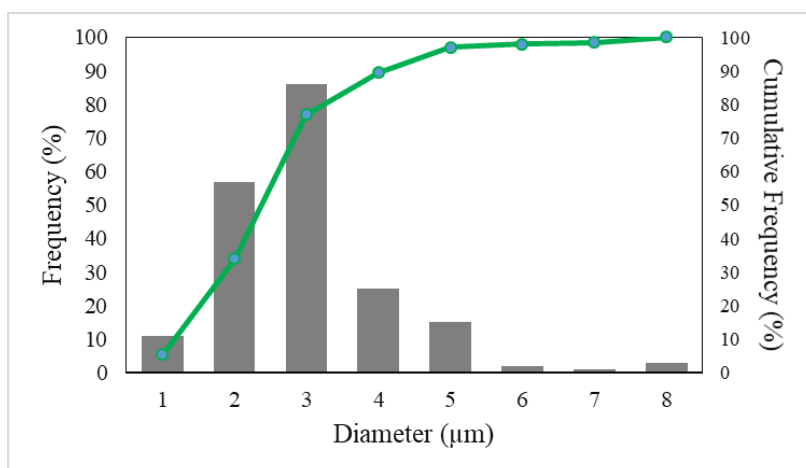
Figure 3.31 Diameter size distribution histogram of PMMA/SF core/shell fibers with an average diameter size of 2.51 µm ± 1.18.

Furthermore, collector shape and distance were altered to produce applicable fiber mats. Rotated drum was used to obtain fibers deposited in a bigger area (Figure 3.32-left). However, they could not be removed from the aluminum collector intact. Alternatively, aluminum plate was utilized in vertical configuration (Figure 3.32-right). Fibers were obtained in a smaller area with an increased thickness for the same volumes of electrospinning solutions. In this version, the electrospun layer could be removed in one piece; however, deformation still occurred and the mesh could be obtained as a layer with inhomogeneous topography.

Alternatively, different types of collector coverages were examined to minimize the adhesion of fibers to the aluminum cover. Filter paper covered metal collector was used to ease the detachment of the mesh. However, fibers were even more tightly attached onto the paper. Then, brushed metal coverage was used; nonetheless, sufficient improvement could not be achieved concerning the removal of fibers.
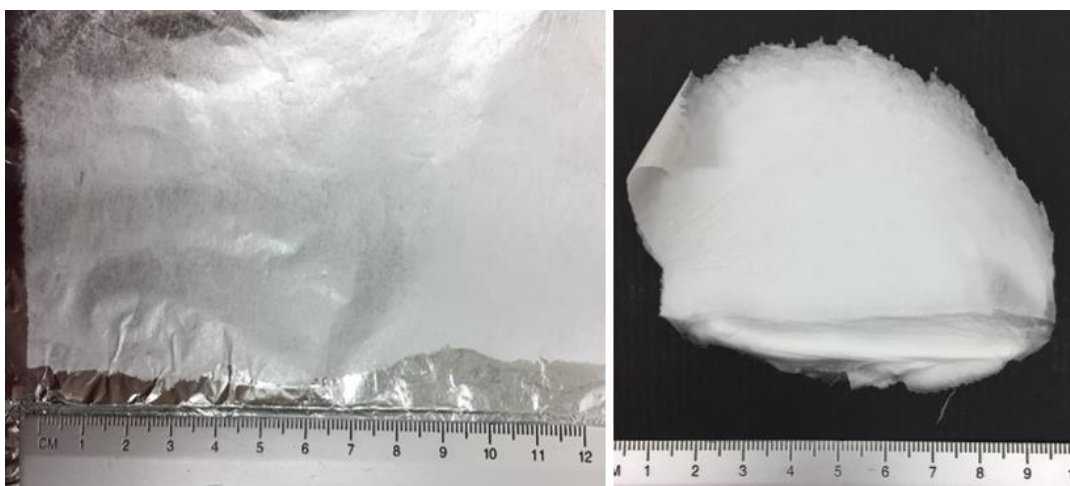
Figure 3.32 PMMA/SF fibrous structures fabricated via coaxial electrospinning technique by using rotating drum collector (left) and vertically positioned collector (right).

In order to obtain non-deformable and homogeneous meshes, a custom-made collector screen was designed by using 3 aluminum plates. The metal plates were attached to each other in a way that the surface for fiber deposition was positioned in negative degree to the syringe axe. Thus, smooth and detachable meshes could be obtained (Figure 3.33). The mesh was removed properly (Figure 3.33-left) and its thickness did not significantly vary along its cross-sectional length (Figure 3.33-right). Moreover, these meshes did not bend spontaneously withstanding against gravitational forces; yet could be bent in purpose. Therefore, it can be interpreted that these meshes were stable and flexible in combination owing to the properties of PMMA and SF, respectively.
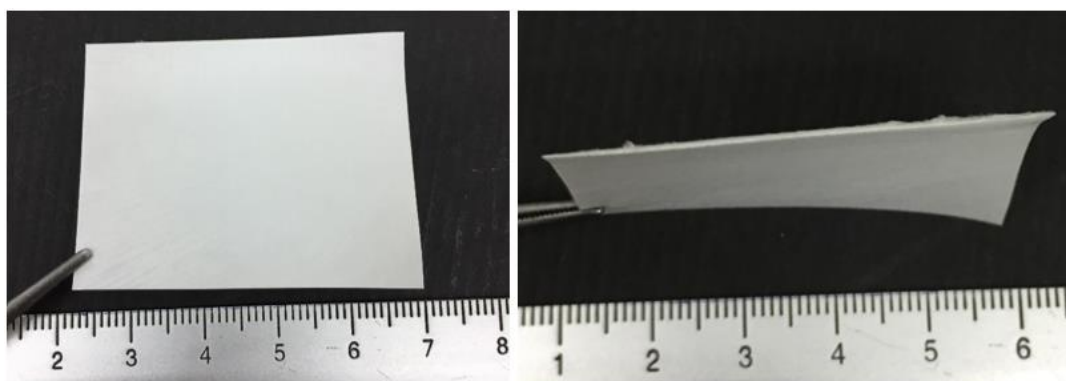
Figure 3.33 PMMA/SF fibrous structures form the surface (left) and cross-sectional view (right) fabricated via coaxial electrospinning technique by using collector in the tilted position.

3.2.1.1.4 Mechanical Tests

Results of mechanical tests are shown in Table 3.1. Neat PMMA meshes exhibited lower UTS value than that of neat SF due to brittleness of PMMA so that PMMA immediately ruptured. UTS values of PMMA/SF fibers were significantly higher than that of neat components which indicated that flexibility of PMMA mesh was improved against tensile forces with the incorporation of SF. Elastic modulus of PMMA/SF mats confirmed this improvement. Neat PMMA and PMMA/SF mats had similar tensile moduli while neat SF had nearly half of their value. It pointed out that SF addition in coaxially electrospun fibers did not significantly change the modulus while having positive impacts on UTS. The superior deformation capacity of SF was obvious in percent strain values of neat SF (around 90%) which was drastically higher than PMMA-containing other groups.

Table 3.1 Mechanical test results of electrospun meshes.

Experimental Groups	UTS (kPa)	Elastic Moduli (kPa)	Strain (%)
Neat PMMA	11.5±1.8	58.2±4.7	3.7±0.5

Neat SF	29.2±3.4	20.9±3.1#	91.8±4.2
PMMA/SF	47.6±3.5	53.6±0.9	16.6±2.9

UTS values were statistically different. # denotes statistically the lowest group. Strain values were statistically different ($p < 0.05$).

During mechanical tests, the flexibility of SF fibers was observed by its stretching whereas PMMA fibers fragmented due to its brittleness (Figure 3.34). On the other hand, PMMA/SF fibers did not deform by stretching or fragmenting as the SF or PMMA fibers did, instead of that, stayed intact until being ruptured at the middle.
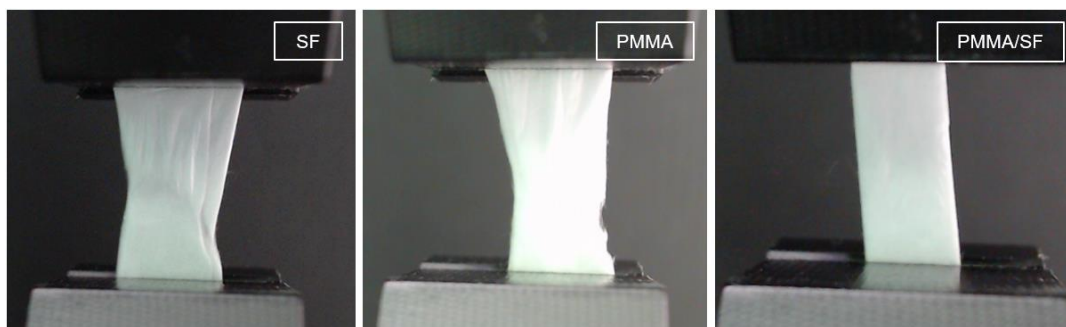
Figure 3.34 Images taken during the tensile tests conducted for the SF, PMMA, and PMMA/SF electrospun meshes.

3.2.1.1.5   Water Contact Angle Measurements

Water contact angle measurements for SF, PMMA, and PMMA/SF mats are shown with representative images (Figure 3.35). The contact angle of SF meshes was calculated as 58.03° ± 5.3 (Figure 3.35A) which was consistent with the hydrophilic nature of SF structures reported in the literature such as contact angles of wild type SF (67.2° ± 0.8) (Kambe, Yamamoto, Kojima, Tamada, & Tomita, 2010), as-cast SF films (51.4° ± 2.6) (H. J. Jin et al., 2005), and pure SF nanofibrous scaffolds (~0°) (K. Zhang et al., 2010). It was obvious that porosity affected the water contact angle of the same biomaterials. Since our electrospun SF meshes has a ribbon-like

microfibers, their porosity was probably lowered; thus, they became moderately hydrophilic when compared to its nanofibrous form (max) or its wild type (min).

The contact angle of PMMA meshes was calculated as $133.12° \pm 4.1$ (Figure 3.35B) because of its hydrophobicity (H. Wei, Zhang, Cheng, Cheng, & Zhuo, 2007). In other studies, the contact angle was determined as 83° for untreated surface of PMMA (Vesel & Mozetic, 2012) and 68° for PMMA films (Ma, Cao, Feng, Ma, & Zou, 2007). This hydrophilicity of PMMA of smooth surfaces was related to the dipole–dipole interactions (Ochoa, Masuelli, & Marchese, 2003). On the other hand, it was reported that surface roughness increased hydrophobicity of the structures (Jiang, Zhao, & Zhai, 2004) such as roughness is created by electrospinning. It was shown that the hydrophilic PMMA films (68°) were converted into super-hydrophobic surfaces (~154°) by the cooperation of the micro/nano-structure and the side group reorientation in the PMMA chains at the topmost (Ma et al., 2007).

In our core-shell PMMA/SF mats with water contact angle was $140° \pm 1.9$ (Figure 3.35C), although the SF-coating has a hydrophilic nature, the PMMA/SF mats exhibited hydrophobic characteristics. This might be due to the entrapment of the surface energy of SF by PMMA core since lowered surface energy causes increment of hydrophobicity (Jiang et al., 2000). Another reason for this phenomenon could be the previously mentioned structural effect (Ma et al., 2007). In other words, the hierarchical micro/nano-roughness was enhanced hydrophobicity further due to its wider fiber diameter distribution than that of PMMA.
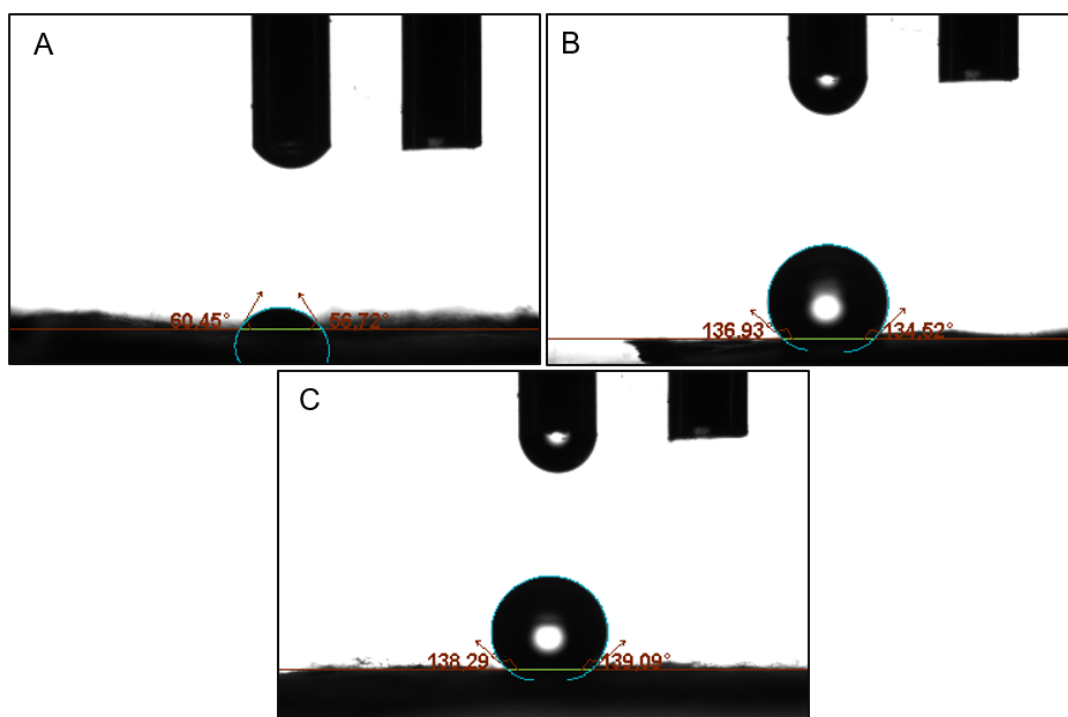
Figure 3.35 Representative images of water contact angles measurements for SF (A), PMMA (B), and PMMA/SF (C) mats.

3.2.1.1.6 *In Vitro* Degradation

The percent weight loss of the SF, PMMA, and PMMA/SF mats was measured in different environments (Figure 3.36). In lysozyme solution, the SF mats lost more than 50% of their initial weights in one day while PMMA (25.13%) and PMMA/SF (27.68%) mats could maintain their structural stability more (Figure 3.36A). It was reported that egg white lysozyme exerts β-glucosaminidase action (Berger & Weiser, 1957) so that it increases the protein degradation (Figure 3.36A). However, lysozyme does not exert α-glucosidase, amylase, lipase, protease, and phosphatase activity (Meyer, Palmer, Thompson, & Khorazo, 1936); therefore, degradation behavior in lipase was also examined (Figure 3.36B). During the lipase incubation, the meshes exhibited a similar trend of degradation with respect to each other. However, PMMA

111

containing mats degraded slightly faster than the neat SF in lipase when compared to the rate in the lysozyme environment.

In vitro degradation of mats in PBS was also examined to study hydrolytic degradation (Figure 3.36C). All the mass losses were observed on the first day for the groups and no significant change was observed during the rest of incubation period. The weight losses of the SF, PMMA, and PMMA/SF were 51, 10, and 48% respectively. These weight loss results demonstrated that the SF mesh that is not crosslinked could conserve about 40-50% of its initial mass in an environment with or without enzyme. However, the PMMA mesh could not degrade more than about 10% of its initial weight in the absence of the enzyme. On the other hand, the degradation profiles of the PMMA/SF mats might be tailored easier that the neat forms of its components since various parameters such as ratio of electrospinning solution of the two components can be altered, hence, the degradation profiles change accordingly.
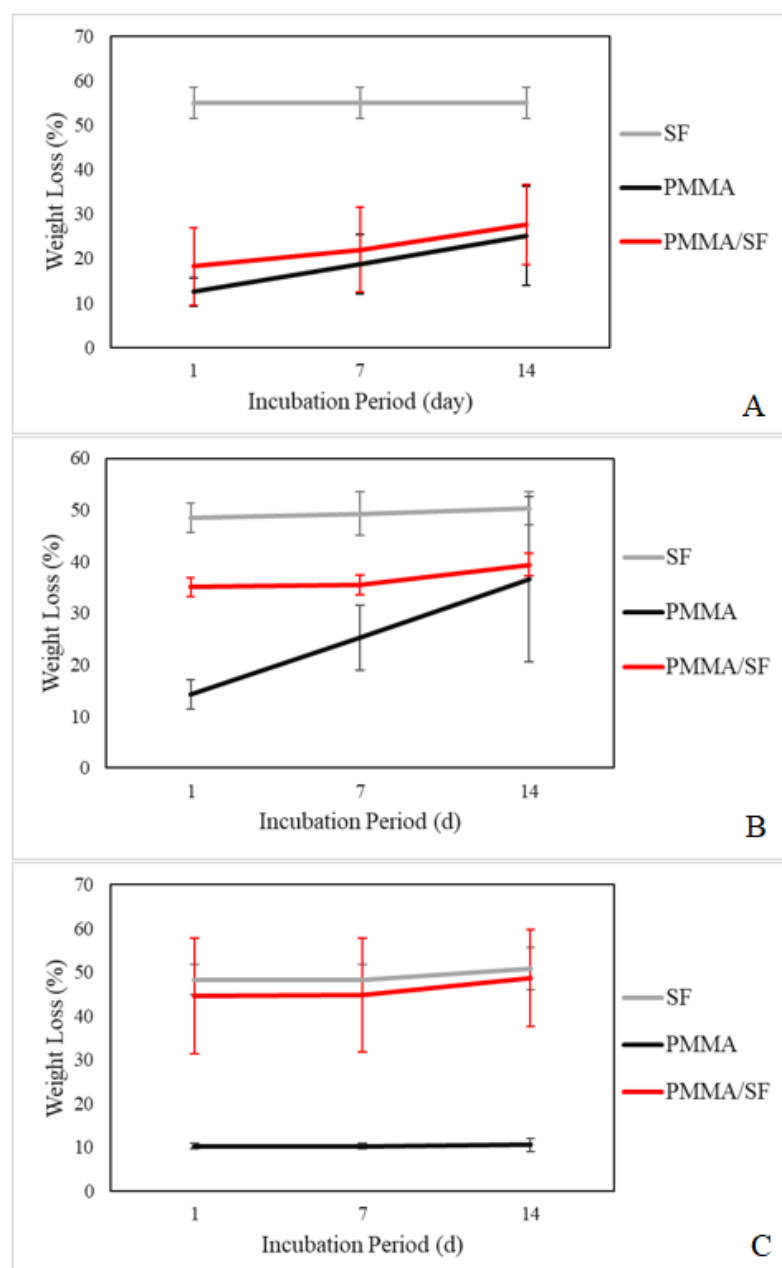
Figure 3.36 *In vitro* degradation of the SF, PMMA, and PMMA/SF electrospun meshes in lysozyme (A), lipase (B), and PBS (C) (n=3).

pH change was recorded in different incubation media (Figure 3.37). In the lysozyme environment, there was no significant difference among the groups which showed lysozyme did not have a selective attack for the specific groups of these materials. However, a slight decrease in pH was observed for PMMA/SF groups in lipase

solution. In PBS, PMMA mats were much stable and weight loss was lower than observed for SF-containing groups. The mats could have different degradation profiles when implanted in different body parts so that the tissue-specific degradation tests should be performed. In our condition, dental tissue contains lower amount of lysozyme activity (Quintarelli & Dellovo, 1963) so that PMMA/SF mats will probably withstand the enzymatic degradation in tooth.
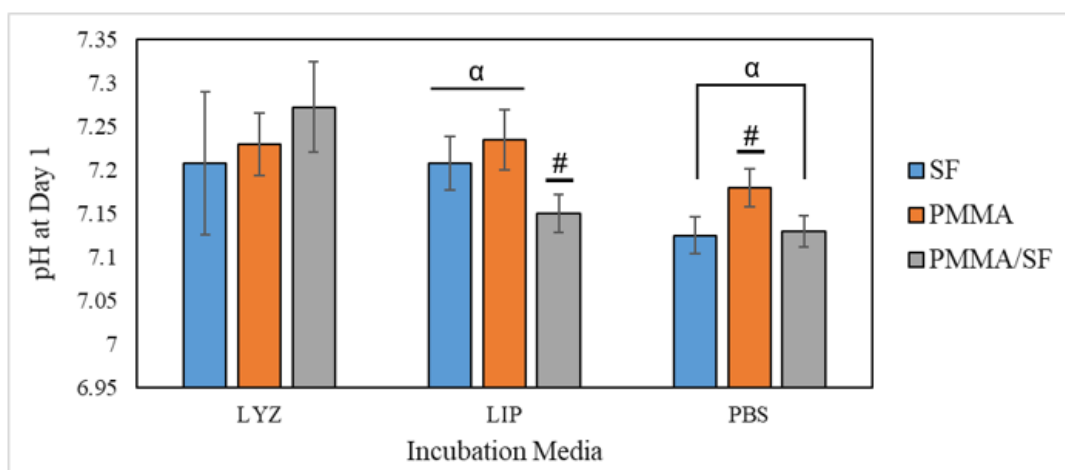
Figure 3.37 pH change of lysozyme, lipase, and PBS media at day 1 in which the SF, PMMA, and PMMA/SF electrospun meshes were incubated at 37°C. "α" denotes the groups statistically different than "#" groups ($p < 0.05$) for that specific media (n=3).

SEM images of SF, PMMA, and PMMA/SF meshes were obtained after two weeks of incubation in PBS to determine morphological alterations in the fibrous structures (Figure 3.38). It was observed that SF fibers did not preserve their ribbon-like fiber form and they fused (Figure 3.38A). This indicated SF could attach and make new bonds among each other and stay intact. On the contrary, PMMA fibers were observed in the same morphology before and after incubation (Figure 3.38B) which showed that the PMMA fibers degraded homogeneously from the fiber surfaces without being fused to each other. In the core-shell form of the PMMA/SF mats, the individual fibers could be differentiated (Figure 3.38C). However, the SF-shell of the fibers were fused at the intercept points of the network while the PMMA-core

114

acted as a separating backbone leading to conservation of porous architecture of the meshes.
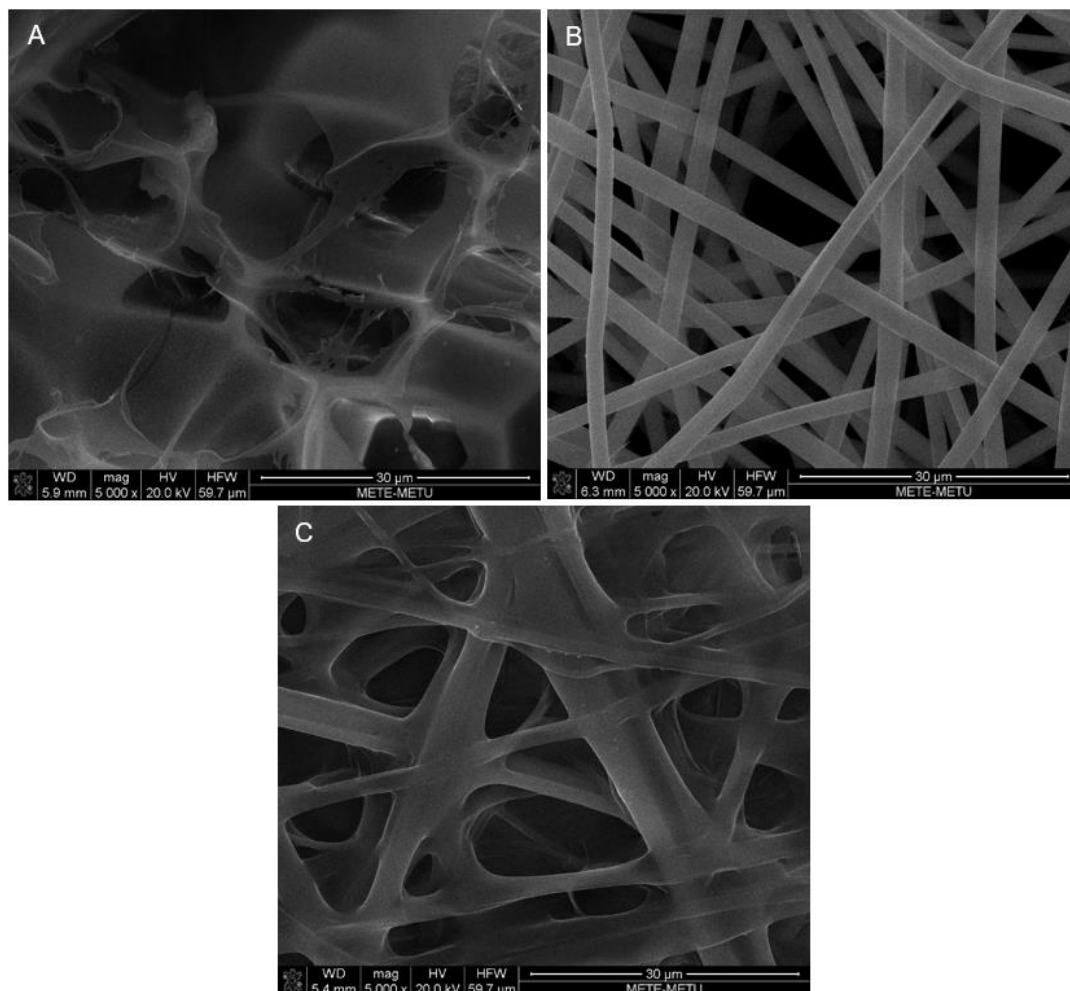
Figure 3.38 SEM images of SF (A), PMMA (B), and PMMA/SF (C) meshes after 14 days of incubation in PBS.

3.2.1.1.7 *In Vitro* Water Uptake Capacity

Water uptake percentages of SF, PMMA, and PMMA/SF incubated in PBS at 37°C for 14 days are given in Figure 3.39. The water uptake capacity of SF mats was 523.1% at day 1 due to dramatic loss of its fibrous structure whereas that value of PMMA mats was 703.3% in agreement with the effect of interconnected pores and

holes within PMMA fibers on hydrophilicity of PMMA surfaces (Varagnolo et al., 2017). For the PMMA/SF mats, that capacity was remarkably amplified up to 1678.6%. Even though the SF meshes should have had the highest capacity to hold water because of its hydrophilicity, the water retention capacity of PMMA/SF was recorded as the highest (~17 fold of its own weight at day 14). This was correlated with the combinational impact of inner porosity-surface hydrophilicity of the PMMA/SF fibers on the water uptake ability. Thus, PMMA/SF preserved its porosity by the help of the PMMA-core and provided a moderate hydrophilicity by the help of the SF-shell.
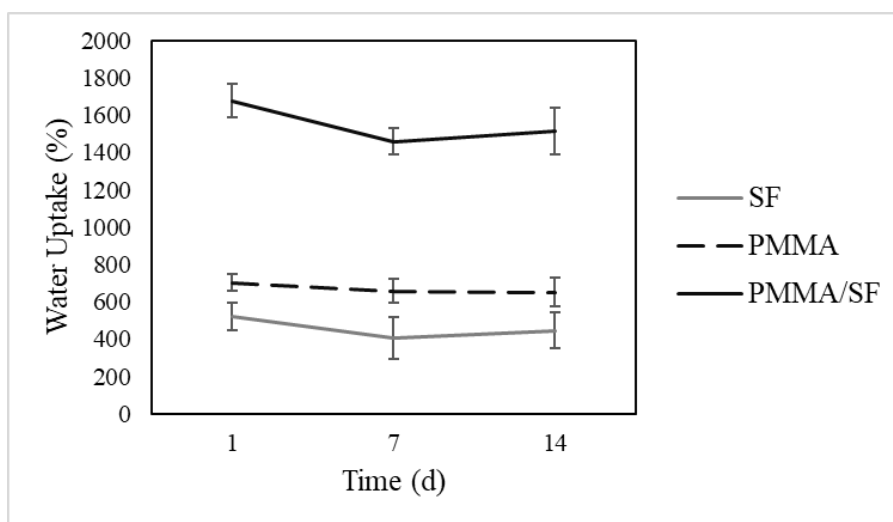
Figure 3.39 Water uptake capacity of the SF, PMMA, and PMMA/SF electrospun meshes in PBS (n=3).

3.2.1.1.8 X-Ray Photoelectron Spectroscopy (XPS)

XPS analyses were conducted to study the chemical composition on the surface of neat SF, neat PMMA, and PMMA/SF coaxially electrospun samples. Besides the neat forms, coaxially electrospun PMMA/SF: 1/2 and 1/3 were examined (Figure 3.40&41) to detect whether PMMA and SF were present at the same spot of PMMA/SF. Otherwise, it could be interpreted that phase separation might occur

116

between PMMA and SF which might be a sign of improper coaxial electrospinning of PMMA/SF.

In SF group, carbon 1s, oxygen 1s, and nitrogen 1s peaks were detected having the atomic percentages of 63.8, 21.2, and 15.0% respectively (Figure 3.40-top). These results were consistent with the unmodified SF films (Bai et al., 2008) and pure electrospun SF nanofibers (K. Zhang et al., 2010) which showed SF was obtained successfully and electrospun without impurity. For the PMMA mats, carbon 1s and oxygen 1s peaks were detected having the atomic percentages of 73.1 and 26.4% respectively (Figure 3.40-bottom). These specified peaks in the XPS spectrum of PMMA were observed (Schulz, Munzert, & Kaiser, 2001). Residual amount of fluorine (F 1s) appeared in the PMMA spectrum. This element might be contributed to the structure during the application of HFIP due to incomplete evaporation and/or incorporation of F atoms into the polymeric chain, which could be considered as negligible (0.5%).

The molecular weight of the components is also one of the important factors for controlling phase separation (L. Li et al., 2011). The morphology of the nanofibers in the presence of phase separation was dependent on the relative ratio of the two polymer components with different Mw (M. Wei, Kang, Sung, & Mead, 2006). Nanofibers composed of high content of polymer with high Mw exhibited co-continuous structure, whereas, the phase morphology, a measure of homogeneity/continuity properties of polymer blends (Mekonnen, Misra, & Mohanty, 2015), changed from co-continuous to core-sheath structure when increasing the content of polymer with low Mw (M. Wei et al., 2006). SF is a high Mw polypeptide composed of 25 kDa (light-chain), 325 kDa (heavy-chain) (H.-J. Jin & Kaplan, 2003) compared to high Mw PMMA (200 kDa). Thus, since PMMA had a lower Mw than that of heavy chain of SF, it partly diffused into the SF-shell layer rather than staying in the core part. Even though, the light chains of SF (25 kDa) would be presented onto the surface of PMMA/SF fibers, there would be a blend of SF and PMMA chains. XPS spectra of two types of PMMA/SF mesh

electrospun with the flow rate ratios of SF/PMMA: 2/1 and 3/1 were examined (Figure 3.41) to understand whether the PMMA core could be covered by SF shell efficaciously. The relative increase in the N 1s peaks from 12.3 to 18.4 % belonging to the SF layer (Figure 3.41-top and bottom, respectively) demonstrated that the fibers were covered more with SF nearly as expected as 2/3 ratio which was calculated in a similar way in the literature (Cai et al., 2002). The other atomic percentages exhibited the blend amount since they were common both for SF and PMMA.
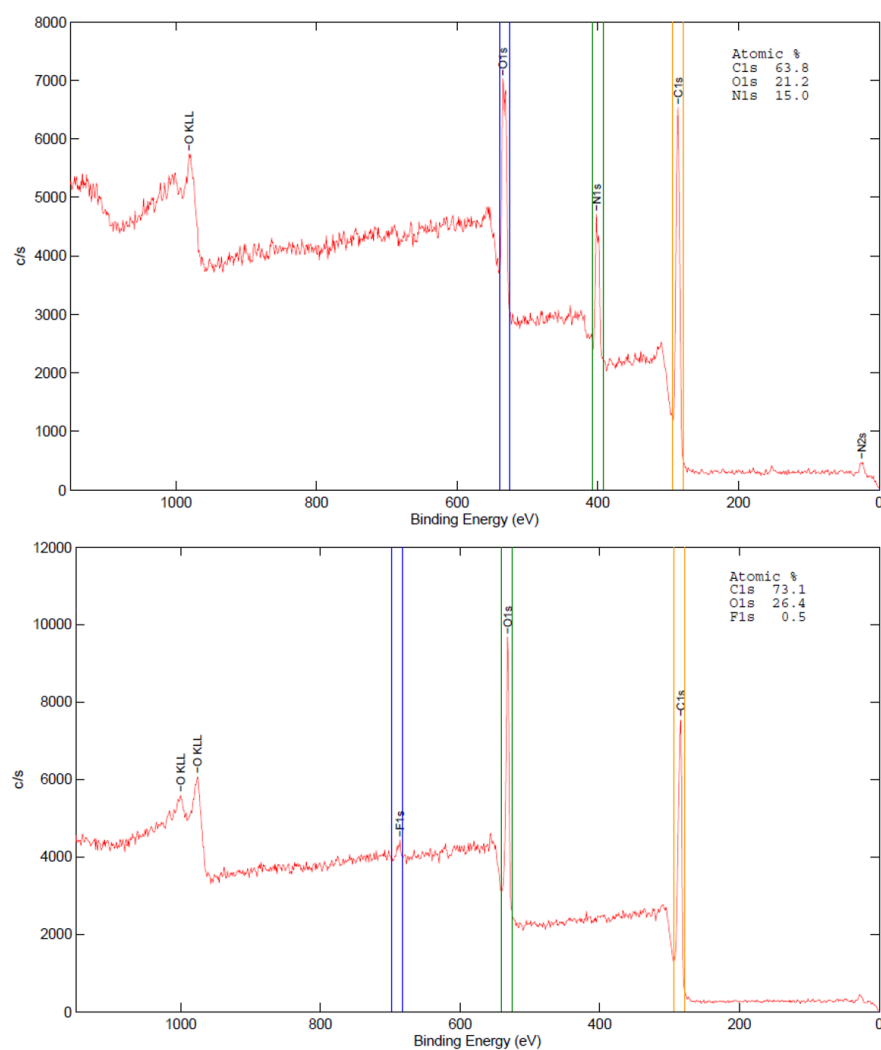
Figure 3.40 XPS spectra of neat SF (top) and neat PMMA (bottom) electrospun mats.
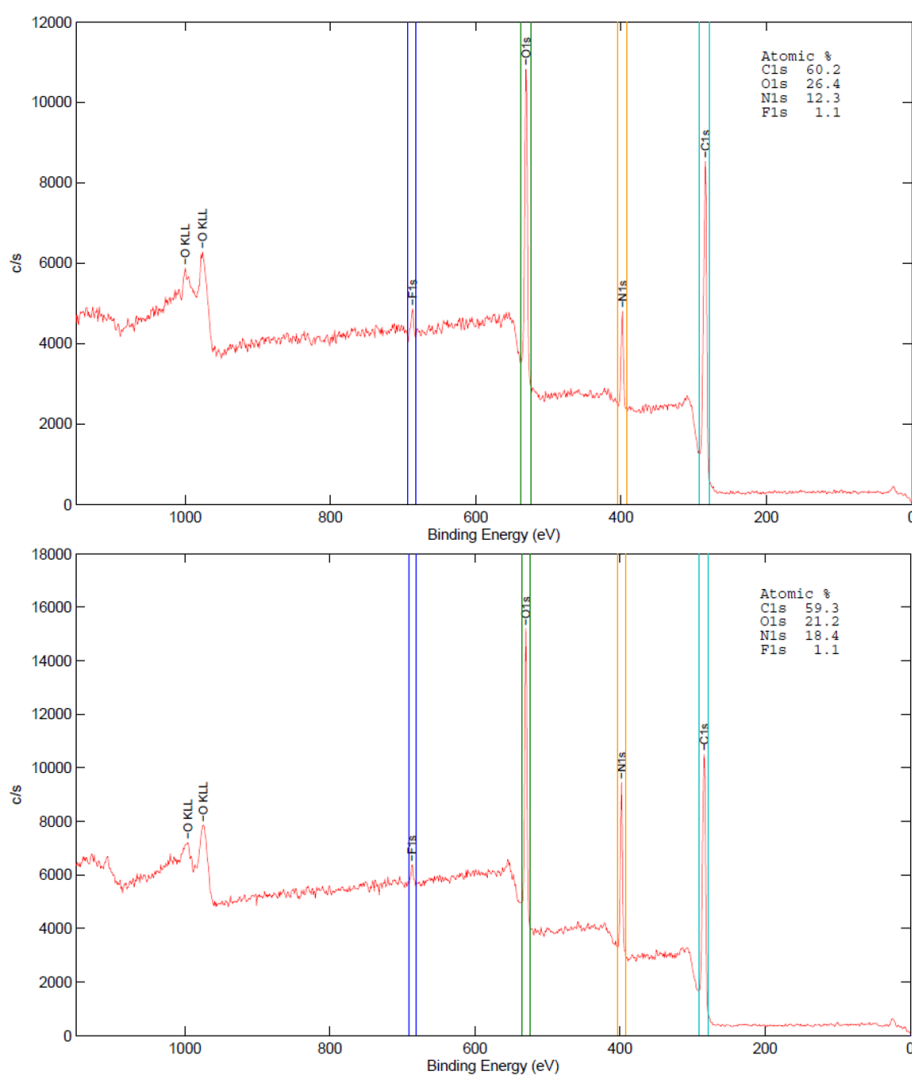
Figure 3.41 XPS spectra of the coaxially electrospun PMMA/SF mats with flow rate ratios of 1/2 (top) and 1/3 (bottom).

3.2.1.1.9 Thermo-Gravimetric Analyses (TGA)

TGA analyses were performed to study the thermal properties of the neat SF, neat PMMA, and PMMA/SF meshes (Figure 3.42). The thermogram of SF included 2 main regions of weight loss clearly seen as the derivative weight change peaks (Figure 3.42-top). In the first loss region appearing within 35-40°C and 100-110°C, water evaporation originating from moisture was observed (Motta, Fambri, &

Migliaresi, 2002). The greatest mass loss rate was observed around 280-350°C which corresponded to fibroin decomposition which involved the breakdown of both i) side chain groups of amino acid residues and ii) peptide bonds of the backbone chain (Freddi, Tsukada, & Beretta, 1999). The remaining amount of SF was 38.7% of its total weight above 600°C which was higher than the remaining mass of electrospun nano-SF (28.5%) at 600°C in another study (K. Wei et al., 2011) which could be associated with a higher level of β-sheet conformation of our SF isolated (Um, Kweon, Park, & Hudson, 2001).

The thermogram of PMMA included 3 regions of weight loss exhibited by derivative weight line (Figure 3.42-bottom). The moisture loss was not observed at the interval of 35-40°C and 100-110°C since PMMA was not hydrophilic. However, a slight mass loss detected above this temperature interval could be related with loss of other low temperature volatile species as reported in the literature (Motta et al., 2002). The gradual decrease in mass at 245-290°C displayed the thermal stability of PMMA with the weak links seen in the radical-polymerized PMMA (Hu, Chen, & Wang, 2004). Prior to the cleavage of head-to-head bonds, removal of these weak links occurred which were defined as the principal initiation sites of degradation (Kashiwagi et al., 1986). Next, the weight loss observed above 300°C showed the degradation of PMMA which was reported to begin at 294°C and finish at 404°C in the literature. (Yunhua Yang & Dan, 2003). However, 13.9% of its mass was still conserved at 600°C in our PMMA thermogram.
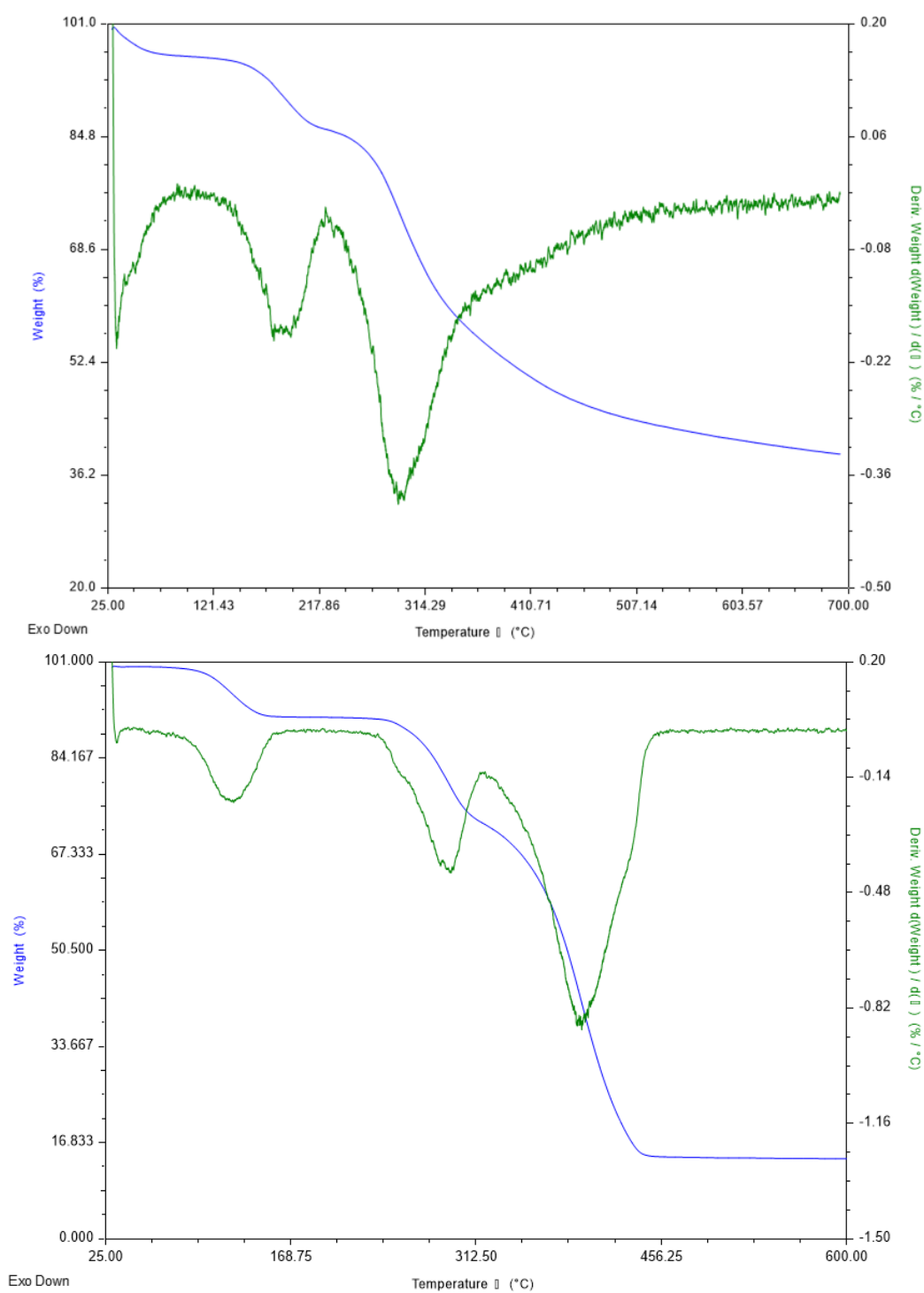
Figure 3.42 TGA curves of neat SF (top) and neat PMMA (bottom) electrospun meshes.

The thermal stability of core-shell PMMA/SF mesh was examined (Figure 3.43). TGA curve of PMMA/SF pointed out that the SF and PMMA components of the structure resulted with a hybrid diagram of degradation. The moisture loss, the loss of residual species, the degradation of SF, and two-step decomposition of PMMA had cumulative effects on the TGA curve of the PMMA/SF mat. The maximum weight loss was recorded in the interval of 290-350°C that corresponded to the overlapping events of backbone decomposition of SF and PMMA. Nonetheless, PMMA/SF continued to lose its weight beyond the point that 13.9% of its weight was left which was the limit for PMMA degradation and this limit was even higher for SF (38.7%). However, the PMMA/SF mats lost its total weight at around 600°C. This unexpected phenomenon could be governed by the distraction of the intramolecular interactions between the same type of polymeric chains with themselves (e.g. β-sheet formation among SF chains). Hence, it might lead to a higher degradation rate due to blending at the interface between the core and the shell.
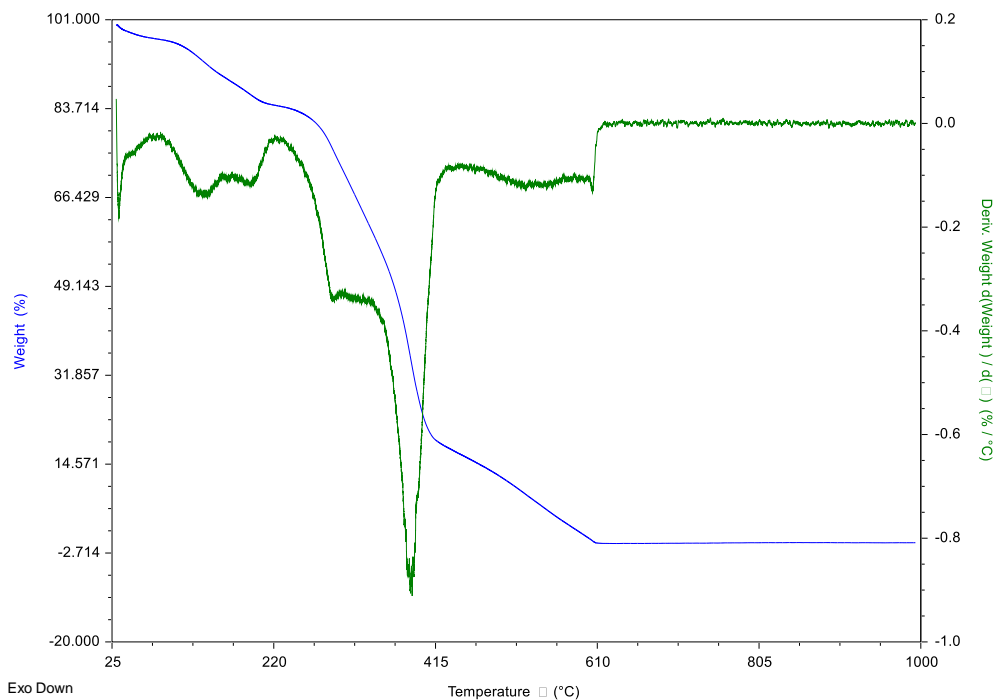
Figure 3.43 TGA curves of the PMMA/SF core-shell meshes.

3.2.1.1.10 Fourier-Transform Infrared-Attenuated Total Reflectance (FTIR-ATR) Spectrophotometry

The FTIR-ATR spectra of SF, PMMA, and PMMA/SF meshes were compared to determine the existence of the specific chemical bonds for the mats (Figure 3.44). The SF meshes exhibited both the amorphous form of random coil of fibroin (α-form: 1538 cm^{-1}) and the antiparallel β-pleated sheets (β-form: 1658 and 1652 cm^{-1}) which were specific to SF (H. J. Jin et al., 2005) (Figure 3.44A). In the spectrum of PMMA, the peaks of CH stretching at 2951 cm^{-1}, C=O stretching at 1721 cm^{-1}, CH_3 stretching at 1449 cm^{-1}, and $-O-CH_3$ stretching at 1159 cm^{-1} were observed that were assigned to the specific peaks of PMMA (Ramesh, Leen, Kumutha, & Arof, 2007) (Figure 3.44B). The FTIR spectrum of PMMA/SF mesh contained all of the peaks assigned for SF and PMMA (Figure 3.41C).
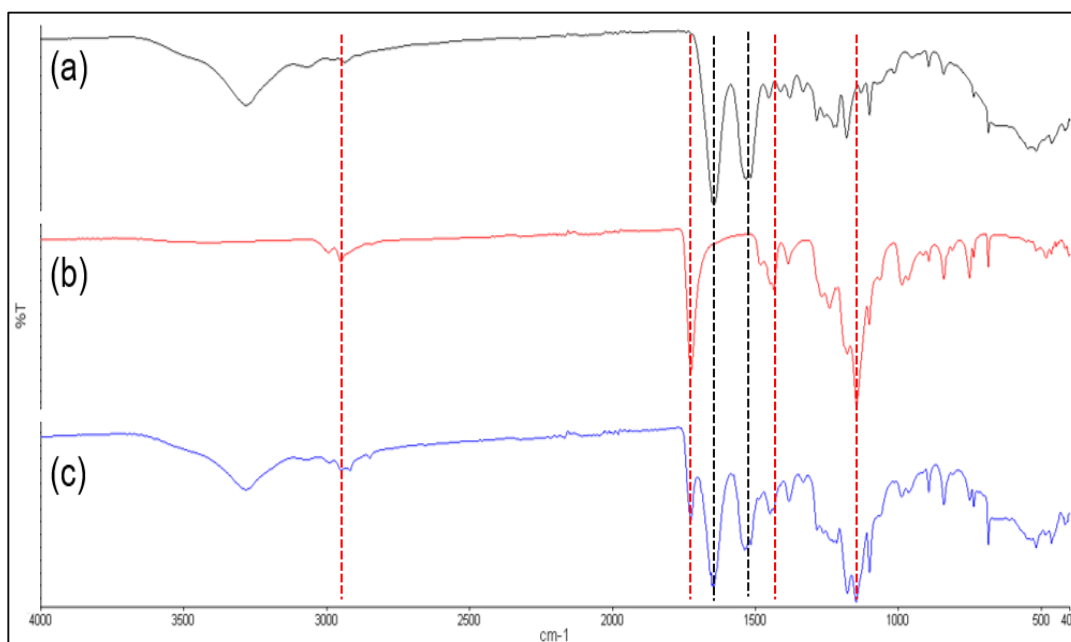
Figure 3.44 FTIR-ATR spectra of SF (A), PMMA (B), and PMMA/SF (C) meshes (Black and red lines represents the peaks assigned to SF and PMMA, respectively).

3.2.1.2 Characterization of GelMA/PecTH Hydrogels

3.2.1.2.1 Proton Nuclear Magnetic Resonance (^{1}H-NMR) Spectroscopy of GelMA

Degree of methacrylation (DM) is defined as the number of methacrylated groups attached to Gel divided by the total number of amine groups (lysine, hydroxylysine) of Gel prior to the reaction (Hoch et al., 2012). Phenylalanine signal (6.9–7.5 ppm) is related with the concentration of the Gel, and the spectra were normalized using MestreNova NMR analysis program. Then the integrated areas of lysine methylene signals (2.8–2.95 ppm) of Gel and GelMA spectra were obtained (Figure 3.45). The expanded region between 5 and 6 ppm in the GelMA spectrum is shown at the inset. Peaks formed between these regions after methacrylation indicate the incorporation of double bonds into the Gel structure. In the Figure 3.42-top, NMR spectra for Gel was presented. NMR results showed that GelMA had about 62.5% DM when the methacrylation reaction was stopped in 1 h; however, 71.9% DM was reached when the methacrylation reaction was stopped in 3 h. Therefore, the last one was used for the following procedures.
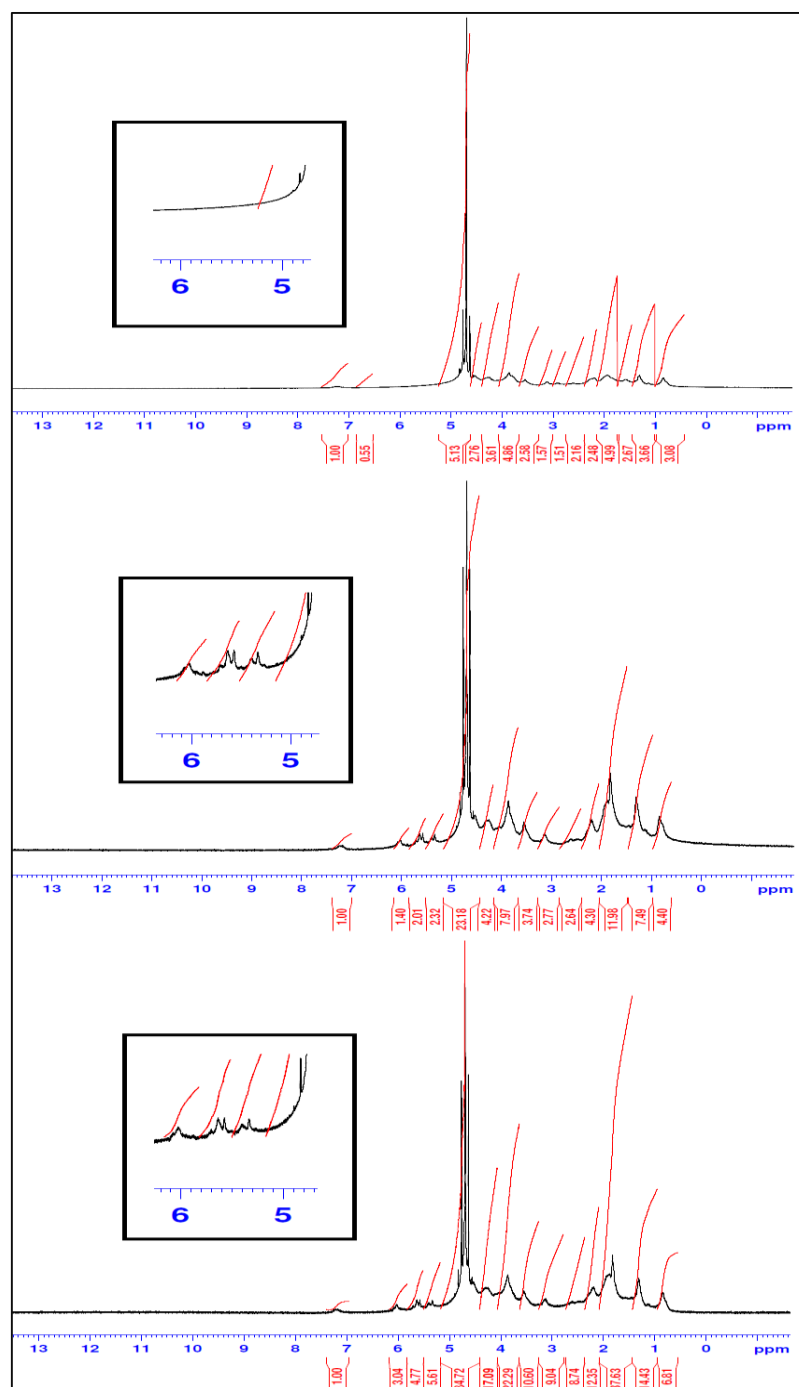
Figure 3.45 ^{1}H-NMR spectra of Gel (top) and GelMA after 1 h-rxn (middle) and 3 h-rxn (bottom).

3.2.1.2.2 Fourier Transform Infrared (FTIR) Spectroscopy of PecTH

FTIR spectrum of Pec and PecTH in the frequency region from 4000 to 500 cm^{-1} is given (Figure 3.46). The IR data of thiolated pectin was as follows: 2573 (SH stretch, weak band, of mercaptans), 1739 (CO stretch of ester), 3247 (OH stretch, broad, of carboxylic group), 1238 (C–O stretch of carboxylic group), 3516, 3551 (OH band of aliphatic alcohol), 1094 (C–O stretch of primary alcohol) (R. Sharma & Ahuja, 2011). The IR data of Pec was as follows: 1736 (CO stretch of ester), 3328 (OH stretch of carboxylic group), 1245 (C–O stretch of carboxylic group), 3445 (OH band of aliphatic alcohol), 1091 (C–O stretch of primary alcohol) (R. Sharma & Ahuja, 2011). Presence of –SH stretch at 2573 and more intensity of CO stretch of ester confirmed the formation of PecTH.
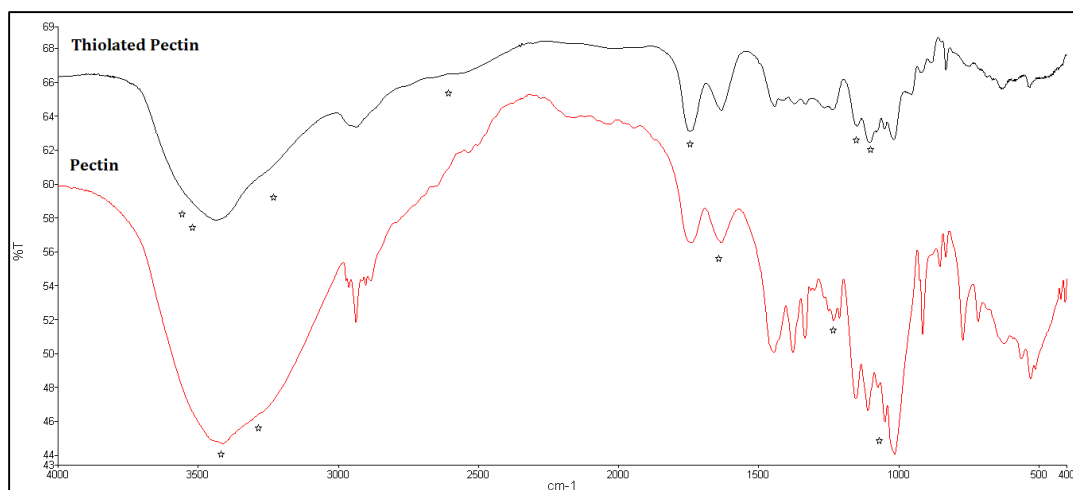
Figure 3.46 FTIR spectra of Pec and PecTH. "*" symbols indicate specific bands for Pec and PecTH.

3.2.1.2.3 Optimization of Fiber Incorporation into Hydrogels

The pulverized PMMA/SF mats were monitored. Firstly, PMMA/SF mats pulverized via cryo-mill were examined (Figure 3.47). In the first cycle of cryo-milling, the fibrous meshes were observable however their porosity decreased due to hit by cryo-

126

mill balls (Figure 3.47-top). In the second cycle, the fibers were united at the surface even though the fibrous structure maintained beneath the surface (Figure 3.47-middle). In the third cycle, there were no visible fibers and its morphology turned to a bulk (Figure 3.47-bottom). Consequently, none of the products after any cycle of cryo-milling was acceptable for further use. Since their morphology totally or partially changed and porosity was lost which is crucial for cell migration and/or determined release behavior. Thus, cryo-milling was quitted.

Homogenization of PMMA/SF mats was used as an alternative method to cryo-milling. SEM images showed that the integrity of fibrous structure could not be preserved during homogenization (Figure 3.48). At the end of the first cycle, there were small fibers on the large bulky material (Figure 3.48-top). However, second cycle of homogenization destroyed all fibers (Figure 3.48-bottom). Therefore, homogenization could not be preferred in the further experiments.

Finally, PMMA/SF mats were cut by scissors and approximately 5 mm × 1 mm sized flakes were obtained. Hence, their morphology was able to be maintained (Figure 3.49). These cut fibers were mixed with GelMA and GelMA/PecTH hydrogels and pulverized by the blender so that their particle size was reduced further. Nonetheless, this pulvarizaiton process by the blender could not be achieved in the absence of the hydrogels since the fibrous mats stuck to the peripheral surface of the blender wall when there was no hydrogel in the blender chamber. After the pulverization, the PMMA/SF fibers homogeneously dispersed within the hydrogels with the reduced size, making them injectable hydrogel systems.
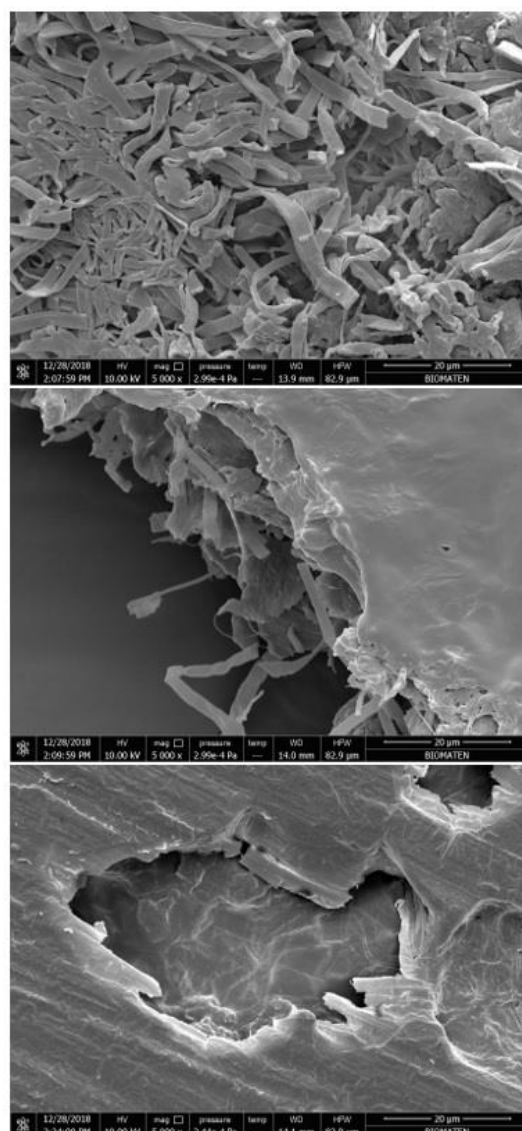
Figure 3.47 SEM images of the pulverized structure of PMMA/SF fibers after cryo-milling in 3 cycles (30 sec × 30 sec × 30 sec).
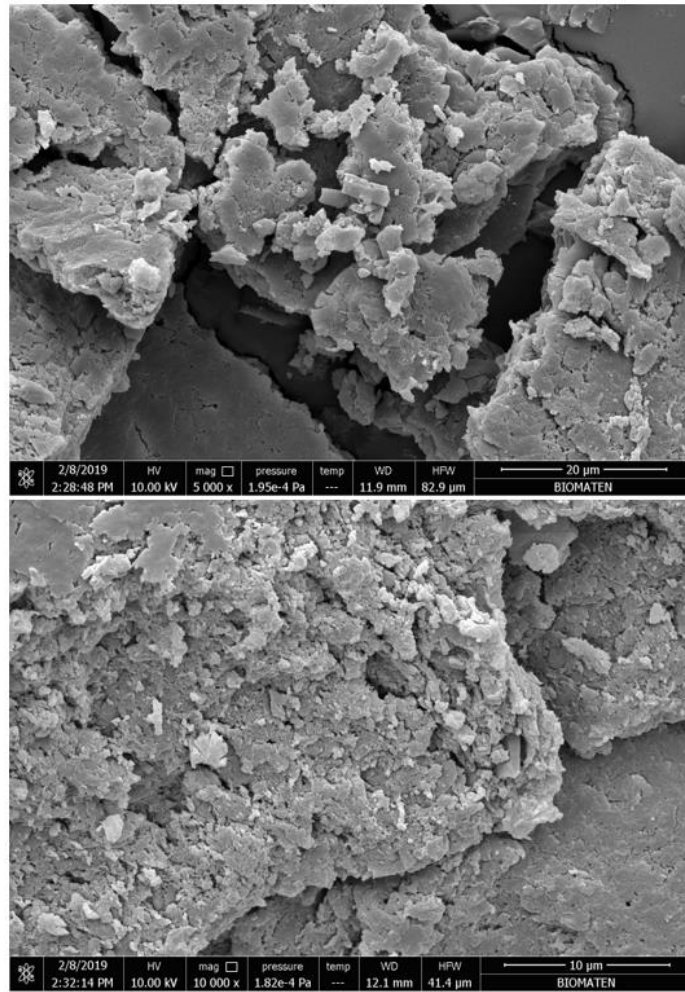
Figure 3.48 SEM images of the pulverized structure of PMMA/SF fibers after homogenization in 2 cycles (2 min × 2 min).
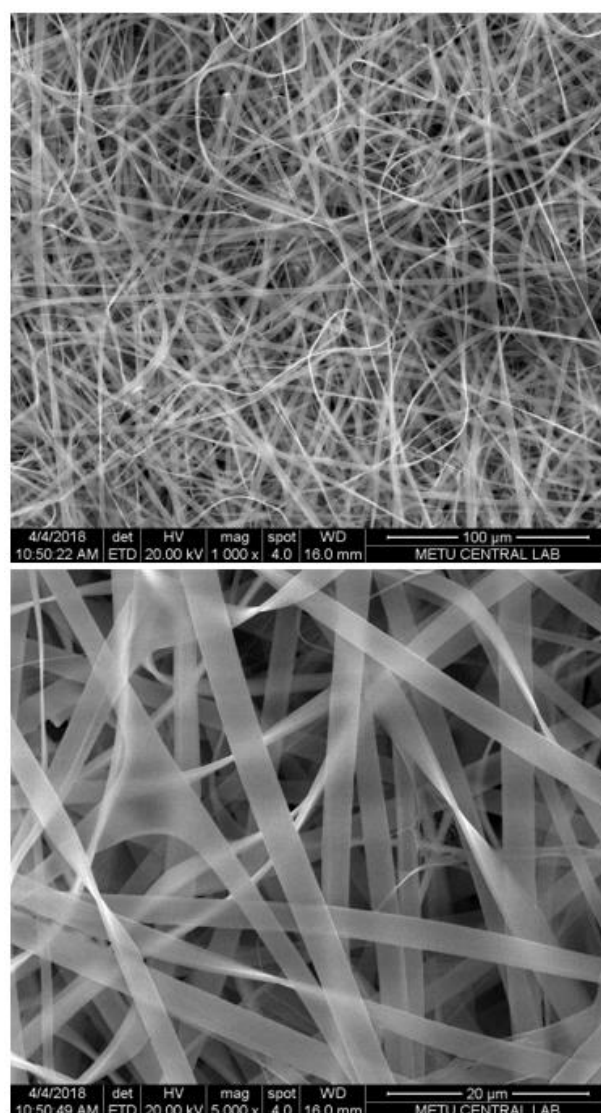
Figure 3.49 PMMA/SF mats cut with a scissor conserves their morphology.

3.2.1.2.4 Degradation Studies

During optimization studies, different GelMA/PecTH (wt/wt) ratios were tested (Figure 3.50). Since its degradation rate was less than the others, 1% of PecTH-containing group inside 10% of GelMA was chosen for further studies.
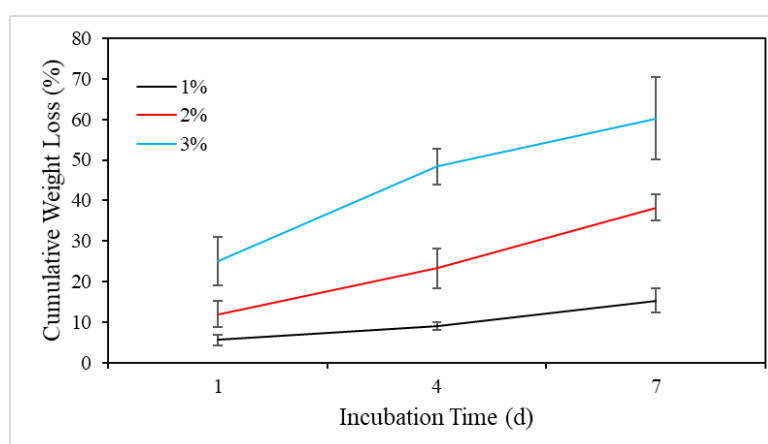
Figure 3.50 Cumulative weight loss of 1, 2, and 3% PecTH-containing GelMA (10%) hydrogels (n=3).

Four experimental groups (GelMA, GelMA/PecTH, GelMA+PMMA/SF, and GelMA/PecTH+PMMA/SF) were used for degradation studies carried out in PBS (Figure 3.51). Weight loss percentages showed that the GelMA group endured against degradation. Additionally, the previously selected PecTH addition (1% of PecTH) did not have a dramatic effect on degradation behavior of GelMA. However, PMMA/SF component altered the degradation profile of the hydrogel systems. For all the time points, GelMA/PecTH+PMMA/SF group had a weight loss statistically higher than all the other groups. This indicated that fibrous structures fastened the degradation process possible by ruining the integrity of hydrogel material. However, approximately 30% weight loss was observed even for this group (GelMA/PecTH+PMMA/SF) at the end of 21 days of incubation. Similarly, it was reported that a composite scaffold fabricated by immersing PGS–PCL fibers into GelMA–HAMA hydrogel precursor solution lost 20-25% of their initial weights in PBS (Eslami et al., 2014).
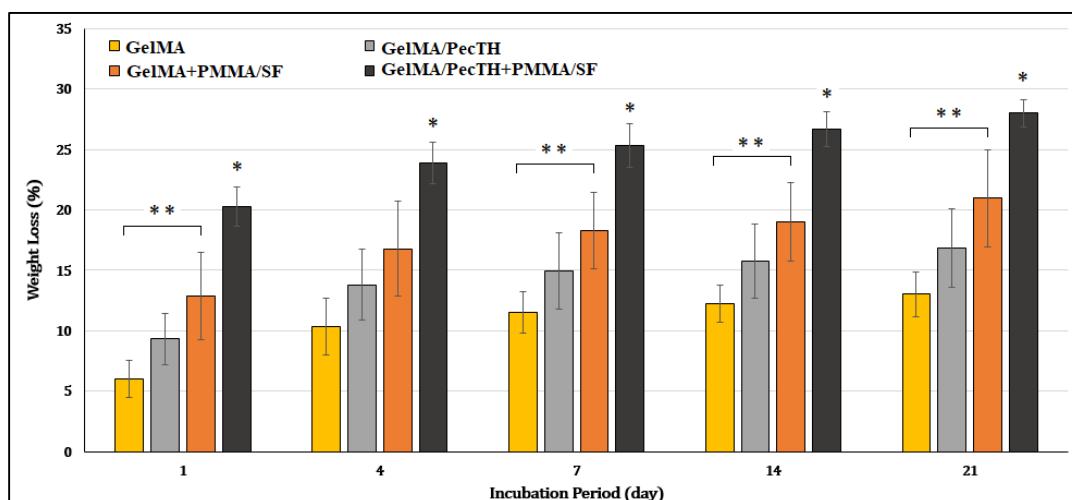
Figure 3.51 Percent weight loss values of GelMA, GelMA/PecTH, GelMA+PMMA/SF, and GelMA/PecTH+PMMA/SF prepared by using scissor cut fibers for 21 days of incubation in PBS at 37°C. "*" symbols indicate statistically different groups than all other groups for its specific time point. "**" symbols indicate statistically difference among the given groups at the specific time point ($p < 0.05$) (n=3).

For better mimicking *in vivo* conditions, degradation behavior of the hydrogel systems was also studied in lysozyme solution (Figure 3.52). Similar trend was observed with PBS incubation. Briefly, after 6 h of incubation in lysozyme, weight remained for the only GelMA group was statistically higher than all other groups at the given time point. Moreover, after 18 h of incubation, weight remained for GelMA/PecTH+PMMA/SF group was statistically lower than all other groups. This finding demonstrated that PMMA/SF addition to these hydrogel systems enhanced the degradation rate of the hydrogels which was contradictory to a previous report which showed that the addition of PLA fibers into hydrogels decrased the degradation rate of the fiber-hydrogel composite (W. Xu, Ma, & Jabbari, 2010). However, this result could be attributed to the hydrophilicity difference between the hydrophobic PLA fibers and the hydrophilic SF covered-PMMA/SF core/shell fibers.
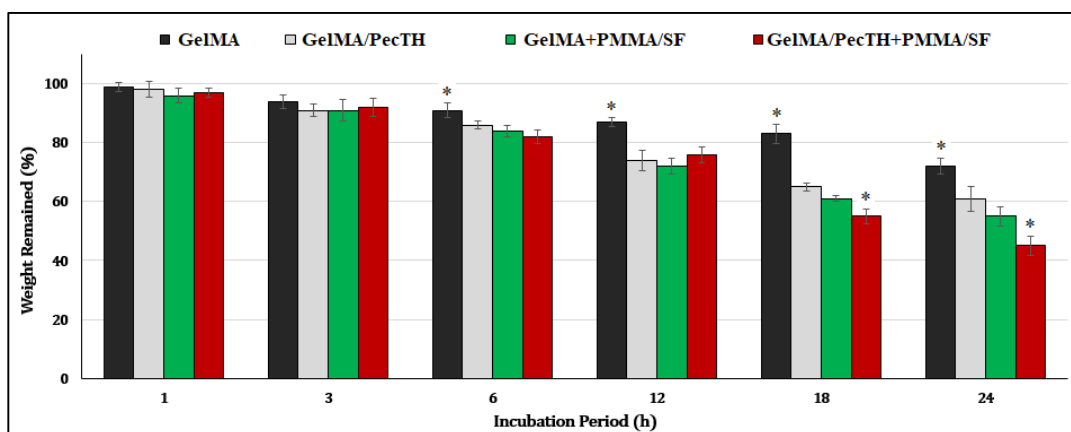
Figure 3.52 Enzymatic degradation profile of GelMA, GelMA/PecTH, GelMA+PMMA/SF, and GelMA/PecTH+PMMA/SF prepared by using scissor cut fibers for 24 h in lysozyme (1 mg/mL) at 37°C. "*" symbols indicate statistically different groups than all other groups at the given time point ($p < 0.05$) (n=3).

3.2.1.2.5 Water Retention

The effect of PecTH percent on water retention was investigated during optimization studies (Figure 3.53). It has been shown that the water retention of hydrogels increased as the PecTH amount was increased. (Note: 1% of PecTH-containing group inside 10% of GelMA had already been chosen for further studies.)
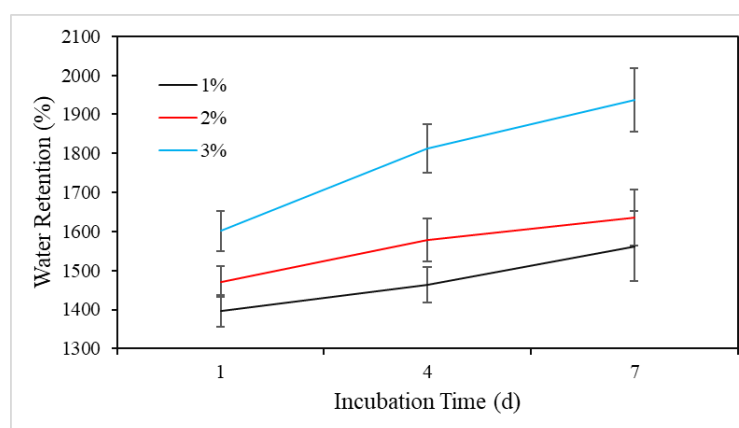
Figure 3.53 Water retention capacities of 1, 2, and 3% of PecTH-containing group inside 10% of GelMA hydrogels (n=3).

Water uptake capacity results of GelMA, GelMA/PecTH, GelMA+PMMA/SF, and GelMA/PecTH+PMMA/SF groups are presented in Figure 3.54. All groups could hold water at least 12 times of their weights. In detail, the lower water uptake capacity was observed in GelMA+PMMA/SF whereas the highest one was observed in GelMA/PecTH+PMMA/SF group. Therefore, water retention percent remarkably increased when PecTH was incorporated to the hydrogel. Similarly, GelMA group had a lower water uptake capacity than GelMA/PecTH group until day 14. This positive effect of PecTH on water retention capacity of the hydrogel system might be arisen from its polysaccharide nature which is known as quite hydrophilic. Similarly, in another study, Pec addition into polyacrylamide caused an increase in water retention capacity of the hydrogels (L. Liu, Cooke, Coffin, Fishman, & Hicks, 2004).
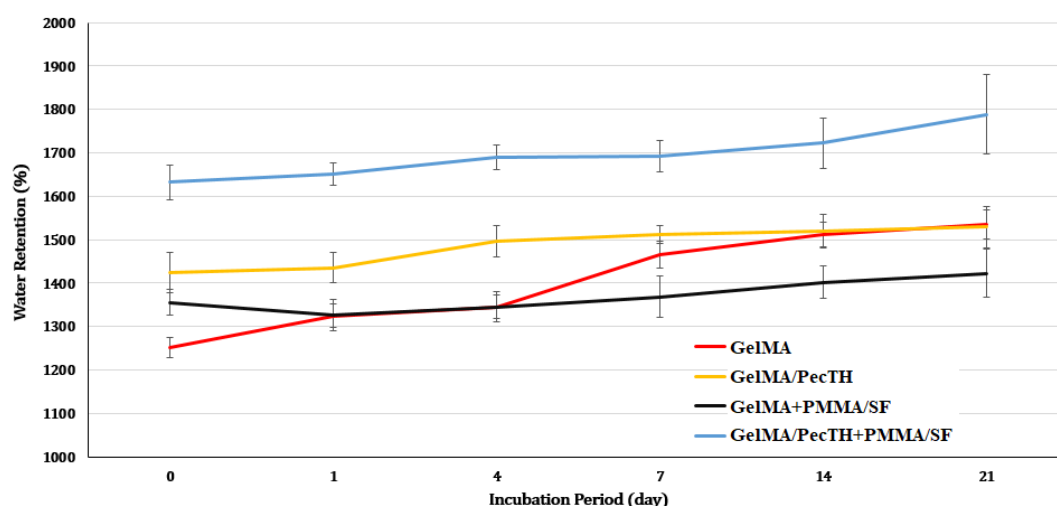
Figure 3.54 Percent water retention values of GelMA, GelMA/PecTH, GelMA+PMMA/SF, and GelMA/PecTH+PMMA/SF prepared by using scissor cut fibers at day 0, 1, 4, 7, 14, and 21 during incubation in PBS at 37°C (n=3).

3.2.1.2.6   Mel Release

In order to determine the release profiles of the Mel-loaded meshes, the standard curve for Mel in PBS was constructed and measurements were conducted at a

wavelength of 222 nm (Appendix E1). Firstly, the absorbance values were collected from a wider interval of concentration in order to determine the sensitivity region. Next, the linear region was constructed the standard curve of Mel in PBS which lied in the interval of 0-7.81 µg/mL of Mel concentration. However, PBS that will be the release environment for the further experiments was not the best solvent for Mel. Hence, the standard curve was also constructed for Mel dissolved in methanol (Appendix E2). The absorbance was read in between 0 and 125 µg/mL of Mel concentration once again. The linear region was detected in the interval of 0-31.25 µg/mL which had a more vertical slope showing that methanol dissolved Mel more effectively. Therefore, the release studies of Mel were decided to be conducted in PBS and then samples were dried. Finally, dry samples were dissolved in methanol to measure the amount of Mel released for the specific time point.

Mel release from the fibers and the fibers inside the hydrogels is represented in Figure 3.55. The release was delayed when Mel-loaded PMMA was at the core of fibers and it was further delayed when the core/shell fibers were placed inside GelMA/PecTH hydrogels. That was an expected result since Mel could not be in contact with the aqueous environment when it was placed inside inner layers of the fibers or/and hydrogels which in turn decrased the release rate.
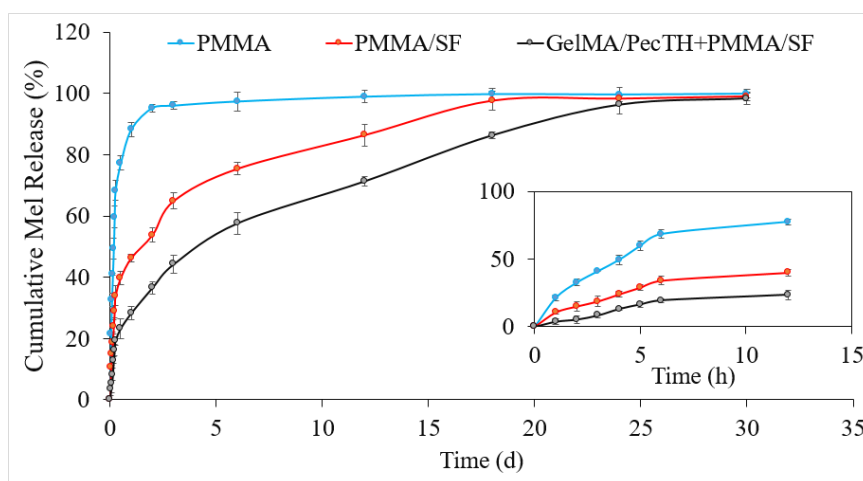
Figure 3.55 Mel Release from the neat PMMA fibers, PMMA/SF core/shell fibers, and GelMA/PecTH+PMMA/SF hydrogels (n=4).

3.2.1.2.7   Td Release

Td release from the fibers and the fibers inside the hydrogels was represented in Figure 3.56. It was shown that Td release was delayed when the core-shell fibers were placed inside GelMA/PecTH hydrogels as it was also observed in the Mel release (Figure 3.55). However, Td release was increased rather than delayed when Td-loaded SF was placed at the shell of fibers when compared to the release amount from the neat SF. Thus, an advanced controlled release of Td and Mel was provided by loading them into the PMMA/SF core/shell fibers, in which Td release was enhanced whereas Mel release was delayed. The tuning of the release profiles of them proceeded by mixing them with the GelMA/PecTH hydrogels. Both of the bioactive agents exhibited the declines in their release rate.
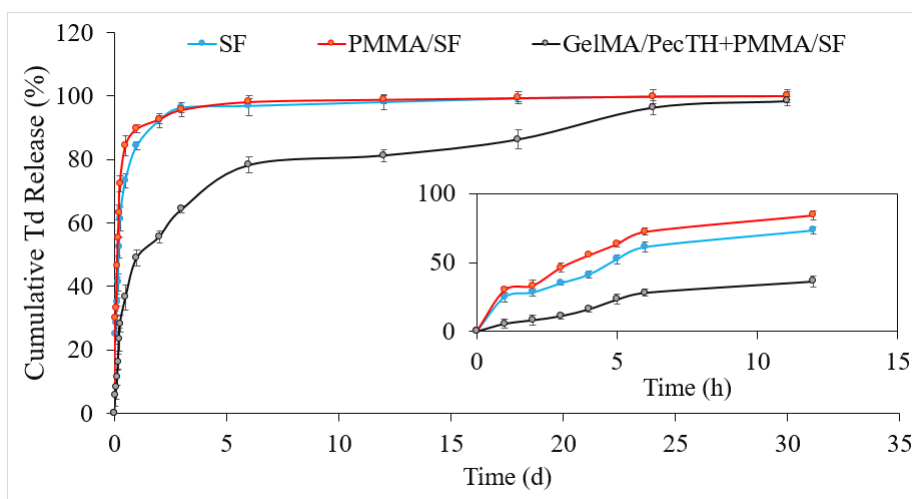
Figure 3.56 Td Release from the neat SF fibers, PMMA/SF core/shell fibers, and GelMA/PecTH+PMMA/SF hydrogels (n=4).

3.2.1.3   Cell Culture Studies for GelMA-Based Hydrogels

3.2.1.3.1   Cell Attachment on Electrospun Fibers

SEM images of DPSC on SF, PMMA, and PMMA fibrous mats were compared to determine suitability of the surfaces for cell adhesion (Figure 3.57). It was clearly observed that SF fibers supported cell adhesion and spreading (Figure 3.57A&B) while the round cells were observed on the PMMA fibers (Figure 3.57C&D). In the literature, it has been demonstrated that human bone marrow cells were attached to the PMMA/hydroxyapatite surfaces and their morphology was not as flat as cells on SF fibers after 10 weeks of incubation (Jäger & Wilke, 2003). It was observed that cells could not intensively proliferate and cover the PMMA fibers due to their strong hydrophobicity which was similar with the results of the current study. However, cells again populated on the PMMA/SF fibers since the SF shell prevented the contact of the cells to the PMMA (Figure 3.57E&F). Cell lawns were observed on the surface of fibrous mats causing the disappearance of the PMMA/SF fibers.
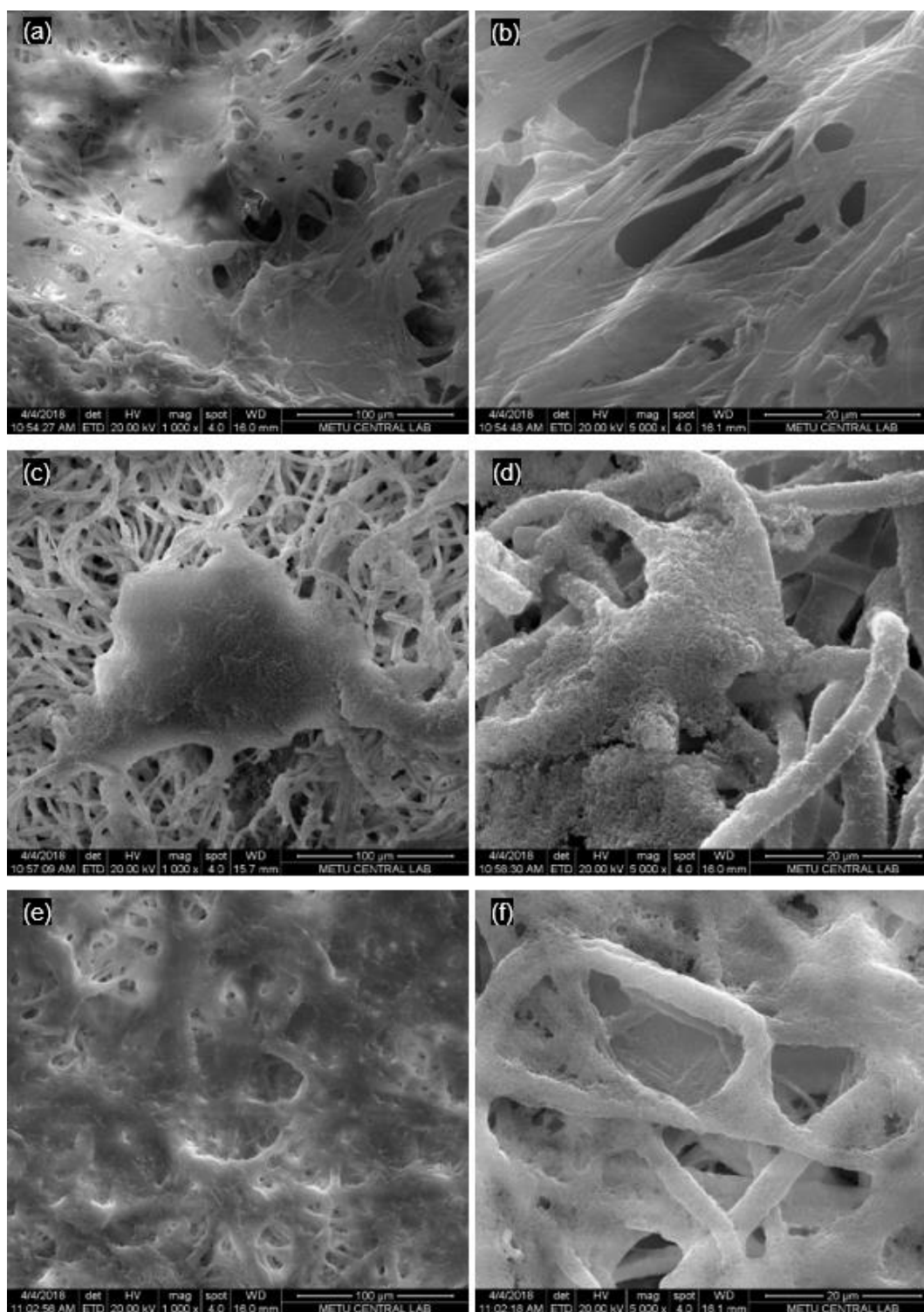
Figure 3.57 SEM images of the neat SF (A&B), the neat PMMA (C&D), and the PMMA/SF (E&F) meshes seeded with DPSC after 7 days of incubation in the cell culture media at 37ºC. (Scale bars for A, C, and E: 100 µm; and B, D, and F: 20 µm.)

3.2.1.3.2   Cell Viability on the Electrospun Fibers

Viability of DPSC on electrospun meshes was measured via Alamar Blue Test and plotted (Figure 3.58). Cells were able to adhere on all types of the surfaces as effectively as on the control group on day 1. The growth rate of cells on the neat PMMA meshes was lower than observed on the other groups. This result was parallel with the SEM examinations which proved the PMMA mats were not substantially suitable for cell attachment so that PMMA surfaces should be coated with a cell-adherent material. Therefore, the coated PMMA/SF surfaces enabled the cells to populate.

At the end of the first week, there was no statistical difference in cell viability between the groups except for the TCPS. It was probably caused by that the control wells and the mats became confluent. Therefore, the cell proliferation decreased in the second week. Finally, the cells again increased their proliferation rate at day 21. However, the PMMA and PMMA/SF groups could not support the cell population which was related with the degradation phenomenon. Since the decomposition of SF layer on the PMMA/SF fibers, the PMMA core was partly exposed beneath the SF surface of the fibrous structures. Thus, the cell adhesion was negatively influenced by the PMMA contact and their cell viability was similar to that observed on the PMMA meshes.
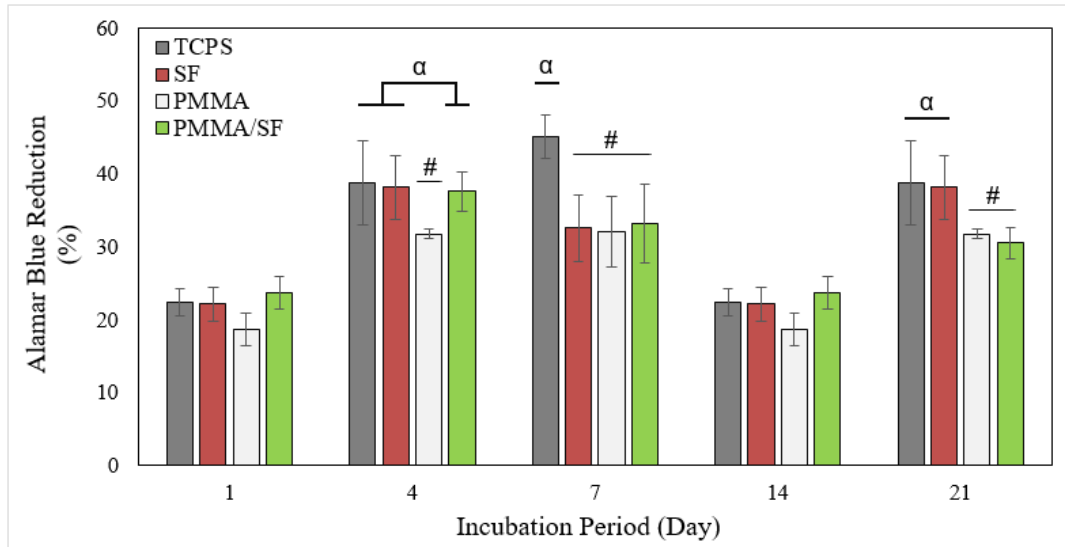
Figure 3.58 Alamar Blue reduction percentages of DPSC on TCPS, SF, PMMA, and PMMA/SF meshes. "α" denoted for the groups statistically different than "#" groups ($p < 0.05$) for the specific time point (n=4).

3.2.1.3.3 Cell Viability with the Hydrogels

Cell viability of DPSC incubated in the media obtained from GelMA-based hydrogel groups containing different amounts of bioactive agents (Mel and Td) were tested (Figure 3.59). Cells responded similarly in all groups on day 1 except for GelMA, GelMA/PecTH, and GelMA+PMMA/SF. Moreover, GelMA/PecTH and GelMA+PMMA/SF groups had higher cell viability than that of bare GelMA which was a sign of the positive impact of incorporations into GelMA on cells. Furthermore, PMMA/SF incorporation influenced the cell viability more than PecTH did at all the time points. This might be attributed to the fact that when there are fibers in the environment, ECM of the native tissues could be mimicked better on which cells could adhere and grow (Sohrabi et al., 2021). Therefore, the cell viability of all of the fiber-containing groups was statistically higher than the bare hydrogels on day 4 too.

140

On day 4, the effect of bioactive agents on cell viability was not obvious for Mel/Td ratios of 3/1 and 1/1 when compared to the empty counterparts (GelMA+PMMA/SF GelMA/PecTH+PMMA/SF); however, Mel/Td:1/3 ratio enhanced the cell viability statistically higher than that of other groups. In other words, the increase in Td amount loaded promoted the Td release and hence the cell proliferation. Besides, Td release was further speeded up and made hydrogel more Td-saturated since Td was loaded into SF (shell part of core/shell fibers). On the other hand, no difference was observed by the alterations in Mel-loading on day 4 since Mel was loaded into the core part (PMMA) of the core/shell fibers.

The previous results were obtained again approximately on day 7 due to the same reasons related to Mel and Td. However, cell viability of GelMA/PecTH+PMMA/SF with Mel/Td:1/3 group was the statistically highest meaning that all components of the hydrogel system (GelMA, PecTH, and PMMA/SF) with Mel/Td:1/3 ratio were required to induce cell proliferation at this level.
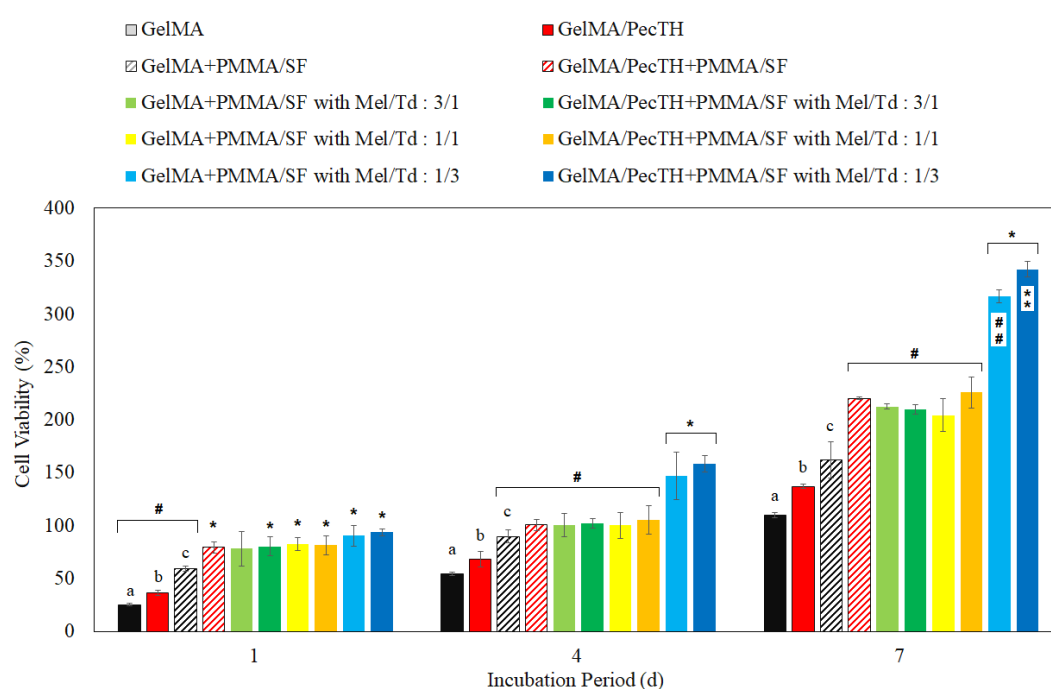
Figure 3.59 Cell viability of DPSC incubated in the media obtained from GelMA-based hydrogel groups. The groups denoted as "a, b, c" are statistically different than

each other on day 1. * denote the groups that are statistically higher that # groups on day 1. The groups denoted as "a, b, c" are statistically different than each other on day 4. * denote the statistically highest groups on day 4 and 7. # denote statistically different groups than the excluded groups on day 4 and 7. The groups denoted as "a, b, c" are statistically different than each other on day 7. ** denotes the group that is statistically higher than ## group on day 7 ($p < 0.05$) (n=4).

3.2.1.3.4 Alkaline Phosphatase (ALP) Enzyme Activity

ALP activity of DPSC incubated in the media obtained from GelMA-based hydrogel groups containing different amounts of bioactive agents (Mel and Td) were tested (Figure 3.60). The presence of bioactive agent-loaded hydrogel systems in the culture environment resulted in a higher ALP activity of cells on day 7 and 14 demonstrating that osteo/odontogenic differentiation of DPSC was enhanced with the release of Mel and Td from the gels. It was observed that Mel/Td:3/1 ratio stimulated the differentiation process more than that of the other ratios (1/1 and 1/3) on day 7 which exhibited Mel was more effective to induce odontogenic differentiation than Td. Moreover, Mel release was lower due to its loading region (the core PMMA) to observe the effect of Mel sooner. Therefore, the Mel effect on DPSC could be seen later (on day 14) for the rest of the Mel/Td-containing groups (namely, GelMA/PecTH+PMMA/SF with Mel/Td:1/1 and 1/3).

142
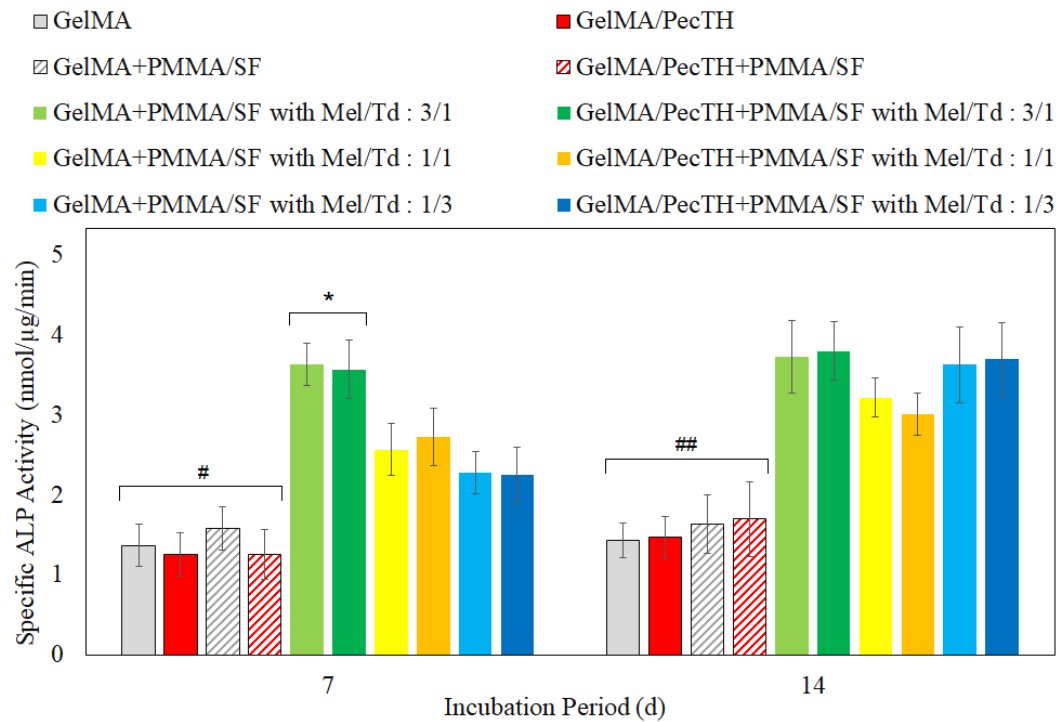
Figure 3.60 Specific ALP activity of DPSC incubated in the media obtained from GelMA-based hydrogel groups at 37ºC with an initial density of 1000 cells/well (n=4). * denotes statistically the highest groups on day 7. # denotes statistically the lowest groups on day 7. ## denotes statistically the lowest groups on day 14 ($p < 0.05$).

3.2.1.3.5 Morphological Analyses

The fluorescence images were obtained to examine the morphology of the cells using a fluorescence microscope will be shared during the thesis defence.

3.2.1.3.6 Gene Expression Studies

Osteo/odontogenic differentiation levels of DPSC exposed to GelMA-based hydrogel groups were analyzed by measurirng COL1A1 gene expression (Figure 3.61). All hydrogel groups displayed higher COL1A1 expression compared to the

control meaning that GelMA-based hydrogels had triggering factors for DPSC to differentiate into osteo/odontogenic lineage. In the literature, GelMA hydrogels were similarly tested and bare GelMA groups resulted with a higher COL1A1 expression of mesenchymal stem cells on day 7 compared to day 1 (Su, Lin, Chen, Lee, & Lin, 2021), confirming the effect of GelMA on osteogenic differentiation of stem cells. Moreover, the fiber-containing hydrogel group (GelMA/PecTH+PMMA/SF) had a higher gene expression level than the only-gel groups which demonstrated the osteo/odontogenic differentiation of DPSC was enhanced in the presence of fibers. In another study, it was reported that random electrospun fibers distributed within hydrogels led to an upregulation of COL1A1 expression of human vascular and avascular meniscus cells when compared to aligned fibers (Baek et al., 2015). This result showed that osteo/odontoblastic ECM was mimicked better by the use of randomly oriented fibers inside the hydrogels.
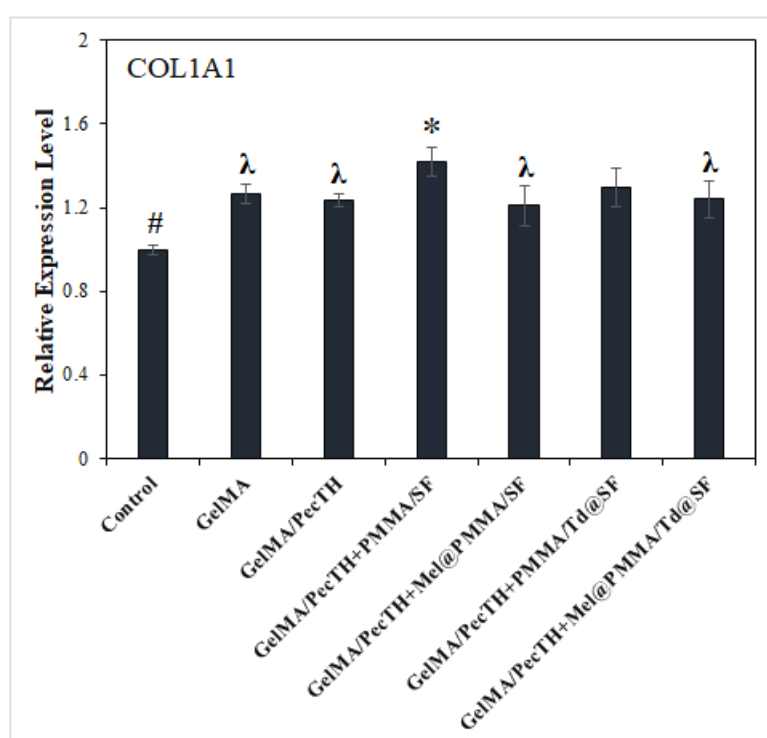
Figure 3.61 Relative COL1A1 gene expression levels of DPSC treated with previously defined test groups on day 7. # detones the statistically lowest group. * denotes statistically different group than λ groups ($p < 0.05$) (n=3).

In order to measure the activation of Wnt/β-catenin pathway taking role in dental regeneration process, Axin-2 gene expression of DPSC was also determined (Figure 3.62). Td-containing GelMA group (GelMA/PecTH+PMMA/Td@SF) showed the highest Axin-2 expression level while Mel and Td-containing ones had still higher levels of Axin-2 than the control. Therefore, it was observed that Td and Mel had a positive influence on the upregulation of Axin-2. Normally, Td was effective on early time point like day 1 as it was previously reported (Neves et al., 2017a; Zaugg et al., 2020) and seen in our results previously obtained for HA-based hydrogels (Figure 3.18); however, when Td was loaded into SF part of the core/shell fibers and the fibers were incorporated into GelMA/PecTH hydrogels, Td release was delayed and could have resulted in stimulation of Axin-2 expression of DPSC on day 7.
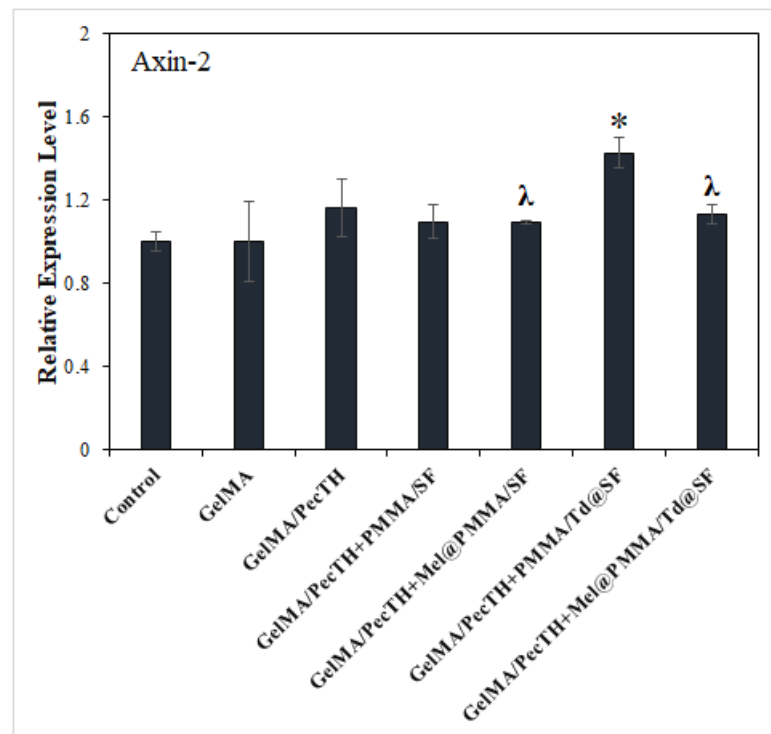
Figure 3.62 Relative Axin-2 gene expression levels of DPSC treated with previously defined test groups on day 7. * detones the statistically highest group. λ denotes statistically different groups than the control ($p < 0.05$).

DSPP gene expression of DPSC incubated with the hydrogel groups was higher than the control showing that odontoblastic differentiation was enhanced in all hydrogel

groups (Figure 3.63). Moreover, Mel-containing hydrogels had a statistically higher level of DSPP expression compared to the empty hydrogel/fiber counterpart (GelMA/PecTH+PMMA/SF). Similarly, DPSC exhibited higher DSPP expression level in the presence of Mel (Q. Liu et al., 2017).
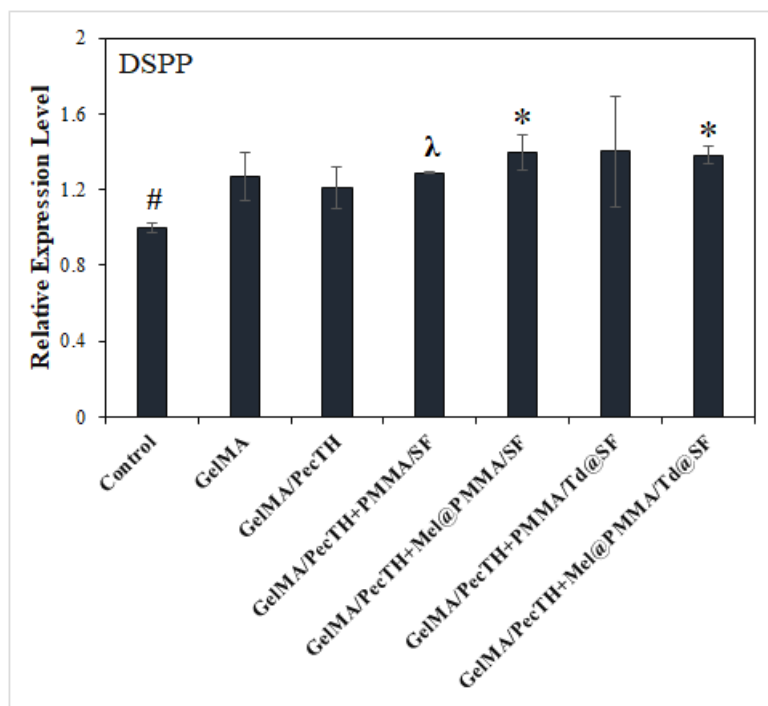
Figure 3.63 Relative DSPP gene expression levels of DPSC treated with previously defined test groups on day 7. # detones the statistically lowest group. * denotes statistically different groups than λ group ($p < 0.05$) (n=3).

The upregulation of DMP1 expression of DPSC was remarkably promoted in the Mel and Td-loaded group (GelMA/PecTH+Mel@PMMA/Td@SF) (Figure 3.64). Furthermore, only Mel-containing and only Td-containing groups, namely GelMA/PecTH+Mel@PMMA/SF and GelMA/PecTH+PMMA/Td@SF, showed statistically higher DMP1 gene expression than the other groups' which contain none of them. This result demonstrated that Mel and Td alone and together posessed stimulatory effect on odontoblastic differentiation of DPSC. DMP1 gene expression result also suggested that co-release of Mel and Td might have synegistic effect.

146
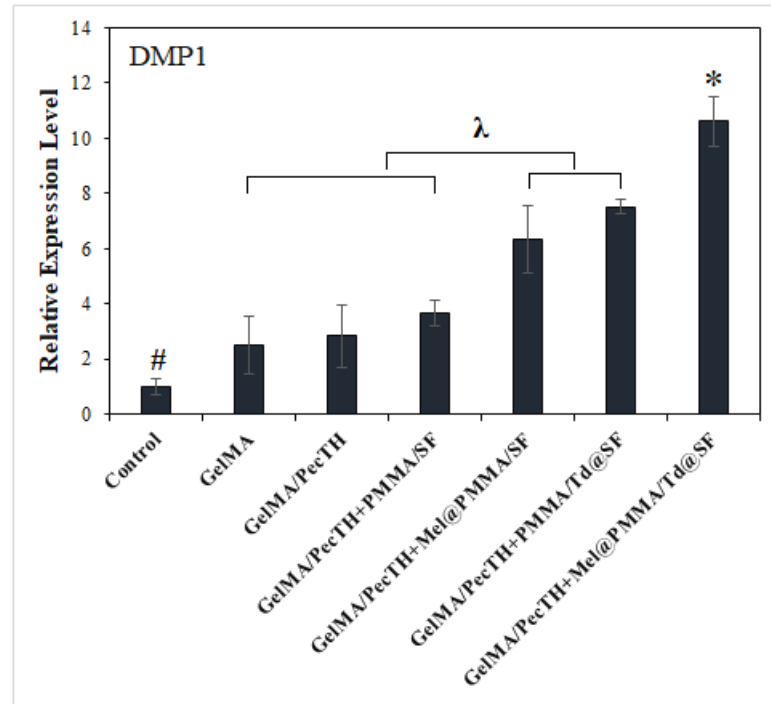
Figure 3.64 Relative DMP1 gene expression levels of DPSC treated with previously defined test groups on day 7. # detones the statistically lowest group. # detones the statistically highest group. λ denotes statistically different groups ($p < 0.05$) (n=3).

CHAPTER 4

CONCLUSION

Developing injectable scaffolds to trigger pulp regeneration effectively remains challenging. In this thesis study, two types of injectable hydrogel systems, namely hyaluronic acid (HA)-based and Gelatin methacryloyl (GelMA)-based hydrogels, were prepared for vital pulp regeneration.

During the development of Type-I hydrogels, multifunctional Tideglusib (Td)-loaded HA injectable hydrogels containing Rg1-loaded chitosan microspheres (CSM) have been developed for the first time and evaluated *in vitro* as a new formulation for vital pulp regeneration. Basically, HA was utilized as a raw biomaterial to construct hydrogels (HAH) and it was loaded with Td since the effect of Td on odontogenic differentiation forces tissue engineers towards drug repurposing of this Alzheimer's Disease drug for dental regeneration. Td release from hydrogels and co-release of Td and Rg1 from hydrogels containing Rg1-loaded microspheres were studied for the first time. The sustained release of Td from HAH facilitated the biomineralization of DPSC. The hydrogels were further incorporated with Rg1-loaded CSM to stimulate vascularization of newly-formed pulp after injection since Rg1 is a green and powerful plant extract to induce vascularization. RT-PCR results confirmed odontogenic and angiogenic differentiation differentiation of DPSC treated with Td-loaded hydrogels incorporated with Rg1-loaded microspheres as well as angiogenic gene expression of HUVEC were shown. Moreover, angiogenic effect of Rg1-containing hydrogel groups was proven on Matrigel *in vitro*. In addition to the highly practical preparation procedure and injectability, these results make this hydrogel microsphere system (Td-loaded HAH with Rg1-loaded CSM) a promising vital pulp regeneration strategy in vascularized endodontic regenerative dentistry. Besides, Td-loaded HAH can be considered as a

separate injectable scaffold to stimulate odontogenic differentiation as well as Rg1-loaded CSM may be used alone to induce vascularization.

During the development of Type-II hydrogels, fiber containing GelMA/Thiolated Pectin (PecTH) were prepared for the fisrt time. The fiber part was fabricated by coaxial electrospinning method and the uniform core/shell poly methyl methacrylate (PMMA)/silk fibroin (SF) fibers were obtained with a ratio of 1/3. The characterization studies of PMMA/SF fibers confirmed that PMMA and SF had brittle/hydrophobic and flexible/hydrophilic properties, respectively. After cytocompatibilty of the hydrogels was shown using DPSC, the fibers were pulvarized and mixed with GelMA/PecTH hydrogels simulatenously. Melatonin (Mel) and Td were loaded into PMMA and SF in different ratios (3/1, 1/1, and 1/3), respectively. Cell viability of DPSC increased when Mel/Td ratio was 1/3 whereas ALP activity level of DPSC increased when Mel/Td ratio was 3/1. Second ratio was used to trigger odontoplastic differentiation of DPSC *in vitro*. Gene expression studies showed that GelMA/PecTH hydrogels incorpotared with Mel and Td-loaded PMMA/SF fibers had the potential to upregulate the odontoblastic marker genes, especially DMP1, of DPSC. *In vivo* evaluations are needed to test the feasibility and potential of these hydrogels for vital pulp regeneration.

REFERENCES

Ahmadian, E., Eftekhari, A., Dizaj, S. M., Sharifi, S., Mokhtarpour, M., Nasibova, A. N., . . . Samiei, M. (2019). The effect of hyaluronic acid hydrogels on dental pulp stem cells behavior. *International journal of biological macromolecules, 140*, 245-254.

Ajay Sharma, L., Love, R. M., Ali, M. A., Sharma, A., Macari, S., Avadhani, A., & Dias, G. J. (2017). Healing response of rat pulp treated with an injectable keratin hydrogel. *Journal of Applied Biomaterials Functional Materials, 15*(3), 244-250.

Al-Sibani, M., Al-Harrasi, A., & Neubert, R. H. (2016). Study of the effect of mixing approach on cross-linking efficiency of hyaluronic acid-based hydrogel cross-linked with 1, 4-butanediol diglycidyl ether. *European Journal of Pharmaceutical Sciences, 91*, 131-137.

Alpan, A. L., Çalisir, M., Kizildag, A., Özdede, M., & Özmen, Ö. (2020). Effects of a glycogen synthase kinase 3 inhibitor tideglusib on bone regeneration with calvarial defects. *Journal of Craniofacial Surgery, 31*(5), 1477-1482.

Anusavice, K. J., Shen, C., & Rawls, H. R. (2013). *Phillips' science of dental materials*: Elsevier Health Sciences.

Asakura, T., Koyanagi, R., Nishiyama, N., Kuboyama, N., Kiba, H., & Abiko, Y. (2011). Bone regeneration on the epicondyle of the femur supported by silk fibroin-based scaffold: a model system for dental surgery. *Journal of Insect Biotechnology and Sericology, 80*(1), 1_025-021_030.

Asgary, S., Nazarian, H., Khojasteh, A., & Shokouhinejad, N. (2014). Gene expression and cytokine release during odontogenic differentiation of human dental pulp stem cells induced by 2 endodontic biomaterials. *Journal of endodontics, 40*(3), 387-392.

Atari, M., Barajas, M., Hernández-Alfaro, F., Gil, C., Fabregat, M., Ferres Padro, E., . . . Casals, N. (2011). Isolation of pluripotent stem cells from human third molar dental pulp. *Histology and histopathology, 26*(7), 1057.

Attele, A. S., Wu, J. A., & Yuan, C.-S. (1999). Ginseng pharmacology: multiple constituents and multiple actions. *Biochemical pharmacology, 58*(11), 1685-1693.

Baek, J., Chen, X., Sovani, S., Jin, S., Grogan, S. P., & D'Lima, D. D. (2015). Meniscus tissue engineering using a novel combination of electrospun scaffolds and human meniscus cells embedded within an extracellular matrix hydrogel. *Journal of Orthopaedic Research, 33*(4), 572-583.

Bai, L., Zhu, L., Min, S., Liu, L., Cai, Y., & Yao, J. (2008). Surface modification and properties of Bombyx mori silk fibroin films by antimicrobial peptide. *Applied Surface Science, 254*(10), 2988-2995.

Bakopoulou, A., Leyhausen, G., Volk, J., Tsiftsoglou, A., Garefis, P., Koidis, P., & Geurtsen, W. (2011). Comparative analysis of in vitro osteo/odontogenic differentiation potential of human dental pulp stem cells (DPSCs) and stem

cells from the apical papilla (SCAP). *Archives of Oral Biology, 56*(7), 709-721.

Barbucci, R., Lamponi, S., Borzacchiello, A., Ambrosio, L., Fini, M., Torricelli, P., & Giardino, R. (2002). Hyaluronic acid hydrogel in the treatment of osteoarthritis. *Biomaterials, 23*(23), 4503-4513.

Baruah, J., Hitzman, R., Zhang, J., Chaudhuri, S., Mastej, V., & Wary, K. K. (2017). The allosteric glycogen synthase kinase-3 inhibitor NP12 limits myocardial remodeling and promotes angiogenesis in an acute myocardial infarction model. *Journal of Biological Chemistry, 292*(50), 20785-20798.

Berès, F., Isaac, J., Mouton, L., Rouzière, S., Berdal, A., Simon, S., & Dessombz, A. (2016). Comparative physicochemical analysis of pulp stone and dentin. *Journal of endodontics, 42*(3), 432-438.

Berger, L. R., & Weiser, R. S. (1957). The β-glucosaminidase activity of egg-white lysozyme. *Biochimica et biophysica acta, 26*(3), 517-521.

Bernkop-Schnürch, A. (2005). Thiomers: a new generation of mucoadhesive polymers. *Advanced drug delivery reviews, 57*(11), 1569-1582.

Bernkop-Schnürch, A., Hornof, M., & Zoidl, T. (2003). Thiolated polymers—thiomers: synthesis and in vitro evaluation of chitosan–2-iminothiolane conjugates. *International journal of pharmaceutics, 260*(2), 229-237.

Bernkop-Schnürch, A., Kast, C. E., & Richter, M. F. (2001). Improvement in the mucoadhesive properties of alginate by the covalent attachment of cysteine. *Journal of controlled release, 71*(3), 277-285.

Bhushani, J. A., & Anandharamakrishnan, C. (2014). Electrospinning and electrospraying techniques: Potential food based applications. *Trends in Food Science Technology, 38*(1), 21-33.

Birjandi, A. A., Suzano, F. R., & Sharpe, P. T. (2020). Drug Repurposing in Dentistry; towards Application of Small Molecules in Dentin Repair. *International Journal of Molecular Sciences, 21*(17), 6394.

Blasiak, J., Kasznicki, J., Drzewoski, J., Pawlowska, E., Szczepanska, J., & Reiter, R. J. (2011). Perspectives on the use of melatonin to reduce cytotoxic and genotoxic effects of methacrylate-based dental materials. *Journal of pineal research, 51*(2), 157-162.

Cai, K., Yao, K., Lin, S., Yang, Z., Li, X., Xie, H., . . . Gao, L. (2002). Poly (D, L-lactic acid) surfaces modified by silk fibroin: effects on the culture of osteoblast in vitro. *Biomaterials, 23*(4), 1153-1160.

Cao, C., Yang, C., Qu, X., Han, B., & Wang, X. (2020). Effects of the injectable glycol-chitosan based hydrogel on the proliferation and differentiation of human dental pulp cells. *Journal of Peking University, 52*(1), 10-17.

Carpentier, G., Berndt, S., Ferratge, S., Rasband, W., Cuendet, M., Uzan, G., & Albanese, P. (2020). Angiogenesis Analyzer for imageJ—A comparative morphometric analysis of "endothelial tube formation Assay" and "fibrin Bead Assay". *Scientific reports, 10*(1), 1-13.

Chang, B., Ahuja, N., Ma, C., & Liu, X. (2017). Injectable scaffolds: Preparation and application in dental and craniofacial regeneration. *Materials Science Engineering: R: Reports, 111*, 1-26.

Cheewatanakornkool, K., Niratisai, S., Manchun, S., Dass, C. R., & Sriamornsak, P. (2017). Thiolated pectin–doxorubicin conjugates: Synthesis, characterization and anticancer activity studies. *Carbohydrate polymers, 174*, 493-506.

Chen, K.-L., Yeh, Y.-Y., Lung, J., Yang, Y.-C., & Yuan, K. (2016). Mineralization effect of hyaluronan on dental pulp cells via CD44. *Journal of endodontics, 42*(5), 711-716.

Chen, Z.-H., Ren, X.-L., Zhou, H.-H., & Li, X.-D. (2012). The role of hyaluronic acid in biomineralization. *Frontiers of Materials Science, 6*(4), 283-296.

Cho, Y. A., Noh, K., Jue, S. S., Lee, S. Y., & Kim, E. C. (2015). Melatonin promotes hepatic differentiation of human dental pulp stem cells: clinical implications for the prevention of liver fibrosis. *Journal of pineal research, 58*(1), 127-135.

Chrepa, V., Austah, O., & Diogenes, A. (2017). Evaluation of a commercially available hyaluronic acid hydrogel (Restylane) as injectable scaffold for dental pulp regeneration: an in vitro evaluation. *Journal of endodontics, 43*(2), 257-262.

Cicciù, M., Fiorillo, L., & Cervino, G. (2019). Chitosan use in dentistry: A systematic review of recent clinical studies. *Marine drugs, 17*(7), 417.

Clifford, A., D'Elia, A., Deering, J., Lee, B. E., Grandfield, K., & Zhitomirsky, I. (2020). Electrochemical fabrication and characterization of pectin hydrogel composite materials for bone tissue repair. *ACS Applied Polymer Materials, 2*(8), 3390-3396.

Comeau-Gauthier, M., Tarchala, M., Luna, J. L. R.-G., Harvey, E., & Merle, G. (2020). Unleashing β-catenin with a new anti-Alzheimer drug for bone tissue regeneration. *Injury*.

Dang, Q., Liu, C., Wang, Y., Yan, J., Wan, H., & Fan, B. (2016). Characterization and biocompatibility of injectable microspheres-loaded hydrogel for methotrexate delivery. *Carbohydrate polymers, 136*, 516-526.

Degidi, M., Artese, L., Scarano, A., Perrotti, V., Gehrke, P., & Piattelli, A. (2006). Inflammatory infiltrate, microvessel density, nitric oxide synthase expression, vascular endothelial growth factor expression, and proliferative activity in peri-implant soft tissues around titanium and zirconium oxide healing caps. *Journal of Periodontology, 77*(1), 73-80.

Dicharry, R. M., Ye, P., Saha, G., Waxman, E., Asandei, A. D., & Parnas, R. S. (2006). Wheat Gluten− Thiolated poly (vinyl alcohol) blends with improved mechanical properties. *Biomacromolecules, 7*(10), 2837-2844.

Dissanayaka, W. L., Hargreaves, K. M., Jin, L., Samaranayake, L. P., & Zhang, C. (2015). The interplay of dental pulp stem cells and endothelial cells in an injectable peptide hydrogel on angiogenesis and pulp regeneration in vivo. *Tissue Engineering Part A, 21*(3-4), 550-563.

Duarte Campos, D. F., Zhang, S., Kreimendahl, F., Köpf, M., Fischer, H., Vogt, M., . . . Esteves-Oliveira, M. (2020). Hand-held bioprinting for de novo vascular formation applicable to dental pulp regeneration. *Connective Tissue Research, 61*(2), 205-215.

Dubocovich, M. L., Rivera-Bermudez, M. A., Gerdin, M. J., & Masana, M. I. (2003). Molecular pharmacology, regulation and function of mammalian melatonin receptors. *Frontiers in bioscience: a journal and virtual library, 8*, d1093-1108.

Ducret, M., Montembault, A., Josse, J., Pasdeloup, M., Celle, A., Benchrih, R., . . . Farges, J.-C. (2019). Design and characterization of a chitosan-enriched fibrin hydrogel for human dental pulp regeneration. *Dental Materials, 35*(4), 523-533.

Dziadek, M., Zima, A., Cichoń, E., Czechowska, J., & Ślósarczyk, A. (2020). Biomicroconcretes based on the hybrid HAp/CTS granules, α-TCP and pectins as a novel injectable bone substitutes. *Materials Letters, 265*, 127457.

Eppley, B. L. (2005). Biomechanical testing of alloplastic PMMA cranioplasty materials. *Journal of Craniofacial Surgery, 16*(1), 140-143.

Erisken, C., Kalyon, D. M., Zhou, J., Kim, S. G., & Mao, J. J. (2015). Viscoelastic properties of dental pulp tissue and ramifications on biomaterial development for pulp regeneration. *Journal of endodontics, 41*(10), 1711-1717.

Eslami, M., Vrana, N. E., Zorlutuna, P., Sant, S., Jung, S., Masoumi, N., . . . Khademhosseini, A. (2014). Fiber-reinforced hydrogel scaffolds for heart valve tissue engineering. *Journal of Biomaterials Applications, 29*(3), 399-410.

Fan, M., Ma, Y., Zhang, Z., Mao, J., Tan, H., & Hu, X. (2015). Biodegradable hyaluronic acid hydrogels to control release of dexamethasone through aqueous Diels–Alder chemistry for adipose tissue engineering. *Materials Science Engineering: C, 56*, 311-317.

Farges, J.-C., Alliot-Licht, B., Renard, E., Ducret, M., Gaudin, A., Smith, A. J., & Cooper, P. R. (2015). Dental pulp defence and repair mechanisms in dental caries. *Mediators of inflammation, 2015*.

Fehrenbach, M. J., & Popowics, T. (2015). *Illustrated dental embryology, histology, and anatomy*: Elsevier Health Sciences.

Ferroni, L., Gardin, C., Sivolella, S., Brunello, G., Berengo, M., Piattelli, A., . . . Zavan, B. (2015). A hyaluronan-based scaffold for the in vitro construction of dental pulp-like tissue. *International Journal of Molecular Sciences, 16*(3), 4666-4681.

Fiaschi, P., Pavanello, M., Imperato, A., Dallolio, V., Accogli, A., Capra, V., . . . Piatelli, G. (2016). Surgical results of cranioplasty with a polymethylmethacrylate customized cranial implant in pediatric patients: a single-center experience. *Journal of Neurosurgery: Pediatrics, 17*(6), 705-710.

Fraser, J. R. E., Laurent, T. C., & Laurent, U. (1997). Hyaluronan: its nature, distribution, functions and turnover. *Journal of internal medicine, 242*(1), 27-33.

Frazer, R. Q., Byron, R. T., Osborne, P. B., & West, K. P. (2005). PMMA: an essential material in medicine and dentistry. *Journal of long-term effects of medical implants, 15*(6).

Freddi, G., Tsukada, M., & Beretta, S. (1999). Structure and physical properties of silk fibroin/polyacrylamide blend films. *Journal of applied polymer science, 71*(10), 1563-1571.

Fu, J., Zhao, S. D., Liu, H. J., Yuan, Q. H., Liu, S. M., Zhang, Y. M., . . . Hao, A. J. (2011). Melatonin promotes proliferation and differentiation of neural stem cells subjected to hypoxia in vitro. *Journal of pineal research, 51*(1), 104-112.

Fuks, A. B. (2008). Vital pulp therapy with new materials for primary teeth: new directions and treatment perspectives. *Pediatric dentistry, 30*(3), 211-219.

Gaihre, B., Uswatta, S., & Jayasuriya, A. C. (2017). Reconstruction of craniomaxillofacial bone defects using tissue-engineering strategies with injectable and non-injectable scaffolds. *Journal of functional biomaterials, 8*(4), 49.

Galano, A., Tan, D. X., & Reiter, R. J. (2011). Melatonin as a natural ally against oxidative stress: a physicochemical examination. *Journal of pineal research, 51*(1), 1-16.

Galis, Z. S., & Khatri, J. J. (2002). Matrix metalloproteinases in vascular remodeling and atherogenesis: the good, the bad, and the ugly. *Circulation research, 90*(3), 251-262.

Galler, K. M., & D'Souza, R. N. (2011). Tissue engineering approaches for regenerative dentistry. *Regenerative medicine, 6*(1), 111-124.

Garzon, I., Martin-Piedra, M., Carriel, V., Alaminos, M., Liu, X., & D'Souza, R. (2018). Bioactive injectable aggregates with nanofibrous microspheres and human dental pulp stem cells: A translational strategy in dental endodontics. *Journal of Tissue Engineering Regenerative Medicine, 12*(1), 204-216.

Ghorbani, M., Roshangar, L., & Rad, J. S. (2020). Development of reinforced chitosan/pectin scaffold by using the cellulose nanocrystals as nanofillers: An injectable hydrogel for tissue engineering. *European Polymer Journal, 130*, 109697.

Goldberg, M., & Hirata, A. (2017). The dental pulp: composition, properties and functions. *JSM Dentistry, 5*(1), 1079.

Gomez-Sosa, J., Caviedes-Bucheli, J., Diaz-Barrera, L., & Munoz, H. (2019). Gene expression of growth factors with angiogenic potential in human dental pulp tissue from teeth with complete and incomplete root development. *International endodontic journal, 52*(12), 1716-1722.

Gong, Q., Wang, R., Jiang, H., Lin, Z., & Ling, J. (2012). Alteration of microRNA expression of human dental pulp cells during odontogenic differentiation. *Journal of Endodontics, 38*(10), 1348-1354.

Groult, S., Buwalda, S., & Budtova, T. (2021). Pectin hydrogels, aerogels, cryogels and xerogels: Influence of drying on structural and release properties. *European Polymer Journal, 149*, 110386.

Hannahan, J. P., & Eleazer, P. D. (2008). Comparison of success of implants versus endodontically treated teeth. *Journal of endodontics, 34*(11), 1302-1305.

Hoch, E., Schuh, C., Hirth, T., Tovar, G. E., & Borchers, K. (2012). Stiff gelatin hydrogels can be photo-chemically synthesized from low viscous gelatin solutions using molecularly functionalized gelatin with a high degree of methacrylation. *Journal of Materials Science: Materials in Medicine, 23*(11), 2607-2617.

Hu, Y.-H., Chen, C.-Y., & Wang, C.-C. (2004). Viscoelastic properties and thermal degradation kinetics of silica/PMMA nanocomposites. *Polymer Degradation and Stability, 84*(3), 545-553.

Huang, G., & Huang, H. (2018). Application of hyaluronic acid as carriers in drug delivery. *Drug Delivery, 25*(1), 766-772.

Huang, S. C., Wu, B. C., Kao, C. T., Huang, T. H., Hung, C. J., & Shie, M. Y. (2015). Role of the p38 pathway in mineral trioxide aggregate-induced cell viability and angiogenesis-related proteins of dental pulp cell in vitro. *International endodontic journal, 48*(3), 236-245.

Inuyama, Y., Kitamura, C., Nishihara, T., Morotomi, T., Nagayoshi, M., Tabata, Y., . . . Terashita, M. (2010). Effects of hyaluronic acid sponge as a scaffold on odontoblastic cell line and amputated dental pulp. *Journal of Biomedical Materials Research Part B: Applied Biomaterials, 92*(1), 120-128.

Ishihara, K., Ueda, T., & Nakabayashi, N. (1990). Preparation of phospholipid polymers and their properties as polymer hydrogel membranes. *Polymer, 22*(5), 355-360.

Jäger, M., & Wilke, A. (2003). Comprehensive biocompatibility testing of a new PMMA-HA bone cement versus conventional PMMA cement in vitro. *Journal of Biomaterials Science, Polymer Edition, 14*(11), 1283-1298.

Jeong, C. H., Yune, J. H., Kwon, H. C., Shin, D.-M., Sohn, H., Lee, K. H., . . . Kim, E. K. (2021). In vitro toxicity assessment of crosslinking agents used in hyaluronic acid dermal filler. *Toxicology in Vitro, 70*, 105034.

Jiang, L., Wang, R., Yang, B., Li, T., Tryk, D., Fujishima, A., . . . Zhu, D. (2000). Binary cooperative complementary nanoscale interfacial materials. *Pure and applied chemistry, 72*(1-2), 73-81.

Jiang, L., Zhao, Y., & Zhai, J. (2004). A lotus-leaf-like superhydrophobic surface: a porous microsphere/nanofiber composite film prepared by electrohydrodynamics. *Angewandte Chemie, 116*(33), 4438-4441.

Jin, H.-J., & Kaplan, D. L. (2003). Mechanism of silk processing in insects and spiders. *Nature, 424*(6952), 1057.

Jin, H. J., Park, J., Karageorgiou, V., Kim, U. J., Valluzzi, R., Cebe, P., & Kaplan, D. L. (2005). Water-Stable Silk Films with Reduced β-Sheet Content. *Advanced Functional Materials, 15*(8), 1241-1247.

Jones, T., Kefi, A., Sun, S., Cho, M., & Alapati, S. (2016). An optimized injectable hydrogel scaffold supports human dental pulp stem cell viability and spreading. *Advances in Medicine, 2016*.

Jung-Hynes, B., Reiter, R. J., & Ahmad, N. (2010). Sirtuins, melatonin and circadian rhythms: building a bridge between aging and cancer. *Journal of pineal research, 48*(1), 9-19.

Jung, J., & Oh, J. (2014). Swelling characterization of photo-cross-linked gelatin methacrylate spherical microgels for bioencapsulation. *e-Polymers, 14*(3), 161-168.

Jung, Y.-J., Hyun, H.-K., Kim, Y.-J., & Jang, K.-T. (2009). Effect of collagenase and esterase on resin-dentin interface: A comparative study between a total-etch adhesive and a self-etch adhesive. *American journal of dentistry, 22*(5), 295.

Kambe, Y., Yamamoto, K., Kojima, K., Tamada, Y., & Tomita, N. (2010). Effects of RGDS sequence genetically interfused in the silk fibroin light chain protein on chondrocyte adhesion and cartilage synthesis. *Biomaterials, 31*(29), 7503-7511.

Kashiwagi, T., Inaba, A., Brown, J. E., Hatada, K., Kitayama, T., & Masuda, E. (1986). Effects of weak linkages on the thermal and oxidative degradation of poly (methyl methacrylates). *Macromolecules, 19*(8), 2160-2168.

Kawamura, H., Li, X., Goishi, K., van Meeteren, L. A., Jakobsson, L., Cébe-Suarez, S., . . . Kjellén, L. (2008). Neuropilin-1 in regulation of VEGF-induced activation of p38MAPK and endothelial cell organization. *Blood, 112*(9), 3638-3649.

Kayabolen, A., Keskin, D., Aykan, A., Karslıoglu, Y., Zor, F., & Tezcaner, A. (2017). Native extracellular matrix/fibroin hydrogels for adipose tissue engineering with enhanced vascularization. *Biomedical Materials, 12*(3), 035007.

Khayat, A., Monteiro, N., Smith, E., Pagni, S., Zhang, W., Khademhosseini, A., & Yelick, P. (2017). GelMA-encapsulated hDPSCs and HUVECs for dental pulp regeneration. *Journal of Dental Research, 96*(2), 192-199.

Kim, J., Park, Y., Tae, G., Lee, K. B., Hwang, S. J., Kim, I. S., . . . Sun, K. (2008). Synthesis and characterization of matrix metalloprotease sensitive-low molecular weight hyaluronic acid based hydrogels. *Journal of Materials Science: Materials in Medicine, 19*(11), 3311-3318.

Kim, K.-H., Jeong, L., Park, H.-N., Shin, S.-Y., Park, W.-H., Lee, S.-C., . . . Lee, Y.-M. (2005). Biological efficacy of silk fibroin nanofiber membranes for guided bone regeneration. *Journal of biotechnology, 120*(3), 327-339.

Kmiec, M., Pighinelli, L., Tedesco, M., Silva, M., & Reis, V. (2017). Chitosan-properties and applications in dentistry. *Adv Tissue Eng Regen Med Open Access, 2*(4), 00035.

Konieczny, P., Selma-Soriano, E., Rapisarda, A. S., Fernandez-Costa, J. M., Perez-Alonso, M., & Artero, R. (2017). Myotonic dystrophy: candidate small molecule therapeutics. *Drug discovery today, 22*(11), 1740-1748.

Krauland, A. H., Leitner, V. M., & Bernkop-Schnürch, A. (2003). Improvement in the in situ gelling properties of deacetylated gellan gum by the immobilization of thiol groups. *Journal of pharmaceutical sciences, 92*(6), 1234-1241.

Kuang, R., Zhang, Z., Jin, X., Hu, J., Shi, S., Ni, L., & Ma, P. X. (2016). Nanofibrous spongy microspheres for the delivery of hypoxia-primed human dental pulp stem cells to regenerate vascularized dental pulp. *Acta biomaterialia, 33*, 225-234.

Langer, R., & Tirrell, D. A. (2004). Designing materials for biology and medicine. *Nature, 428*(6982), 487-492.

Lee, S.-H., & Shin, H. (2007). Matrices and scaffolds for delivery of bioactive molecules in bone and cartilage tissue engineering. *Advanced drug delivery reviews, 59*(4), 339-359.

Leung, K. W., Cheng, Y.-K., Mak, N. K., Chan, K. K., Fan, T. D., & Wong, R. N. (2006). Signaling pathway of ginsenoside-Rg1 leading to nitric oxide production in endothelial cells. *FEBS Letters, 580*(13), 3211-3216.

Li, F., Zhao, Y., & Song, Y. (2010). Core-shell nanofibers: nano channel and capsule by coaxial electrospinning. *Nanofibers, 2*, 418-438.

Li, J., & Zhuang, S. (2020). Antibacterial activity of chitosan and its derivatives and their interaction mechanism with bacteria: Current state and perspectives. *European Polymer Journal, 138*, 109984.

Li, L., Li, H., Qian, Y., Li, X., Singh, G. K., Zhong, L., . . . Yang, L. (2011). Electrospun poly (ε-caprolactone)/silk fibroin core-sheath nanofibers and their potential applications in tissue engineering and drug release. *International journal of biological macromolecules, 49*(2), 223-232.

Li, M., Jia, W., Zhang, X., Weng, H., Gu, G., & Chen, Z. (2021). Hyaluronic acid oligosaccharides modified mineralized collagen and chitosan with enhanced osteoinductive properties for bone tissue engineering. *Carbohydrate polymers, 260*, 117780.

Li, X., Ma, C., Xie, X., Sun, H., & Liu, X. (2016). Pulp regeneration in a full-length human tooth root using a hierarchical nanofibrous microsphere system. *Acta biomaterialia, 35*, 57-67.

Lin, K. M.-C., Hsu, C.-H., & Rajasekaran, S. (2008). Angiogenic evaluation of ginsenoside Rg1 from Panax ginseng in fluorescent transgenic mice. *Vascular Pharmacology, 49*(1), 37-43.

Liu, J., Zhou, H., Fan, W., Dong, W., Fu, S., He, H., & Huang, F. (2013). Melatonin influences proliferation and differentiation of rat dental papilla cells in vitro and dentine formation in vivo by altering mitochondrial activity. *Journal of pineal research, 54*(2), 170-178.

Liu, L., Cooke, P. H., Coffin, D. R., Fishman, M. L., & Hicks, K. B. (2004). Pectin and polyacrylamide composite hydrogels: effect of pectin on structural and dynamic mechanical properties. *Journal of Applied Polymer Science, 92*(3), 1893-1901.

Liu, Q., Fan, W., He, Y., Zhang, F., Guan, X., Deng, Q., . . . Huang, F. (2017). Effects of melatonin on the proliferation and differentiation of human dental pulp cells. *Archives of Oral Biology, 83*, 33-39.

Lovász, B. V., Lempel, E., Szalma, J., Sétáló, G., Vecsernyés, M., & Berta, G. (2021). Influence of TEGDMA monomer on MMP-2, MMP-8, and MMP-9

production and collagenase activity in pulp cells. *Clinical Oral Investigations, 25*(4), 2269-2279.

Lovestone, S., Boada, M., Dubois, B., Hüll, M., Rinne, J. O., Huppertz, H.-J., . . . Leon, T. (2015). A phase II trial of tideglusib in Alzheimer's disease. *Journal of Alzheimer's Disease, 45*(1), 75-88.

Ma, Y., Cao, X., Feng, X., Ma, Y., & Zou, H. (2007). Fabrication of super-hydrophobic film from PMMA with intrinsic water contact angle below 90. *Polymer, 48*(26), 7455-7460.

Matsunaga, T., Yanagiguchi, K., Yamada, S., Ohara, N., Ikeda, T., & Hayashi, Y. (2006). Chitosan monomer promotes tissue regeneration on dental pulp wounds. *Journal of Biomedical Materials Research Part A, 76*(4), 711-720.

Mei, Y. F., Yamaza, T., Atsuta, I., Danjo, A., Yamashita, Y., Kido, M. A., . . . Tanaka, T. (2007). Sequential expression of endothelial nitric oxide synthase, inducible nitric oxide synthase, and nitrotyrosine in odontoblasts and pulp cells during dentin repair after tooth preparation in rat molars. *Cell Tissue Research, 328*(1), 117-127.

Mekonnen, T., Misra, M., & Mohanty, A. (2015). Processing, performance, and applications of plant and animal protein-based blends and their biocomposites. In *Biocomposites* (pp. 201-235): Elsevier.

Meyer, K., Palmer, J. W., Thompson, R., & Khorazo, D. (1936). On the mechanism of lysozyme action. *Journal of Biological Chemistry, 113*(2), 479-486.

Moreira, H. R., Munarin, F., Gentilini, R., Visai, L., Granja, P. L., Tanzi, M. C., & Petrini, P. (2014). Injectable pectin hydrogels produced by internal gelation: pH dependence of gelling and rheological properties. *Carbohydrate polymers, 103*, 339-347.

Moreira, M. S., Sarra, G., Carvalho, G. L., Gonçalves, F., Caballero-Flores, H. V., Pedroni, A. C. F., . . . Marques, M. M. (2021). Physical and Biological Properties of a Chitosan Hydrogel Scaffold Associated to Photobiomodulation Therapy for Dental Pulp Regeneration: An In Vitro and In Vivo Study. *BioMed Research International, 2021*.

Mori, T., Okumura, M., Matsuura, M., Ueno, K., Tokura, S., Okamoto, Y., . . . Fujinaga, T. (1997). Effects of chitin and its derivatives on the proliferation and cytokine production of fibroblasts in vitro. *Biomaterials, 18*(13), 947-951.

Morotomi, T., Washio, A., & Kitamura, C. (2019). Current and future options for dental pulp therapy. *Japanese Dental Science Review, 55*(1), 5-11.

Motta, A., Fambri, L., & Migliaresi, C. (2002). Regenerated silk fibroin films: thermal and dynamic mechanical analysis. *Macromolecular Chemistry and Physics, 203*(10-11), 1658-1665.

Nair, P. (2006). On the causes of persistent apical periodontitis: a review. *International endodontic journal, 39*(4), 249-281.

Nanci, A. (2007). *Ten cate's oral histology-pageburst on vitalsource: development, structure, and function*: Elsevier Health Sciences.

Neves, V. C., Babb, R., Chandrasekaran, D., & Sharpe, P. T. (2017a). Promotion of natural tooth repair by small molecule GSK3 antagonists. *Scientific reports, 7*(1), 1-7.

Neves, V. C., Babb, R., Chandrasekaran, D., & Sharpe, P. T. (2017b). Promotion of natural tooth repair by small molecule GSK3 antagonists. *Scientific reports, 7*, 39654.

Nichol, J. W., Koshy, S. T., Bae, H., Hwang, C. M., Yamanlar, S., & Khademhosseini, A. (2010). Cell-laden microengineered gelatin methacrylate hydrogels. *Biomaterials, 31*(21), 5536-5544.

Ochoa, N., Masuelli, M., & Marchese, J. (2003). Effect of hydrophilicity on fouling of an emulsified oil wastewater with PVDF/PMMA membranes. *Journal of Membrane Science, 226*(1-2), 203-211.

Pan, T., Song, W., Cao, X., & Wang, Y. (2016). 3D bioplotting of gelatin/alginate scaffolds for tissue engineering: influence of crosslinking degree and pore architecture on physicochemical properties. *Journal of Materials Science Technology, 32*(9), 889-900.

Pankajakshan, D., Voytik-Harbin, S. L., Nör, J. E., & Bottino, M. C. (2020). Injectable highly tunable Oligomeric collagen matrices for dental tissue regeneration. *ACS Applied Biomaterials, 3*(2), 859-868.

Pashley, D. H., Livingston, M., & Greenhill, J. (1978). Regional resistances to fluid flow in human dentine in vitro. *Archives of Oral Biology, 23*(9), 807-810.

Patterson, J., Siew, R., Herring, S. W., Lin, A. S., Guldberg, R., & Stayton, P. S. (2010). Hyaluronic acid hydrogels with controlled degradation properties for oriented bone regeneration. *Biomaterials, 31*(26), 6772-6781.

Pedano, M. S., Li, X., Camargo, B., Hauben, E., De Vleeschauwer, S., Yoshihara, K., . . . Van Meerbeek, B. (2020). Injectable phosphopullulan-functionalized calcium-silicate cement for pulp-tissue engineering: An in-vivo and ex-vivo study. *Dental Materials, 36*(4), 512-526.

Peluso, G., Petillo, O., Ranieri, M., Santin, M., Ambrosic, L., Calabró, D., . . . Balsamo, G. (1994). Chitosan-mediated stimulation of macrophage function. *Biomaterials, 15*(15), 1215-1220.

Peppas, N. A., Hilt, J. Z., Khademhosseini, A., & Langer, R. (2006). Hydrogels in biology and medicine: from molecular principles to bionanotechnology. *Advanced Materials, 18*(11), 1345-1360.

Peppas, N. A., & Langer, R. (1994). New challenges in biomaterials. *Science, 263*(5154), 1715-1721.

Perera, G., Hombach, J., & Bernkop-Schnürch, A. (2010). Hydrophobic thiolation of pectin with 4-aminothiophenol: synthesis and in vitro characterization. *Aaps Pharmscitech, 11*(1), 174-180.

Prada, I., Micó-Muñoz, P., Giner-Lluesma, T., Micó-Martínez, P., Muwaquet-Rodríguez, S., & Albero-Monteagudo, A. (2019). Update of the therapeutic planning of irrigation and intracanal medication in root canal treatment. A literature review. *Journal of clinical experimental dentistry, 11*(2), e185.

Prasad, B., Gupta, V., Devanna, N., & Jayasurya, K. (2014). Microspheres as drug delivery system-a review. *Glob Trends Pharm Sci, 5*, 1961-1972.

Quintarelli, G., & Dellovo, M. C. (1963). Mucopolysaccharide histochemistry of rat tooth germs. *Zeitschrift für Zellforschung und mikroskopische Anatomie Abt. Histochemie, 3*(3), 195-207.

Qutachi, O., Vetsch, J. R., Gill, D., Cox, H., Scurr, D. J., Hofmann, S., . . . Rahman, C. V. (2014). Injectable and porous PLGA microspheres that form highly porous scaffolds at body temperature. *Acta biomaterialia, 10*(12), 5090-5098.

Rabiatul, A., Lokanathan, Y., Rohaina, C., Chowdhury, S. R., Aminuddin, B., & Ruszymah, B. (2015). Surface modification of electrospun poly (methyl methacrylate)(PMMA) nanofibers for the development of in vitro respiratory epithelium model. *Journal of Biomaterials Science, Polymer Edition, 26*(17), 1297-1311.

Rad, R. M., Atila, D., Akgün, E. E., Evis, Z., Keskin, D., & Tezcaner, A. (2019). Evaluation of human dental pulp stem cells behavior on a novel nanobiocomposite scaffold prepared for regenerative endodontics. *Materials Science Engineering: C, 100*, 928-948.

Ramesh, S., Leen, K. H., Kumutha, K., & Arof, A. (2007). FTIR studies of PVC/PMMA blend based polymer electrolytes. *Spectrochimica Acta Part A: Molecular and Biomolecular Spectroscopy, 66*(4-5), 1237-1242.

Ratner, B. D., Hoffman, A. S., Schoen, F. J., & Lemons, J. E. (2004). *Biomaterials science: an introduction to materials in medicine*: Academic press.

Ribeiro, J. S., Bordini, E. A., Ferreira, J. A., Mei, L., Dubey, N., Fenno, J. C., . . . Bottino, M. C. (2020). Injectable MMP-responsive nanotube-modified gelatin hydrogel for dental infection ablation. *ACS Applied Materials Interfaces, 12*(14), 16006-16017.

Riccio, M., Maraldi, T., Pisciotta, A., La Sala, G. B., Ferrari, A., Bruzzesi, G., . . . De Pol, A. (2012). Fibroin scaffold repairs critical-size bone defects in vivo supported by human amniotic fluid and dental pulp stem cells. *Tissue Engineering Part A, 18*(9-10), 1006-1013.

Rockwood, D. N., Preda, R. C., Yücel, T., Wang, X., Lovett, M. L., & Kaplan, D. L. (2011). Materials fabrication from Bombyx mori silk fibroin. *Nature protocols, 6*(10), 1612.

Rodríguez-Lozano, F., García-Bernal, D., Aznar-Cervantes, S., Ros-Roca, M., Algueró, M., Atucha, N., . . . Cenis, J. (2014). Effects of composite films of silk fibroin and graphene oxide on the proliferation, cell viability and mesenchymal phenotype of periodontal ligament stem cells. *Journal of Materials Science: Materials in Medicine, 25*(12), 2731-2741.

Saghiri, M. A., Asatourian, A., Sorenson, C. M., & Sheibani, N. (2015). Role of angiogenesis in endodontics: contributions of stem cells and proangiogenic and antiangiogenic factors to dental pulp regeneration. *Journal of endodontics, 41*(6), 797-803.

Scatena, L., Brown, M., & Richmond, G. (2001). Water at hydrophobic surfaces: Weak hydrogen bonding and strong orientation effects. *Science, 292*(5518), 908-912.

Schulz, U., Munzert, P., & Kaiser, N. (2001). Surface modification of PMMA by DC glow discharge and microwave plasma treatment for the improvement of coating adhesion. *Surface and coatings technology, 142*, 507-511.

Seidlits, S. K., Drinnan, C. T., Petersen, R. R., Shear, J. B., Suggs, L. J., & Schmidt, C. E. (2011). Fibronectin–hyaluronic acid composite hydrogels for three-dimensional endothelial cell culture. *Acta biomaterialia, 7*(6), 2401-2409.

Sharma, L. A., & Love, R. M. (2019). Scaffolds for regeneration of the pulp–dentine complex. In *Handbook of Tissue Engineering Scaffolds: Volume One* (pp. 459-478): Elsevier.

Sharma, R., & Ahuja, M. (2011). Thiolated pectin: Synthesis, characterization and evaluation as a mucoadhesive polymer. *Carbohydrate polymers, 85*(3), 658-663.

Shioya, T., Koga, Y., Fujimoto, K., & Ishida, R. (1988). Micro-mechanism of dynamic crack propagation in brittle materials. *Le Journal de Physique Colloques, 49*(C3), C3-253-C253-260.

Siepmann, J., Faisant, N., Akiki, J., Richard, J., & Benoit, J. (2004). Effect of the size of biodegradable microparticles on drug release: experiment and theory. *Journal of Controlled Release, 96*(1), 123-134.

Silva, C. R., Babo, P. S., Gulino, M., Costa, L., Oliveira, J. M., Silva-Correia, J., . . . Gomes, M. E. (2018). Injectable and tunable hyaluronic acid hydrogels releasing chemotactic and angiogenic growth factors for endodontic regeneration. *Acta biomaterialia, 77*, 155-171.

Sirousazar, M., Kokabi, M., & Hassan, Z. (2012). Swelling behavior and structural characteristics of polyvinyl alcohol/montmorillonite nanocomposite hydrogels. *Journal of Applied Polymer Science, 123*(1), 50-58.

Snead, M. L. (2008). Whole-tooth regeneration: it takes a village of scientists, clinicians, and patients. *Journal of dental education, 72*(8), 903-911.

Sohrabi, A., Hosseini, M., Abazari, M. F., Karizi, S. Z., Oskouei, S. A. S., Hajati-Birgani, N., . . . Askari, M. (2021). Wnt pathway activator delivery by poly (lactide-co-glycolide)/silk fibroin composite nanofibers promotes dental pulp stem cell osteogenesis. *Journal of Drug Delivery Science Technology, 61*, 102223.

Sriamornsak, P., Thirawong, N., Nunthanid, J., Puttipipatkhachorn, S., Thongborisute, J., & Takeuchi, H. (2008). Atomic force microscopy imaging of novel self-assembling pectin–liposome nanocomplexes. *Carbohydrate Polymers, 71*(2), 324-329.

Sriamornsak, P., Wattanakorn, N., Nunthanid, J., & Puttipipatkhachorn, S. (2008). Mucoadhesion of pectin as evidence by wettability and chain interpenetration. *Carbohydrate Polymers, 74*(3), 458-467.

Stevens, M. M. (2008). Biomaterials for bone tissue engineering. *Materials Today, 11*(5), 18-25.

Su, J. J.-M., Lin, C.-H., Chen, H., Lee, S.-Y., & Lin, Y.-M. (2021). Biofabrication of Cell-Laden Gelatin Methacryloyl Hydrogels with Incorporation of

Silanized Hydroxyapatite by Visible Light Projection. *Polymers, 13*(14), 2354.

Tachibana, R., Tatehara, S., Kumasaka, S., Tokuyama, R., & Satomura, K. (2014). Effect of melatonin on human dental papilla cells. *International journal of molecular sciences, 15*(10), 17304-17317.

Tan, D.-X., Pöeggeler, B., Reiter, R. J., Chen, L.-D., Chen, S., Lucien, M. C., & Barlow-Walden, L. R. (1993). The pineal hormone melatonin inhibits DNA-adduct formation induced by the chemical carcinogen safrole in vivo. *Cancer letters, 70*(1), 65-71.

Tan, L., Wang, J., Yin, S., Zhu, W., Zhou, G., Cao, Y., & Cen, L. (2015). Regeneration of dentin–pulp-like tissue using an injectable tissue engineering technique. *RSC advances, 5*(73), 59723-59737.

Tang, Z., Chen, H., He, H., & Ma, C. (2019). Assays for alkaline phosphatase activity: progress and prospects. *Trends in Analytical Chemistry, 113*, 32-43.

Thompson, C., Chase, G. G., Yarin, A., & Reneker, D. (2007). Effects of parameters on nanofiber diameter determined from electrospinning model. *Polymer, 48*(23), 6913-6922.

Tihan, T. G., Ionita, M. D., Popescu, R. G., & Iordachescu, D. (2009). Effect of hydrophilic–hydrophobic balance on biocompatibility of poly (methyl methacrylate)(PMMA)–hydroxyapatite (HA) composites. *Materials Chemistry and Physics, 118*(2), 265-269.

Toker, S., Tezcaner, A., & Evis, Z. (2011). Microstructure, microhardness, and biocompatibility characteristics of yttrium hydroxyapatite doped with fluoride. *Journal of Biomedical Materials Research Part B: Applied Biomaterials, 96*(2), 207-217.

Tolosa, E., Litvan, I., Höglinger, G. U., Burn, D., Lees, A., Andrés, M. V., . . . Del Ser, T. (2014). A phase 2 trial of the GSK-3 inhibitor tideglusib in progressive supranuclear palsy. *Movement Disorders, 29*(4), 470-478.

Ueno, H., Yamada, H., Tanaka, I., Kaba, N., Matsuura, M., Okumura, M., . . . Fujinaga, T. (1999). Accelerating effects of chitosan for healing at early phase of experimental open wound in dogs. *Biomaterials, 20*(15), 1407-1414.

Um, I. C., Kweon, H., Park, Y. H., & Hudson, S. (2001). Structural characteristics and properties of the regenerated silk fibroin prepared from formic acid. *International journal of biological macromolecules, 29*(2), 91-97.

Van Den Bulcke, A. I., Bogdanov, B., De Rooze, N., Schacht, E. H., Cornelissen, M., & Berghmans, H. (2000). Structural and rheological properties of methacrylamide modified gelatin hydrogels. *Biomacromolecules, 1*(1), 31-38.

Varagnolo, S., Raccanello, F., Pierno, M., Mistura, G., Moffa, M., Persano, L., & Pisignano, D. (2017). Highly sticky surfaces made by electrospun polymer nanofibers. *RSC advances, 7*(10), 5836-5842.

Veerayutthwilai, O., Byers, M., Pham, T. T., Darveau, R., & Dale, B. (2007). Differential regulation of immune responses by odontoblasts. *Oral microbiology immunology, 22*(1), 5-13.

Vesel, A., & Mozetic, M. (2012). Surface modification and ageing of PMMA polymer by oxygen plasma treatment. *Vacuum, 86*(6), 634-637.

Wang, H., Zhang, Y., Shao, H., & Hu, X. (2005). Electrospun ultra-fine silk fibroin fibers from aqueous solutions. *Journal of materials science, 40*(20), 5359-5363.

Wang, J., Ma, H., Jin, X., Hu, J., Liu, X., Ni, L., & Ma, P. X. (2011). The effect of scaffold architecture on odontogenic differentiation of human dental pulp stem cells. *Biomaterials, 32*(31), 7822-7830.

Wang, P., Wei, X., Zhang, F., Yang, K., Qu, C., Luo, H., & He, L. (2014). Ginsenoside Rg1 of Panax ginseng stimulates the proliferation, odontogenic/osteogenic differentiation and gene expression profiles of human dental pulp stem cells. *Phytomedicine, 21*(2), 177-183.

Wang, P., Wei, X., Zhou, Y., Wang, Y. P., Yang, K., Zhang, F. J., & Jiang, R. (2012). Effect of ginsenoside Rg1 on proliferation and differentiation of human dental pulp cells in vitro. *Australian Dental Journal, 57*(2), 157-165.

Wang, W., Meng, Q., Li, Q., Liu, J., Zhou, M., Jin, Z., & Zhao, K. (2020). Chitosan derivatives and their application in biomedicine. *International Journal of Molecular Sciences, 21*(2), 487.

Wei, H., Zhang, X., Cheng, C., Cheng, S.-X., & Zhuo, R.-X. (2007). Self-assembled, thermosensitive micelles of a star block copolymer based on PMMA and PNIPAAm for controlled drug delivery. *Biomaterials, 28*(1), 99-107.

Wei, K., Li, Y., Kim, K. O., Nakagawa, Y., Kim, B. S., Abe, K., . . . Kim, I. S. (2011). Fabrication of nano-hydroxyapatite on electrospun silk fibroin nanofiber and their effects in osteoblastic behavior. *Journal of Biomedical Materials Research Part A, 97*(3), 272-280.

Wei, M., Kang, B., Sung, C., & Mead, J. (2006). Core-Sheath Structure in Electrospun Nanofibers from Polymer Blends. *Macromolecular materials and engineering, 291*(11), 1307-1314.

Wende, F. J., Gohil, S., Nord, L. I., Kenne, A. H., & Sandström, C. (2017). 1D NMR methods for determination of degree of cross-linking and BDDE substitution positions in HA hydrogels. *Carbohydrate polymers, 157*, 1525-1530.

Woloszyk, A., Dircksen, S. H., Bostanci, N., Müller, R., Hofmann, S., & Mitsiadis, T. A. (2014). Influence of the mechanical environment on the engineering of mineralised tissues using human dental pulp stem cells and silk fibroin scaffolds. *PloS one, 9*(10), e111010.

Wöltgens, J., Vingerling, P., & Witjes, F. (1980). Chemical evidence of two separate apatite phases in human enamel. *Archives of Oral Biology, 25*(6), 435-436.

Xing, Z.-C., Han, S.-J., Shin, Y.-S., Koo, T.-H., Moon, S., Jeong, Y., & Kang, I.-K. (2013). Enhanced osteoblast responses to poly (methyl

methacrylate)/hydroxyapatite electrospun nanocomposites for bone tissue engineering. *Journal of Biomaterials Science, Polymer Edition, 24*(1), 61-76.

Xu, J., Gong, T., Wang, Y., Zou, T., Heng, B., Yang, Y., & Zhang, C. (2018). Inhibition of TGF-β signaling in SHED enhances endothelial differentiation. *Journal of Dental Research, 97*(2), 218-225.

Xu, W., Ma, J., & Jabbari, E. (2010). Material properties and osteogenic differentiation of marrow stromal cells on fiber-reinforced laminated hydrogel nanocomposites. *Acta biomaterialia, 6*(6), 1992-2002.

Xue, Y., Chen, H., Xu, C., Yu, D., Xu, H., & Hu, Y. (2020). Synthesis of hyaluronic acid hydrogels by crosslinking the mixture of high-molecular-weight hyaluronic acid and low-molecular-weight hyaluronic acid with 1, 4-butanediol diglycidyl ether. *RSC advances, 10*(12), 7206-7213.

Yang, I.-H., Chen, Y.-S., Li, J.-J., Liang, Y.-J., Lin, T.-C., Jakfar, S., . . . Lin, F.-H. (2021). The development of laminin-alginate microspheres encapsulated with Ginsenoside Rg1 and ADSCs for breast reconstruction after lumpectomy. *Bioactive Materials, 6*(6), 1699-1710.

Yang, J.-w., Zhang, Y.-f., Sun, Z.-y., Song, G.-t., & Chen, Z. (2015). Dental pulp tissue engineering with bFGF-incorporated silk fibroin scaffolds. *Journal of biomaterials applications, 30*(2), 221-229.

Yang, M. (2017). Silk-based biomaterials. *Microscopy Research and Technique, 80*(3), 321-330.

Yang, R., Tan, L., Cen, L., & Zhang, Z. (2016). An injectable scaffold based on crosslinked hyaluronic acid gel for tissue regeneration. *RSC advances, 6*(20), 16838-16850.

Yang, T., Zhang, Q., Xie, L., Zhang, R., Qian, R., Tian, Y., . . . Tian, W. (2021). hDPSC-laden GelMA microspheres fabricated using electrostatic microdroplet method for endodontic regeneration. *Materials Science Engineering: C, 121*, 111850.

Yang, X., Yang, F., Walboomers, X. F., Bian, Z., Fan, M., & Jansen, J. A. (2010). The performance of dental pulp stem cells on nanofibrous PCL/gelatin/nHA scaffolds. *Journal of Biomedical Materials Research Part A, 93*(1), 247-257.

Yang, Y., & Dan, Y. (2003). Preparation of PMMA/SiO 2 composite particles via emulsion polymerization. *Colloid and Polymer Science, 281*(8), 794-799.

Yang, Y., Wang, S., Wang, Y., Wang, X., Wang, Q., & Chen, M. (2014). Advances in self-assembled chitosan nanomaterials for drug delivery. *Biotechnology Advances, 32*(7), 1301-1316.

Yen, A. H.-H., & Sharpe, P. T. (2008). Stem cells and tooth tissue engineering. *Cell and tissue research, 331*(1), 359-372.

Yu, H., Zhang, X., Song, W., Pan, T., Wang, H., Ning, T., . . . Ma, D. (2019). Effects of 3-dimensional bioprinting alginate/gelatin hydrogel scaffold extract on proliferation and differentiation of human dental pulp stem cells. *Journal of endodontics, 45*(6), 706-715.

Zaslansky, P., Friesem, A. A., & Weiner, S. (2006). Structure and mechanical properties of the soft zone separating bulk dentin and enamel in crowns of human teeth: insight into tooth function. *Journal of structural biology, 153*(2), 188-199.

Zaugg, L., Banu, A., Walther, A., Chandrasekaran, D., Babb, R., Salzlechner, C., . . . Sharpe, P. (2020). Translation Approach for Dentine Regeneration Using GSK-3 Antagonists. *Journal of Dental Research, 99*(5), 544-551.

Zeng, W., Huang, J., Hu, X., Xiao, W., Rong, M., Yuan, Z., & Luo, Z. (2011). Ionically cross-linked chitosan microspheres for controlled release of bioactive nerve growth factor. *International journal of pharmaceutics, 421*(2), 283-290.

Zhang, K., Wang, H., Huang, C., Su, Y., Mo, X., & Ikada, Y. (2010). Fabrication of silk fibroin blended P (LLA-CL) nanofibrous scaffolds for tissue engineering. *Journal of Biomedical Materials Research Part A, 93*(3), 984-993.

Zhang, L., Zhang, J., Ling, Y., Chen, C., Liang, A., Peng, Y., . . . Huang, D. (2013). Sustained release of melatonin from poly (lactic-co-glycolic acid)(PLGA) microspheres to induce osteogenesis of human mesenchymal stem cells in vitro. *Journal of pineal research, 54*(1), 24-32.

Zhang, R., Xie, L., Wu, H., Yang, T., Zhang, Q., Tian, Y., . . . He, M. (2020). Alginate/laponite hydrogel microspheres co-encapsulating dental pulp stem cells and VEGF for endodontic regeneration. *Acta biomaterialia, 113*, 305-316.

Zhang, S., Thiebes, A. L., Kreimendahl, F., Ruetten, S., Buhl, E. M., Wolf, M., . . . Apel, C. (2020). Extracellular vesicles-loaded fibrin gel supports rapid neovascularization for dental pulp regeneration. *International Journal of Molecular Sciences, 21*(12), 4226.

Zhang, W., & Yelick, P. C. (2010). Vital pulp therapy—current progress of dental pulp regeneration and revascularization. *International journal of dentistry, Volume 2010*.

Zhang, X.-Z., Lewis, P. J., & Chu, C.-C. (2005). Fabrication and characterization of a smart drug delivery system: microsphere in hydrogel. *Biomaterials, 26*(16), 3299-3309.

Zheng, Y., Feng, Z., You, C., Jin, Y., Hu, X., Wang, X., & Han, C. (2013). In vitro evaluation of Panax notoginseng Rg1 released from collagen/chitosan-gelatin microsphere scaffolds for angiogenesis. *Biomedical Engineering, 12*(1), 1-16.

Zhu, N., Chatzistavrou, X., Papagerakis, P., Ge, L., Qin, M., & Wang, Y. (2019). Silver-doped bioactive glass/chitosan hydrogel with potential application in dental pulp repair. *ACS Biomaterials Science Engineering, 5*(9), 4624-4633.
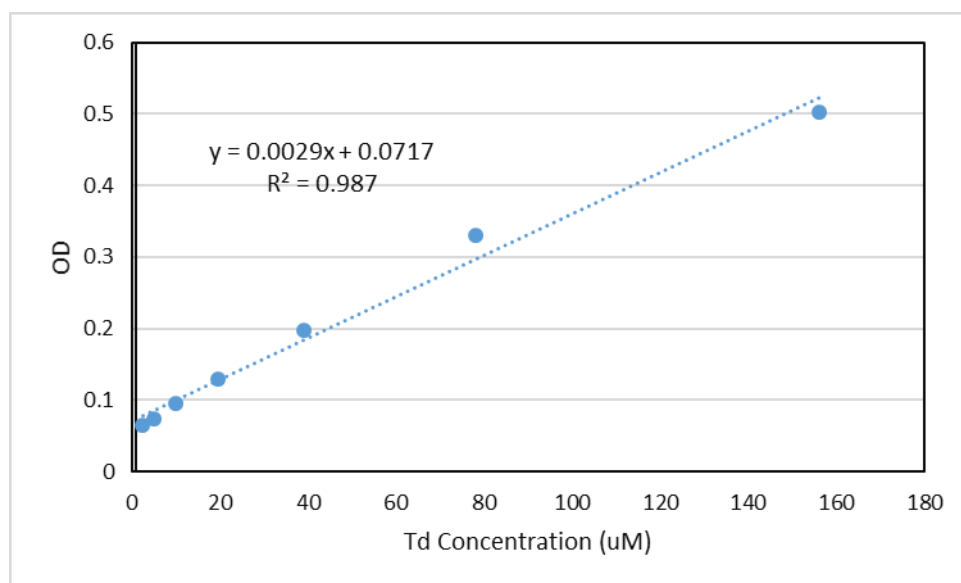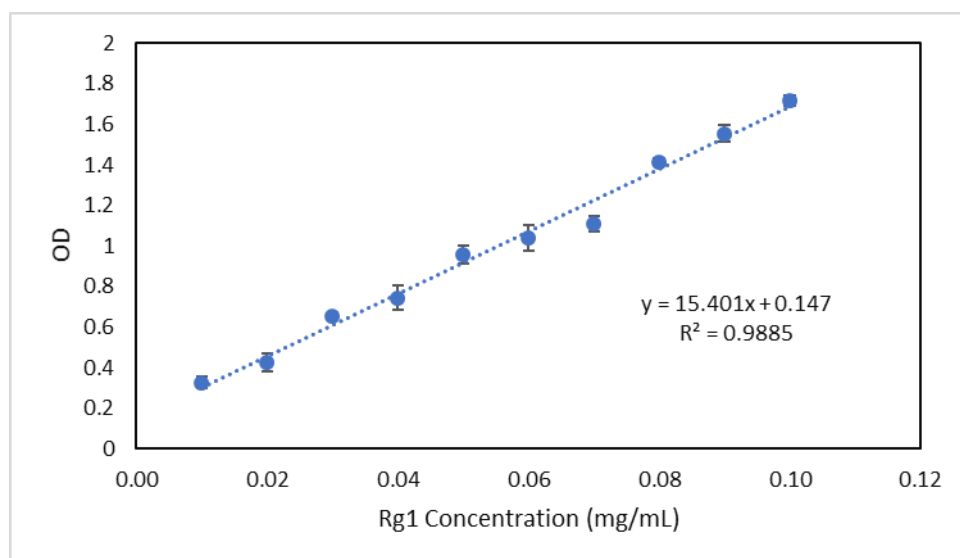
A. Calibration Study of BDDE Removal
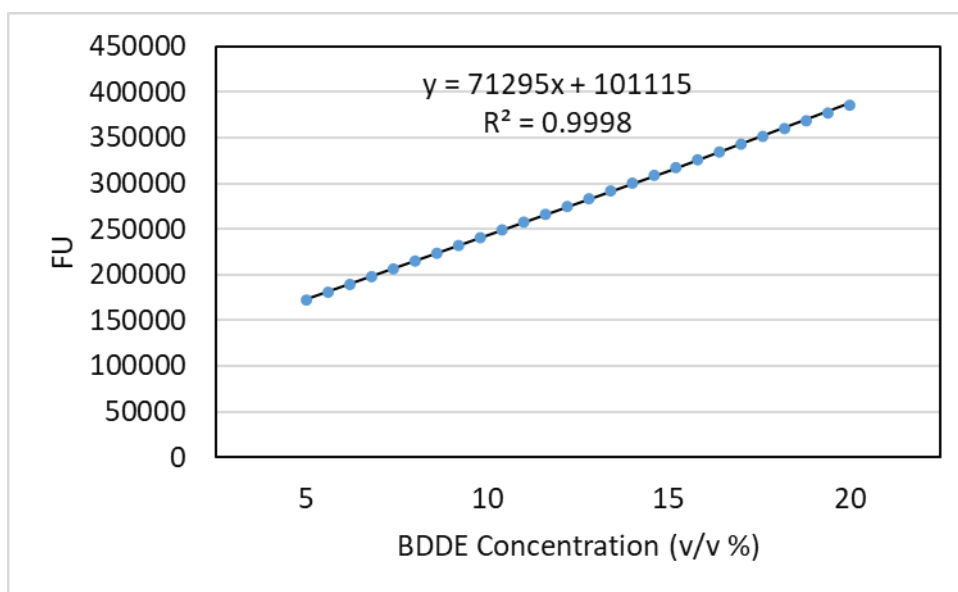
Appendix A1 Figure 65 Standard curve constructed for different concentrations of BDDE.
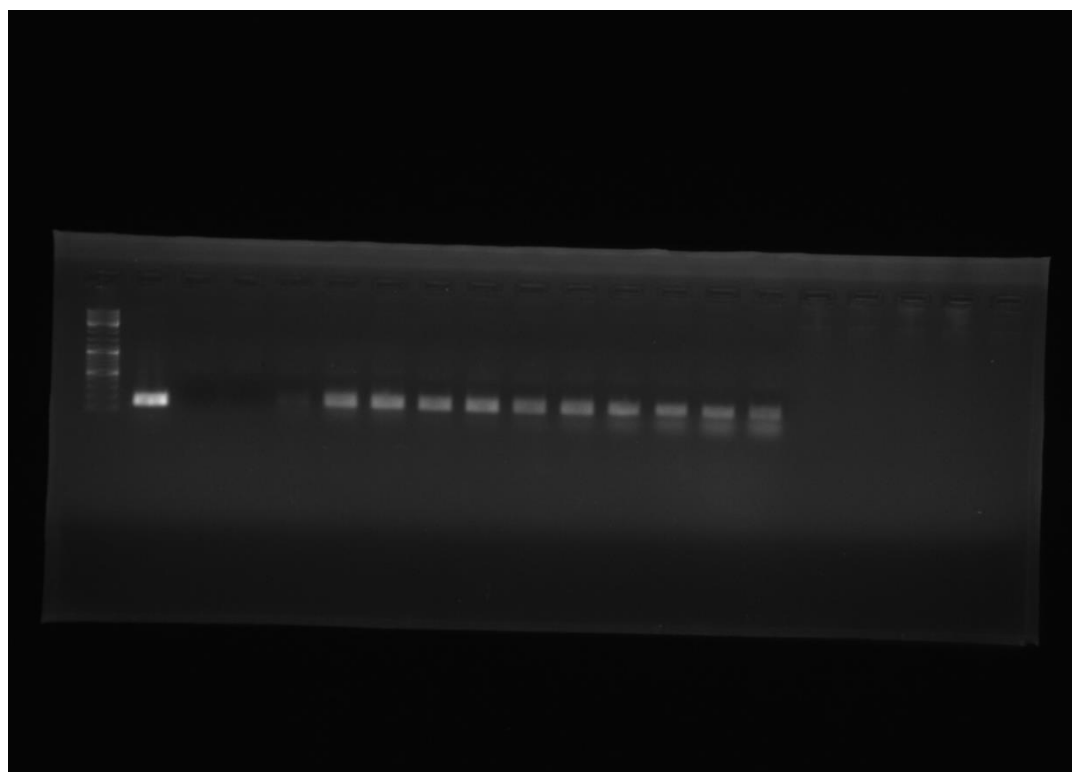
B. Calibration Study of Td Release

Appendix B1 Figure 66 Standard curve constructed for different concentrations of Td in DMSO.

C. Calibration Study of Rg1 Release

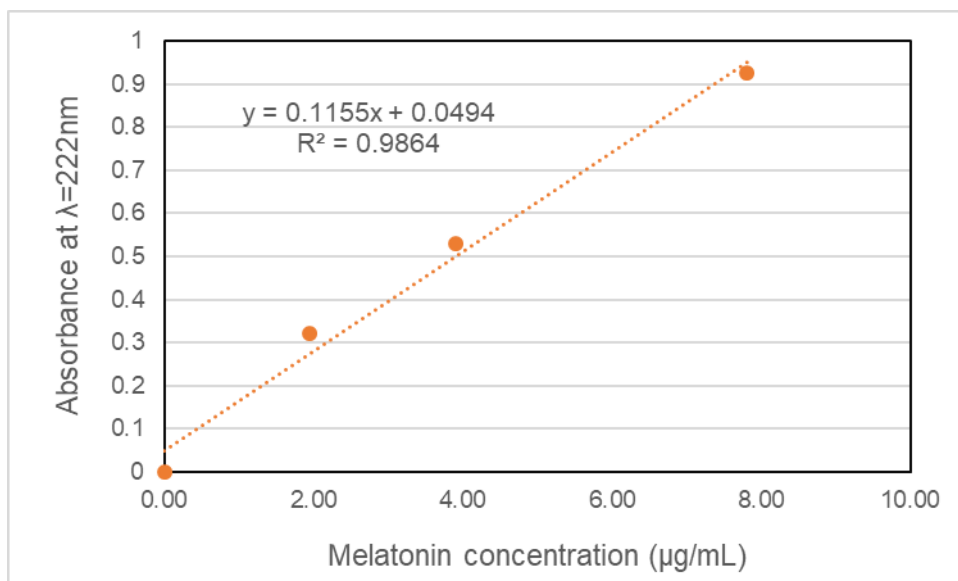Appendix C1 Figure 67 Standard curve constructed for different concentrations of Rg1.
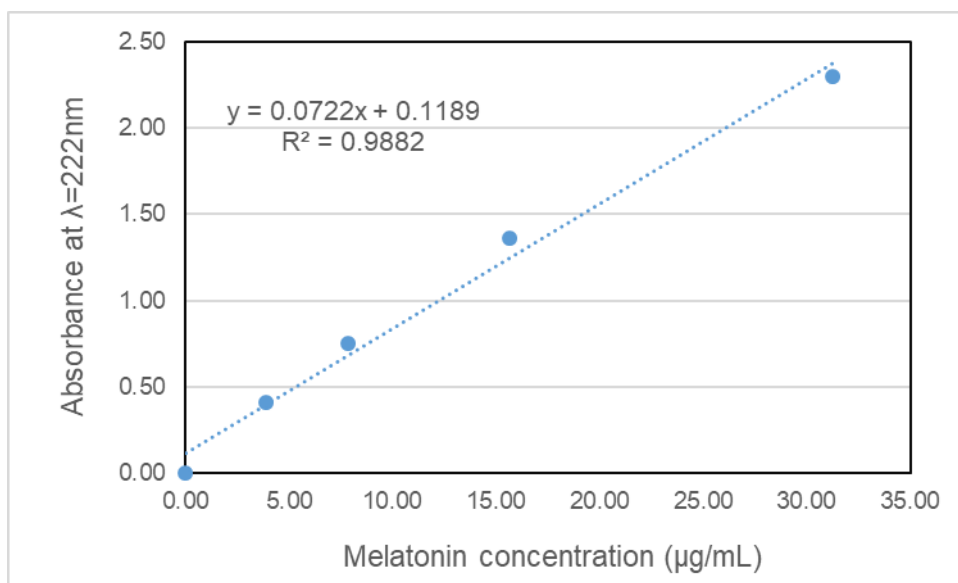
D. Agarose Gel Monitoring of GAPDH

Appendix D1 Figure 68 Agarose gel electrophoresis of DNA obtained from qPCR reaction products of GAPDH calibration study.
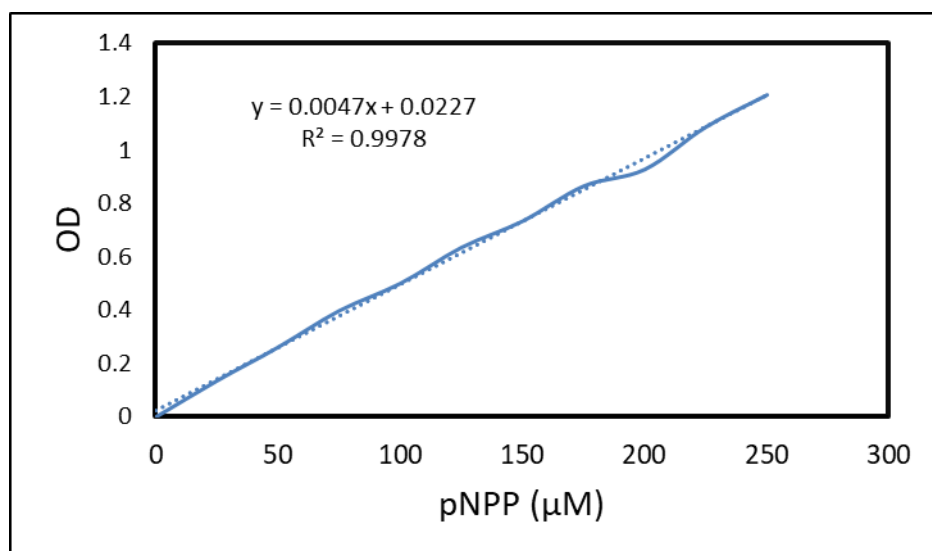
E. Calibration Study of Mel Release

Appendix E1 Figure 69 Standard curve constructed for different concentrations of Mel in PBS.
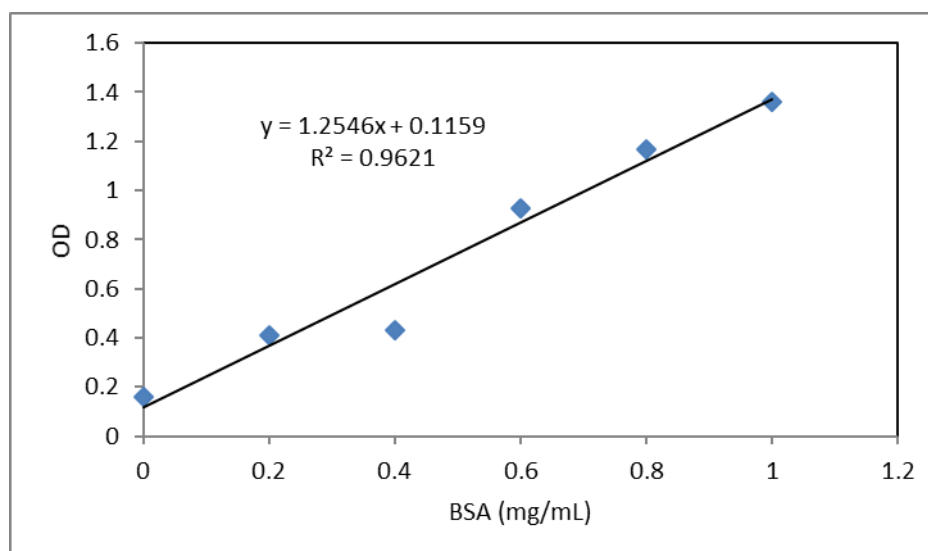

Appendix E2 Figure 70 Standard curve constructed for different concentrations of Mel in methanol.

F. Calibration Study of pNPP

Appendix F1 Figure 71 Standard curve constructed for different concentrations of pNPP.

G. Calibration Study of BCA

Appendix G1 Figure 72 Standard curve constructed for different concentrations of BSA.

CURRICULUM VITAE

PERSONAL INFORMATION

Surname, Name: Atila, Deniz
Nationality: Turkish (TC)
Date and Place of Birth: 16 February 1986, Ankara
Marital Status: Single
Phone: +90 505 279 39 52
Fax: +90 312 210 22 91
email: atila.deniz@metu.edu.tr

EDUCATION

Degree	Institution	Year of Graduation
MS	METU Engineering Sciences	2014
BS	METU Biology	2011
High School	Kaya Bayazıtoğlu High School, Ankara	2005

WORK EXPERIENCE

Year	Place	Enrollment
2013-2020	METU Dept. of Engineering Sciences	Research Assistant
2019-2020	National Health Research Institutes Institutes of Biomedical Engineering and Nanomedicine, Taiwan	Fellowship Student
2010 July	Ankara Uni. Dept. of Molecular Biology	Intern Student

FOREIGN LANGUAGES

Fluent English, Basic Chinese

PUBLICATIONS

1. Atila, D., Keskin, D., & Tezcaner, A. (2015). Cellulose acetate based 3-dimensional electrospun scaffolds for skin tissue engineering applications. Carbohydrate Polymers, 133, 251-261. Doi: 10.1016/j.carbpol.2015.06.109.

2. Atila, D., Keskin, D., & Tezcaner, A. (2016). Crosslinked pullulan/cellulose acetate fibrous scaffolds for bone tissue engineering. Materials Science and Engineering: C, 69, 1103-1115. Doi: 10.1016/j.msec.2016.08.015.

3. Türkkan, S., Atila, D., Akdağ, A., & Tezcaner, A. (2018). Fabrication of functionalized citrus pectin/silk fibroin scaffolds for skin tissue engineering. Journal of Biomedical Materials Research Part B: Applied Biomaterials. 106(7), 2625-2635. Doi: 10.1002/jbm.b.34079.

4. Rad, R. M., Atila, D., Akgün, E. E., Evis, Z., Keskin, D., & Tezcaner, A. (2019). Evaluation of human dental pulp stem cells behavior on a novel nanobiocomposite scaffold prepared for regenerative endodontics. Materials Science and Engineering: C, 100, 928-948. Doi: 10.1016/j.msec.2019.03.022.

5. Dalgic, A. D., Atila, D., Karatas, A., Tezcaner, A., & Keskin, D. (2019). Diatom shell incorporated PHBV/PCL-pullulan co-electrospun scaffold for bone tissue engineering. Materials Science and Engineering: C, 100, 735-746. Doi: 10.1016/j.msec.2019.03.046.

6. Moonesi Rad, R., Atila, D., Evis, Z., Keskin, D., & Tezcaner, A. (2019). Development of a novel functionally graded membrane containing boron-modified bioactive glass nanoparticles for guided bone regeneration. Journal of tissue engineering and regenerative medicine. 13(8), 1331-1345. Doi: 10.1002/term.2877.

7. Atila, D., Karataş, A., Evcin, A., Keskin, D., & Tezcaner, A. (2019). Bacterial cellulose-reinforced boron-doped hydroxyapatite/gelatin scaffolds for bone tissue engineering. Cellulose, 1-21. Doi: 10.1007/s10570-019-02741-1.

8. Akbaba, S., Atila, D., Keskin, D., Tezcaner, T., & Tezcaner, A. (2021). Multilayer Fibroin/Chitosan Oligosaccharide Lactate and Pullulan Immunomodulatory Patch for Treatment of Hernia and Prevention of Intraperitoneal Adhesion. Carbohydrate polymers, 118066. Doi: 10.1016/j.carbpol.2021.118066.